Energy transfer in lanthanide complexes

Clarkson, Ian Michael

Energy Transfer in Lanthanide Complexes

Ian Michael Clarkson

Department of Chemistry
University of Durham

A thesis submitted for the degree of Doctor of Philosophy

1999

Energy Transfer in Lanthanide Complexes

Ian Michael Clarkson, 1999

Abstract

This thesis details investigations into the photophysical properties of lanthanide ions in a number of different systems.

The preparation and characterisation of lanthanide containing surfactant salts of the type $Ln(AOT)_3$ (Ln = Tb, Nd, Eu, AOT = bis-(2-ethylhexyl) sulfosuccinate) is described. Small angle neutron scattering experiments have been used to determine the size and shape of reverse micelles formed by these surfactants in water/cyclohexane microemulsions. The luminescence lifetimes of the lanthanide ions have been used to investigate the solvation environment within reverse micelle systems as a function of water content.

The use of lanthanide complexes based on 1,4,7,10-tetraazacyclododecane bearing phenanthridine antenna in luminescence microscopy has been explored. Samples such as silica particles, onion skin cells and guinea pig heart cells have been imaged. Time-resolved measurements have allowed time gating of the sample from a fluorescent background and lifetime maps of the images have been obtained.

The preparation and characterisation of deuteriated complexes of dota (1,4,7,10-tetraazacyclododecane-1,4,7,10-tetraacetic acid) with lanthanide ions is described. Selective deuteriation of both the ring and arm sites allow the relative quenching effects of C-H/D oscillators to be determined for various lanthanides in a series of structurally well defined complexes.

Finally, investigations into the distance dependence of the energy transfer between aromatic chromophores and lanthanide ions have been undertaken. The synthesis of a model system linking a phenanthridine donor to a europium complex by poly(valine) spacer units is described. Preliminary photophysical results show that the quantum yield of emission by europium decreases as the distance between the donor acceptor pair is increased.

Declaration

The content of this thesis represents the work of the author unless indicated to the contrary or acknowledged by reference. The thesis describes the results of reseach carried out in the Department of Chemistry, University of Durham and also at the Rutherford Appleton Laboratories, Oxfordshire between October 1996 and September 1999. This work has not been submitted for a higher degree in any other academic institution.

Statement of Copyright

Abbreviations

AOT		Aerosol OT, bis(2-ethylhexyl)sulfosuccinate
^{t}Bu		*tert*-butyl
CCD		charge coupled device
CTAB		cetyltrimethylammonium bromide
DCM		dichloromethane
DCM		4-dicyanmethylene-2-methyl-6-(*p*-dimethylaminostyryl-4H-pyran
DDAB		didodecyldimethylammonium bromide
DELFIA		dissociation enhanced lanthanide fluoroimmunoassay
DOTA		1,4,7,10-tetrakis(carboxymethyl)-1,4,7,10-tetraazacyclododecane
DMF		dimethylformamide
Et		ethyl
FTIR		Fourier transform infra red
IC		internal conversion
IR		infra red
	s	strong
	m	medium
	w	weak
	br	broad
IRF		instrument response function
ISC		intersystem crossing
Me		methyl
Ms		methanesulfonyl
Mp		melting point
MS		mass spectroscopy
	DCI	desorbed chemical ionisation
	ESMS	electrospray mass spectrometry
	ES+/-	electrospray positive/negative
	FAB	fast atom bombardment
	M	molecular ion
NMR		
	s	singlet

	d	doublet
	dd	doublet of doublets
	m	multiplet
	t	triplet
	q	quartet
	pent.	pentet
	br	broad
PBS		phosphate buffered saline
^{i}Pr		*iso*-propyl
SANS		small angle neutron scattering
SDS		sodium dodecyl sulfate
TFA		trifluoroethanoic acid
THF		tetrahydrofuran
TLC		thin layer chromatography
Ts		tolylsulfonyl
UV		ultra violet
Vis		visible
VR		vibrational relaxation
YAG		yttrium aluminium garnet

Acknowlegements

Firstly thanks must go to my supervisors David Parker and Andy Beeby without their guidance, support and friendship the past three years would have been impossible.

Thanks to all the people who I have worked with in labs 2, 7, 27 and 133 and have provided me with advice, support and good humour. Special thanks must go to Stephen Faulkner, Justin Perry and Linda Govenlock.

Much of this work would have been impossible without the help of the services here in Durham. Thanks to Alan Kenwright and Ian McKeag for all their expertise in running and interpreting NMR spectra and to Mike Jones and Lara Turner for all their help with mass spectrometry. The glass blowers, Ray and Gordon, and stores men, Jimmy and Joe, have provided invaluble help over course of my work.

Work completed at the Rutherford Appleton Laboratories forms a substantial part of this work and I would like to thank Tony Parker, Kevin Henbest, Stan Botchway and Trevor Powell (University of Oxford) for all their help during our time at the Luminescence Microscope in the Lasers for Science Division. Thanks also to Richard Heenan (RAL) and Julian Eastoe (University of Bristol) for their help with the small angle neutron scattering work.

Finally a big thank you to my long suffering family and friends. Thanks to my Mum, Dad and brother for their continual support throughout my time in Durham. Thanks also to Phil Skinner, Sarah Woodlands, Caroline Smith, Steve Moss, John Clarke, Dan Read, Andy Clase, Allison Jones and Andrew Lamb.

Contents

Chapter 1

Introduction

Chapter 1
Introduction

This thesis describes investigations into the photophysical properties of lanthanide ions in a number of different systems. This chapter is a general introduction and describes basic concepts of luminescence, lanthanide complexation chemistry and the spectroscopic properties of the lanthanides.

1.1 Luminescence

All materials increase their emission of radiation as their temperature is raised, a phenomenon known as incandescence or "hot light". Luminescence, or "cold light", is the phenomenon whereby light is emitted by a material which has not arisen from an increase in its temperature. For emission to occur the material must first absorb energy from a suitable source[1].

Luminescence can be subdivided into a number of categories. If the absorbed energy comes from an exoenergetic chemical reaction, the emitted light is known as chemiluminescence. Triboluminescence involves emission of light on rubbing or crushing crystals, for example sugar. The work described in this thesis concerns photoluminescence, that is, emission of light following absorption of light of the same or higher energy.

Photoluminescence may be further subdivided into fluorescence and phosphorescence. Historically this distinction was based upon the relative lifetime of emission following discontinuation of the excitation. If emission continued after the excitation was stopped the process was known as phosphorescence as opposed to emission which stopped as soon as the excitation was discontinued which was referred to as fluorescence. This definition proved unsatisfactory and has been replaced by a definition based on the spin states of the excited electronic state and the state to which this decays during the transition. If the two states are of the same multiplicity the process is know as fluorescence and if the two states are of different

multiplicity the process is known as phosphorescence[2]. Transitions between electronic levels of different multiplicities are spin forbidden and as a consequence the process of phosphorescence usually has a low rate constant, with the lifetime of the state being 10^{-3}-10 s. Fluorescence is a spin allowed process and as such the excited state has a much shorter lifetime typically in the range of ns to ms. Figure 1.1 shows these transitions for a typical organic molecule on a simplified Jablonski diagram.

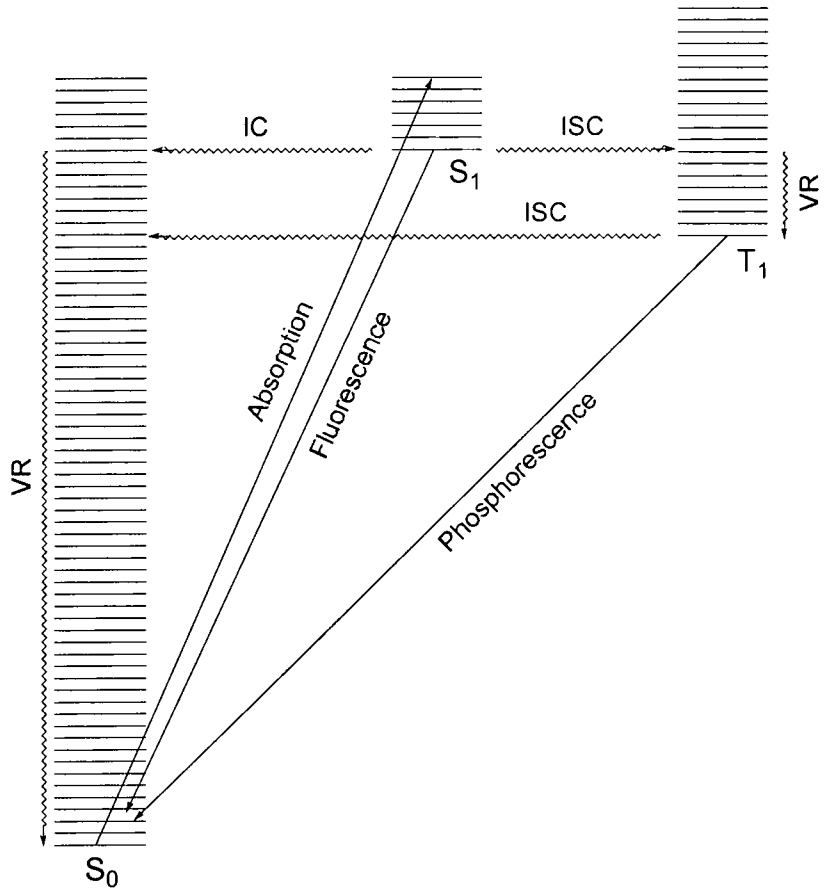

Figure 1.1 Jablonski diagram for a typical organic molecule

The diagram also shows possible deactivation pathways for the molecule including non-radiative quenching of the excited state. The non-radiative decay pathways shown include vibrational relaxation (VR) where a state loses its excess energy to vibrational modes of the surrounding medium. Internal conversion (IC) occurs between isoenergetic levels of the same multiplicity, e.g. the upper levels of S_0, the ground state, with the lower levels of S_1, the first excited singlet state. When this process occurs between isoenergetic levels of different multiplicities the process is

known as intersystem crossing (ISC) e.g. from S_1 to T_1, the first excited triplet state, which populates the T_1 state allowing phosphorescence to occur. Deactivation of the T_1 state may also take place by ISC back to S_0 or it may be quenched by oxygen. This explains why phosphorescence can often only be observed in deoxygenated samples or in solid matrices.

1.2 Lanthanides

1.2.1 General

The lanthanide elements consist of the 14 elements after lanthanum in which the 4f subshell is progressively filled. The outer electronic configuration is generally $[Xe]4f^n5d^06s^2$ with the exceptions being cerium, $[Xe]4f^15d^16s^2$; gadolinium, $[Xe]4f^75d^16s^2$; and lutetium, $[Xe]4f^{14}5d^16s^2$. The aqueous solution chemistry of these elements is dominated by their +3 oxidation state ($[Xe]4f^n$), the exceptions being Ce^{IV} and Eu^{II} which are stable in basic and acidic aqueous media and Pr^{IV}, Tb^{IV}, Nd^{II}, Sm^{II}, Eu^{II}, Dy^{II}, Tm^{II} and Yb^{II} which are metastable in the solid state[3]. Apart from lutetium and lanthanum, the ions all contain partially filled f-shells and as such are paramagnetic[3].

1.2.2 Complexation

Bonding between lanthanide(III) ions and ligands is essentially ionic, the inertness and poor spatial penetration of the 4f electrons eliminating the possibility of π-back bonding as found in d-block chemistry. This leads to the primary co-ordination number and geometry of the complex being determined almost entirely by the packing considerations of the ligands around the ions. The number of atoms in the first co-ordination sphere varies widely from 6 to 12 with 8 or 9 being the most common[3]. Lanthanide aqua ions have a primary co-ordination number which varies across the series with a value of 9 from La^{3+} to Nd^{3+}; 8 from Dy^{3+} through to Lu^{3+} and intermediate values for the remaining ions[4].

Lanthanide ions act as hard acids with a preference to bind hard bases such as oxygen or nitrogen donors over softer donors such as sulfur or phosphorus. More polarisable atoms such as amine nitrogens are preferred to ether oxygens. As co-ordination is

predominantly ionic in nature, charged groups such as carboxylates, phosphonates and phosphinates are favoured. The chelate effect[5] may also be used to increase complex stability: donor atoms are incorporated into chelating rings with 5-membered rings being preferable to 6 membered rings[6]. Further stability may be imparted by incorporating the donor atoms into a macrocycle[7]. This 'macrocyclic' effect is due to enthalpic and entropic effects which vary according to metal and macrocycle[8].

1.2.3 Lanthanide Complexes of 1, 4, 7, 10-tetraazacyclododecane-based Ligands

The ligand 1,4,7,10-tetraazacyclododecane-1,4,7,10-tetraacetic acid, dota, **1**, based on the macrocycle 1,4,7,10-tetraazadodecane, $12N_4$, with appended acetate arms is ideal for lanthanide complexation. It complexes through N and O donors, it is octadentate, it has negatively charged donor groups and it forms 5 membered chelate rings. The structures of several of these complexes are known in the solid state (Eu[9], Gd[10], Lu[11]). The ligand is arranged around the metal in a square antiprismatic geometry with the ninth co-ordination site occupied by a water molecule. The nitrogen atoms are arranged gauche to each other and the ethylene bridges are staggered giving rise to two possible ring conformations either in the δδδδ or the λλλλ form (using the nomenclature of Corey[12]).

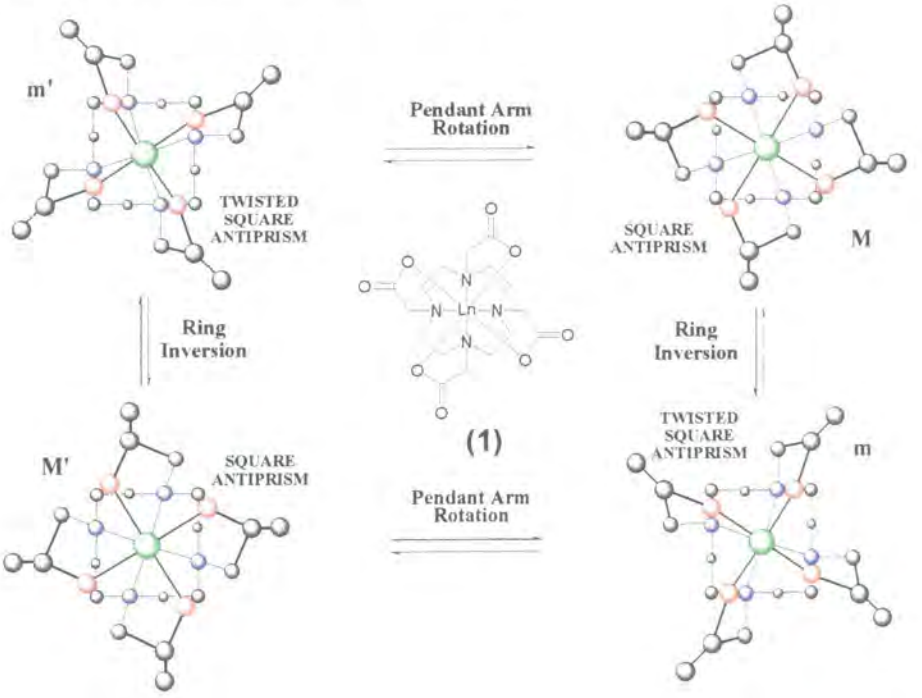

Figure 1.2 Stereoisomerism in lanthanide-DOTA complexes

The acetate arms can either lie in a clockwise or anticlockwise fashion resulting in either a Δ, for an anticlockwise orientation of the arms or a Λ conformation, for a clockwise orientation. The various combinations of these two features, as shown in Figure 1.2, result in two enantiomeric pairs of diasteromers, in total four stereoisomers. M and M', respectively the Λ(δδδδ) and Δ(λλλλ), have a square antiprismatic complexation geometry. The m and m' isomers, respectively the Λ(λλλλ) and Δ(δδδδ), have a twisted square antiprismatic geometry, with a reduced angle of twist about the principal axis.

1.2.4 Spectroscopy

The $4f^n$ electrons give rise to a large number of excited states, shown in Figure 1.3, whose energies are determined by interelectronic repulsions, spin-orbit coupling and ligand field effects.

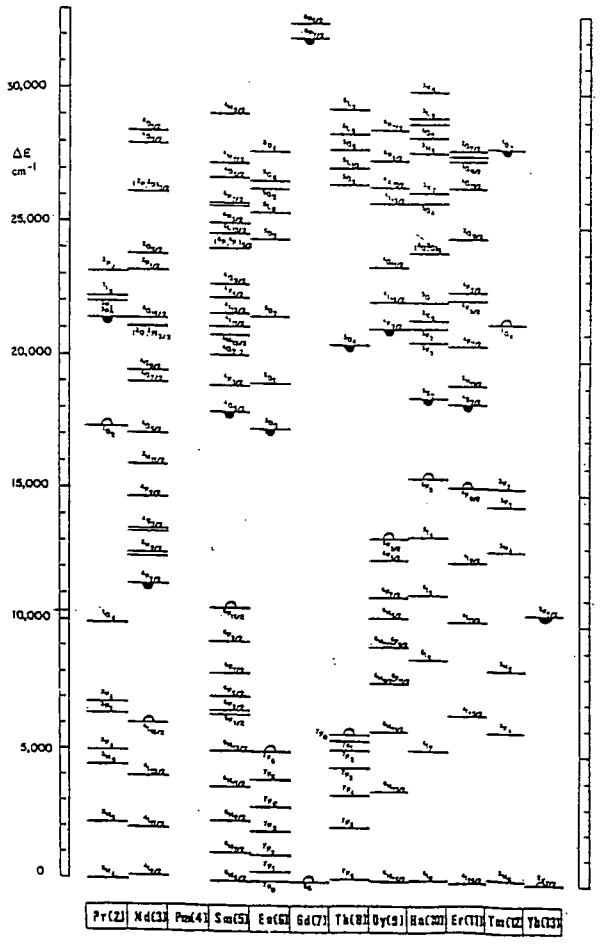

Figure 1.3 Energy level diagram for the lanthanides. Filled circles represent lowest luminescent levels and open circles represent the highest levels of the ground state manifold

The electronic configurations of the lanthanides are described by use of the Russell-Saunders coupling scheme[13]. The 4f electrons are effectively shielded and are minimally involved in bonding, therefore ligand field splittings are small,[14] typically around 10^2 cm^{-1}. In turn, this leads to sharp spectral bands both in absorption and emission with low extinction co-efficients[15] (1-10 dm^3 mol^{-1} cm^{-1}). This may be contrasted with d-block metal complexes where large ligand field splittings (around 1000's of cm^{-1}) lead to broad absorption spectra usually with much higher extinction co-efficients.

The Laporte selection rule for electronic transitions states that the only allowed transitions are those accompanied by a change of parity. If the orbital remains unchanged under an inversion it is gerade, whereas if the signs of the lobes change under inversion it is ungerade. f-Orbitals are ungerade and this means that f→f transitions are forbidden as there is no change in parity. d→d Transitions are forbidden for the same reason, but in the case of these transitions the selection rule is relaxed by interaction with the ligand field which introduces different parity into the d-levels. It has already been stated that these effects are much smaller in the case of the lanthanide ions meaning that the relaxation of the selection rule by introduction of different parity into the 4f wavefunction is much less significant than for d-block complexes. Hence lanthanide ions have much lower extinction co-efficients than those found for the d-block.

1.3 Sensitised luminescence

As a consequence of the low molar extinction co-efficients, the excited state of lanthanide ions are not readily populated using conventional light sources. This problem can be countered either by using powerful excitation sources such as lasers, or by using sensitised emission[16,17]. Sensitised emission increases the effective molar extinction co-efficient by using a strongly absorbing chromophore to absorb the incident radiation followed by energy transfer to the lanthanide resulting in indirect excitation of the lanthanide ion. Sensitised emission was originally observed in europium complexes[18] where irradiation with u. v. light in an area of the spectrum

where only the organic chelating species absorbed caused the characteristic europium luminescence to occur.

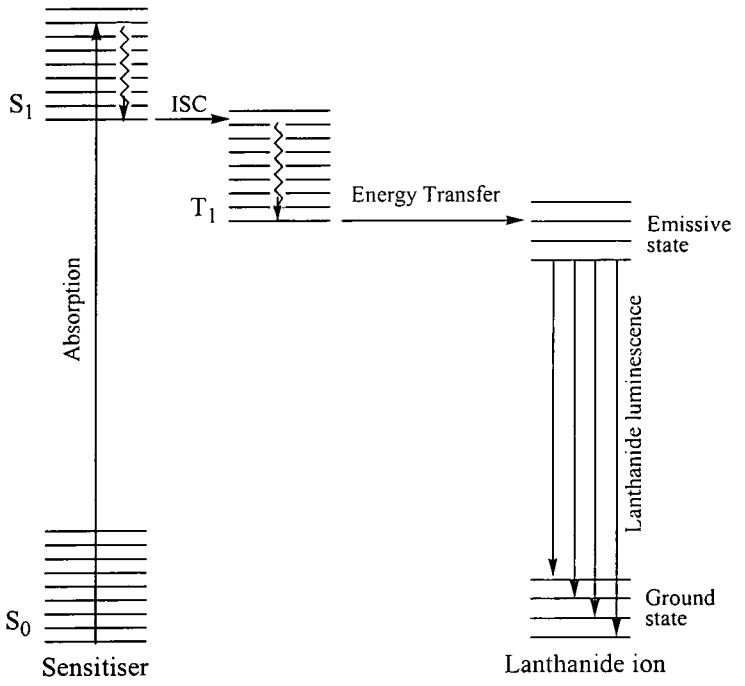

Figure 1.4 Sensitised emission

This process is represented in Figure 1.4. An organic chromophore absorbs energy to give an excited S_1 state, intersystem crossing yields the T_1 state which transfers energy to a lanthanide ion[19,20] resulting in lanthanide luminescence. Direct excitation of the lanthanide is not involved[21]. Transfer of energy from the singlet state can occur but is a minor factor compared with the transfer from the triplet state[22]. The chromophore may be present in solution or may be incorporated into the ligand which is binding the lanthanide[23,24]. The energy transfer is favoured by the sensitiser and the lanthanide being in close proximity. The efficiency is dependent upon the energy difference between the triplet state of the sensitiser and the emissive state of the lanthanide. To prevent thermally activated back energy transfer to the triplet state the energy difference should be greater than 1500 cm^{-1} (at 298 K, kT is *ca.* 208 cm^{-1}).

1.4 Measurement of Lifetimes

A major part of this work involves the measurement of luminescent lifetimes of lanthanide ions. The magnitude of the lifetime determines the method for measurement. The decay is usually a first order process following an exponential decay profile, equation 1.1. The lifetime, τ, is the inverse of the rate constant for decay, k.

$$I = A_0 + A_1\exp(-kt) \qquad \textbf{1.1}$$

where I = intensity after time t

A_0 = intensity after the decay has finished

A_1 = pre-exponential factor

k = rate constant for decay of the excited state.

For ions such as europium and terbium the lifetime can be measured using a spectrofluorimeter. The sample is excited using a short pulse of light and the resulting emission is monitored as a function of time. The lifetime is then obtained by fitting the data to equation 1.1. Figure 1.5 shows typical data, and the resulting fit, obtained for the europium complex of the ligand dota (1,4,7,10-tetraazadocacane-tetraacetate).

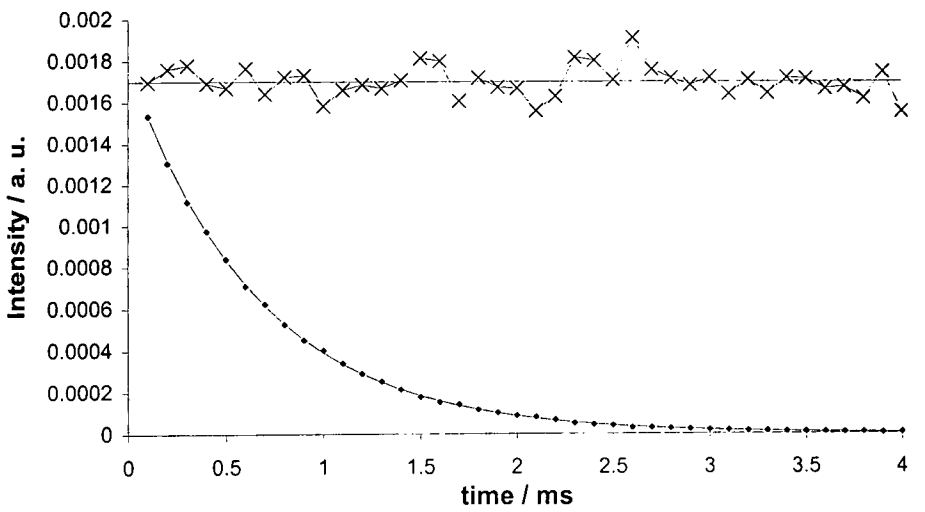

Figure 1.5 The decay (points), fit (line) and residuals (top) for $[Eu(dota)]^-$ in H_2O at 298 K. The data gives k = 1.52 ms^{-1}. λ_{ex} = 397 nm, λ_{em} = 594 nm.

This method cannot be applied to neodymium or ytterbium for two reasons. Firstly, the radiative lifetime ($\tau < 1$ μs) is much less for these two lanthanides than for europium or terbium. Secondly, the wavelength range on the available spectrofluorimeters is insensitive beyond 800 nm and emission from neodymium is at 1055 nm and for ytterbium at 980 nm. For this reason, neodymium lifetimes are measured using a home-made ns-laser pumped fluorimeter, utilising a germanium diode detector. This set-up is more fully explained in chapter 6. The signal collected is a convolution of the response of the instrument and the decay of the neodymium ion. This decay may be modelled by convolving an exponential decay with the measured instrument response[25]. An iterative method is used to compare the model and the experimentally determined signal to yield the lifetime, full details of which can be found in chapter 6. Figure 1.6 shows some typical results for the neodymium complex of dota in H_2O. It can be seen that the fit and decay overlay each other and that the residuals are small and random.

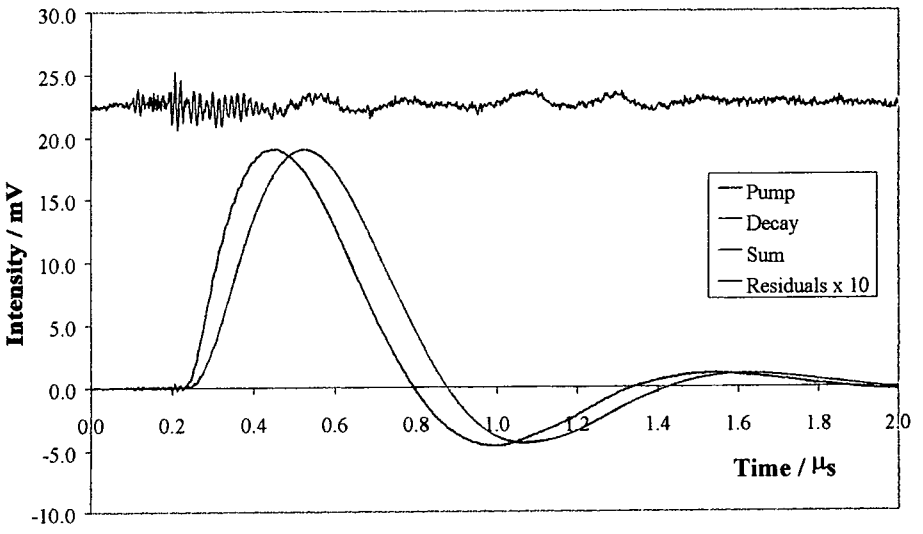

Figure 1.6 The IRF, decay, fit and residuals x 10 for $[Nd(dota)]^-$ in H_2O. The data gives a lifetime of 75.7 ns.

1.5 Deactivation of the Excited State

The excited state of lanthanide(III) ions in solution can be deactivated by energy transfer to high-energy vibrations of solvent molecules or oscillators within the bound ligand. Early studies suggested that the most effective of these was the O-H

oscillator such as that found in any coordinated water molecules. Oscillators such as amide N-H, C-H and C=O were also shown to have a lesser effect[26]. The extent of luminescence quenching was also found to be inversely proportional to the energy gap between the emitting state and the ground state[26,27]. Each oscillator was found to be acting independently in quenching the excited state[28,29]. Figure 1.7 shows the luminescent states for neodymium ($^4F_{3/2}$), europium ($^5D_0$), terbium ($^5D_4$) and ytterbium ($^2F_{5/2}$) and their ground state manifolds. On the same figure the relative energies of the vibrational manifolds for C-H, C-D, O-H and O-D oscillators are depicted. It can be seen that there is relatively efficient coupling between the Yb^{3+} and Eu^{3+} emissive states with the third vibrational overtone of O-H, for terbium with the fourth overtone and for neodymium with the first and second overtones. The Franck-Condon overlap factor becomes less favourable with the higher overtones. This is consistent with the very efficient quenching of neodymium and the less efficient quenching of terbium. The O-D, C-D and N-D oscillators have lower stretching frequencies and therefore energy matching may only occur with higher vibrational overtones. The Franck-Condon factor is therefore less favourable for X-D oscillators than for similar X-H oscillators explaining their less effective quenching of the excited state. For complexes of europium and terbium, X-D oscillators have been estimated to be at least 200 times less effective than the corresponding X-H oscillator[30].

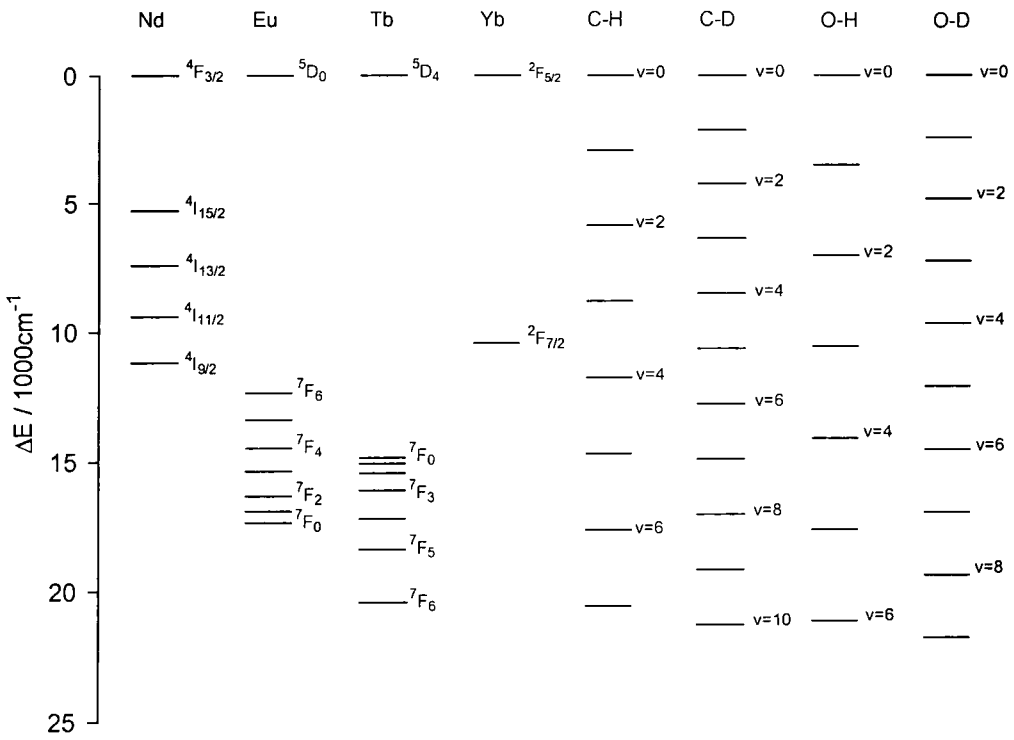

Figure 1.7

The rate constant for depopulation of the lanthanide excited state can be partitioned into the sum of the various contributing processes as shown in equations 1.2 and 1.3.

$$k_{H_2O} = k_{nat} + k_{nr} + \Sigma k_{XH} + \Sigma k_{other} \qquad \textbf{1.2}$$

$$k_{D_2O} = k_{nat} + k_{nr} + \Sigma k_{XD} + \Sigma k_{other} \qquad \textbf{1.3}$$

k_{H_2O/D_2O} observed lifetime in H_2O/D_2O

k_{nat} natural radiative rate constant

k_{nr} non-radiative de-excitation rate constant

$\Sigma k_{XH/D}$ sum of rate constants to proximate matched X-H/D oscillators

Σk_{other} sum of rate constants to proximate matched non-exchangable oscillators

In D_2O, if the exchangeable X-H oscillators do not contribute to vibrational quenching then equation 1.3 can be reduced to equation 1.4.

$$k_{D_2O} = k_{nat} + k_{nr} + \Sigma k_{other} \qquad \textbf{1.4}$$

Subtracting equation 1.4 from equation 1.2 gives equation 1.5.

$$\Delta_k = k_{H_2O} - k_{D_2O} = \Sigma k_{XH} \qquad \textbf{1.5}$$

Given that in aqueous media the predominant quenching mechanism involves O-H oscillators and ignoring other contributions, an expression was derived[36] which related the number of water molecules in the inner co-ordination sphere, q, to the difference in rate constants for quenching in H_2O and D_2O, equation 1.6

$$q = A\,(k_{H_2O} - k_{D_2O}) \qquad \textbf{1.6}$$

q number of water molecules in the inner co-ordination sphere

A proportionality constant

The proportionality constant, A, is a measure of the sensitivity of the lanthanide to vibronic quenching by O-H oscillators. Some values of A are shown in Table 1.1. The estimated uncertainty in calculations of q for europium and terbium was assessed to be ± 0.5 This error in the assessment of q values may be due to the effect of 'outer-sphere' water, water not directly co-ordinated to the metal but diffusing sufficiently close to the complex to effect vibrational relaxation of the excited state of the metal. Evidence for this comes from such complexes as the tetra benzyl phosphinate complex, **2**.

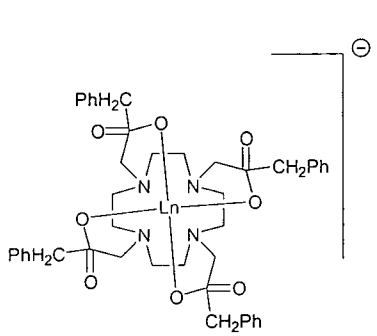

2

These are known to have no bound water[31,32] for the europium, yttrium, gadolinium and ytterbium complexes. However the europium, terbium and ytterbium complexes have a decreased lifetime in H_2O compared with D_2O, this represents quenching by non-bound, 'outer-sphere' water.[33]

A similar method has been applied to quantify the effect of amine N-H oscillators[34,35] using ethylenediamine complexes of europium and terbium in DMSO. This does not give a well defined system but rather a distribution of the 1:1, 1:2 and 1:3 stoicheometries in a dynamic equilibrium. With this non-ideal system, it was found that in complexes of europium an N-H oscillator is 1.5 times more effective than an O-H oscillator at quenching the excited state, while for terbium complexes N-H oscillators were half as effective as O-H oscillators [34].

Lanthanide	*A* / s	Reference
Tb^{3+}	4.2×10^{-3}	36
Eu^{3+}	1.05×10^{-3}	36
Nd^{3+}	3.6×10^{-7}	37
Yb^{3+}	1.0×10^{-6}	38

Table 1.1 '*A*' values for selected lanthanides

1.6 Effect of C-H/D Oscillators

C-H oscillators can also quench the excited states of lanthanide ions. This is usually a smaller effect than for O-H oscillators as C-H oscillators are weaker. Furthermore energy matching with the oscillator is more difficult as C-H oscillators have a sharper energy than the hydrogen bond broadened profile of an O-H oscillator. C-H Oscillators in a ligand are always more distant than bound O-H oscillators, this is another contributing factor to their reduced efficiency in quenching the excited states of lanthanide ions.

Early work focused on the effect of deuteriation in the solvent molecules[26,28]. The rate constants of luminescence of the europium(III) and neodymium(III)[37] ions in

non- and perdeuteriated solvents were measured and some typical results are summarised in Table 1.2.

		k / s^{-1}		$\Delta k / s^{-1}$	Reference
Salt	Solvent	Protiated	Deuteriated		
$Eu(ClO_4)_3$	DMSO	667	351	316	28
$Eu(ClO_4)_3$	Acetonitrile	1290	714	576	28
$Eu(NO_3)_3$	Acetone	2630	847	1780	26
$Nd(ClO_4)_3$	DMSO	5.88×10^5	1.11×10^5	4.77×10^5	37
$Nd(ClO_4)_3$	MeOD†	3.45×10^6	2.10×10^6	1.35×10^6	37

Table 1.2 Rate constants of luminescence for europium and neodymium in protiated and deuteriated solvents. († The data shown are for the deuteriation of the C-H oscillators; in each case the hydroxyl is deuteriated.)

From the data in Table 1.2, it can be seen that deuteriation of the C-H oscillators increases the lifetime of the excited state.

The quenching effect of C-H oscillators on lanthanide luminescence has also been investigated for the C-H oscillators of various ligands. The polydentate hemispherands **3a-d** have been synthesised with deuterium incorporated at various positions[39]. These hemispherands form neutral complexes with lanthanide ions and have recently been used in an investigation of the quenching effect of C-H oscillators on lanthanide luminescence.

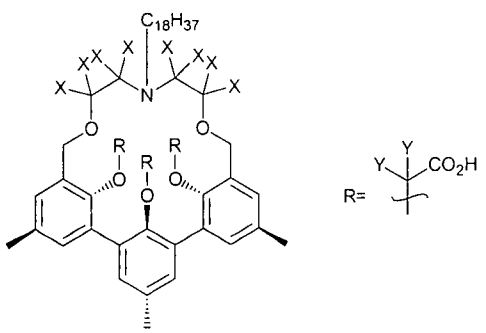

	X	Y
3a	H	H
3b	D	H
3c	H	D
3d	D	D

An increase in luminescence emission intensity was observed with increasing ligand deuteriation, in the order **3d** > **3b** > **3c** > **3a**. This increased intensity is caused by the deuteriated analogues quenching the excited state less. Lifetime measurements showed that deuteriation of the 8-aza-crown bridge positions (X = D) led to an increase in the luminescent lifetime by a factor of about 1.5. Deuteriation of the pendant arms was shown to have no significant effect on the luminescence lifetime. This effect is attributed to the distance dependence of energy transfer: the distance from the europium ion to the hydrogen atoms of the pendent arms ((3.86 - 4.87) ± 0.21 Å[†]) is significantly longer than the distance to the hydrogen atoms of the aza bridge ((3.54 - 4.26) ± 0.17 Å[†]), hence the efficiency of quenching by the aza bridge hydrogens is less. The rate constant for quenching by aza bridge C-H oscillators in this molecule, **3a**, is calculated as 310 ms^{-1}, that is, a contribution of *ca.* 40 s^{-1} per C-H.

The luminescence properties of ligands **3a** and **3b** have been investigated in their complexes with various other lanthanides[40]. Samarium, terbium, dysprosium, praseodymium, neodymium and ytterbium complexes were all shown to have increased luminescence emission intensity and lifetimes following ligand deuteriation. The complex **[Sm.3]** had a luminescent lifetime increase of 1.5 and the quenching effect per C-H was determined to be 0.75 ms^{-1}. For terbium, a doubling of the luminescence intensity was observed upon ligand deuteriation and the rate constant for quenching per C-H was determined to be <0.0025 s^{-1}. This reduced rate constant, relative to samarium is due to the increased energy gap between the emissive state and the ground state for terbium. As a consequence higher C-H/D overtones are involved in the energy transfer process with a less favourable Franck-Condon overlap. Dysprosium and praesodymium also increased their luminescence intensity upon ligand deuteriation. In the case of praesodymium the enhancement was not as high as was originally surmised, a possible reason is that the magnitude of the energy gap is resonant with the first overtone of a C-D oscillator. As a result, the C-D oscillator is relatively effective at quenching the excited state, so deuteriation

[†] From molecular dynamics calculations.

does not lead to as large a luminescence enhancement as would be expected. The quenching of neodymium by C-H oscillators was found to be very efficient, with a rate constant of 17.8 ms^{-1} per C-H. For ytterbium a rate constant of quenching of 2.6 ms^{-1} per C-H oscillator was determined.

1.7 Mechanism of Energy Transfer

Electronic energy transfer is the simultaneous relaxation of a molecule in an excited state, the donor (D), and the excitation of a molecule or ion in a lower-lying state, the acceptor(A), the overall process is represented by equation 1.7.

$$D^* + A \rightarrow D + A^* \qquad \textbf{1.7}$$

The simplest mechanism is a radiative process where the donor emits light (equation 1.8) which is subsequently re-absorbed by the acceptor (equation 1.9)[41,42]. This mechanism is dependent on the quantum yield of emission of D*, the overlap of the emission profile of D* with the absorption profile of A, the amount and the light absorbing properties of A. The trivial mechanism is favoured when all these factors are maximised.

$$D^* \rightarrow D + h\nu \qquad \textbf{1.8}$$

$$h\nu + A \rightarrow A^* \qquad \textbf{1.9}$$

Energy transfer can also occur via non-radiative processes. There are two different mechanisms which are generally believed to account for the non-radiative interaction: the Förster and the Dexter mechanisms. Both mechanisms require a spectral overlap between the emission spectrum of the donor and the absorption spectrum of the acceptor.

The Förster mechanism[42,43,44] proceeds via a dipole-dipole coupling between the donor and acceptor - a coulombic interaction. The excited state of the donor is assumed to behave like a field generated by a classically oscillating dipole. The resulting electric charge oscillation causes electrostatic forces to be exerted on the

electronic systems of surrounding molecules. Thus an excited molecule may cause the electrons in a ground state molecule to oscillate in much the same way as does the electric field of a light wave. For the excited state of the acceptor to occur a resonance condition must be met, in this case $\Delta E(D^* \rightarrow D) = \Delta E(A \rightarrow A^*)$. This mechanism gives the rate of energy transfer, k_{ET}, as a function of the separation of the donor and acceptor, R_{DA}, equation 1.10.

$$k_{ET} = k\frac{\kappa^2 k_D^o}{R_{DA}^6} J(\varepsilon_A) \qquad \textbf{1.10}$$

k is a constant determined by the experimental conditions being used, that is, the refractive index of the solvent and the concentrations of the species. The interaction is dependent on the orientation of the two dipoles in space, this is taken into account by the term κ^2, for a randomly distribution of dipoles this factor is constant and equal to □. The rate of energy transfer is also dependent on the pure radiative lifetime of D, k_D°, this is theoretically related to the oscillator strength of the $D^* \rightarrow D$ transition. The process is related to the spectral overlap between the absorption and emission curves, this factor is taken into account by $J(\varepsilon_A)$. The process is subject to some selection rules. There can be no change in the spin of the donor or acceptor and the multiplicities of the excited donor and acceptor must be the same as those of the ground state donor and acceptor respectively.

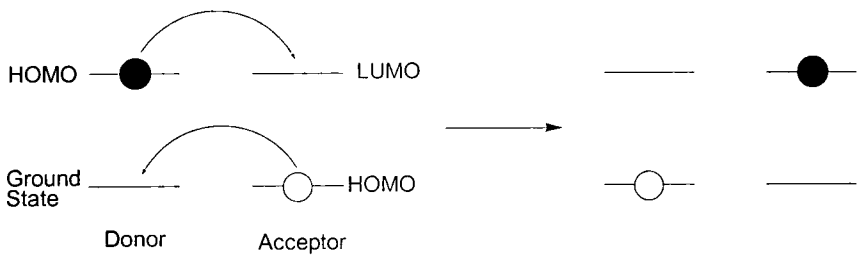

Figure 1.8 Diagrammatic representation of the Dexter mechanism of energy transfer.

The Dexter mechanism[42,45] considers transfer processes involving forbidden transitions not only allowed transitions as for the Förster mechanism. It is an exchange interaction involving mutual electron exchange between the sensitiser and acceptor, with a conservation of multiplicity of the system, as shown in Figure 1.8.

For this to occur the electronic orbitals of the donor and acceptor species must overlap.

$$k_{ET} = KJ \exp(-2R_{DA}/L) \qquad 1.11$$

Equation 1.11 shows that the rate of energy transfer reduces exponentially with increasing distance between the donor and acceptor, R_{DA}. This is due to the fact that electron densities usually fall off exponentially as the distance from the nucleus increases. The rate is also related to the specific orbital interactions, K, and the spectral overlap integral normalised for the absorption coefficient of the acceptor, J, and the donor-acceptor pairs van der Waals radii, L.

The main differences between the two mechanisms are in the distance dependent nature of the rate of energy transfer. The coulombic, dipole-induced energy transfer decreasing as R_{DA}^{-6} whereas the exchange mechanism decreases as $\exp(-2R_{DA}/L)$. The rate of energy transfer for the coulombic mechanism is dependent on the oscillator strengths of the $D^* \rightarrow D$ and the $A \rightarrow A^*$ transitions whereas for the exchange mechanism is independent of these. The efficiency of the energy transfer process for the coulombic mechanism is mainly dependent on the oscillator strength of the $A \rightarrow A^*$ transition and the quantum yield of the donor, Φ_D, whereas the efficiency of energy transfer by exchange is not directly related to an experimental quantity. Despite these differences both mechanisms highlight the importance of J the spectral overlap between the donor emission and the acceptor absorbance spectra.

1.8 Thesis Structure

Chapter 2 describes an investigation of the luminescent and structural properties of various lanthanide-containing reverse micelle systems. The variation of the luminescent lifetime as a function of the H_2O/D_2O content allowed an investigation of the solvation state of the lanthanide. Chapter 3 demonstrates the use of sensitised emission from lanthanide complexes to perform time-resolved measurements in luminescent microscopy. Chapter 4 describes the synthesis of dota complexes of various lanthanides with both the ring and arm positions deuteriated. This allowed

an investigation into the effect of ligand deuteriation in the lanthanide (Eu, Tb, Nd and Yb) complexes of dota. Chapter 5 describes the synthesis of model donor-acceptor systems suitable for the study of the distance dependence of energy transfer; some preliminary photophysical results are presented.

1.9 References for Chapter 1

[1] *Luminescence Probes,* Bunzli J.-C. G., in *Lanthanide Probes in Chemical and Earth Sciences,* eds. Bunzli J.-C. G., Chopin G. R., Elsevier, Amsterdam, 1989.

[2] *Photochemistry,* Wayne C. E., Wayne R. P., Oxford University Press, 1996.

[3] *Chemistry of the Elements,* Greenwood N. N., Earnshaw A., Pergamon, 1994.

[4] David F. H., Fourest B., *New J. Chem.*, **1997**, 21, 167.

[5] Schwarzenbach, *Helv. Chim. Acta.*, **1952**, 35, 2344.

[6] Hancock R. D., Martell A. E., *Chem. Rev.,* **1989**, 89, 1875.

[7] Cabbiness D. K., Margerum D. W., *J. Am. Chem. Soc.*, **1969**, 91, 6540.

[8] Lindoy L. F., 'The Chemistry of Macrocyclic Ligand Complexes', Cambridge University Press, Cambridge, 1989.

[9] Spirlet M., Rebizant J., Desreux J. F., Loncin M. F., *Inorg. Chem.*, **1984**, 23, 359.

[10] Dubost J. P., Leger J. M., Langlois M. H., Meyer D., Schaefer M., *C. R. Acad. Sci., Ser. 2,* **1991**, 312, 349.

[11] Aime S., Barge A., Botta M., Fasano M., Ayala J. D., Bombieri G., *Inorg. Chem. Acta,* **1996,** 246, 423.

[12] Corey E. J., Bailar J. C., *J. Am. Chem. Soc.*, **1959**, 81, 2620.

[13] *Lanthanides and Actinides,* Cotton S., Oxford University Press, 1991.

[14] Sabbatini N., Guardigli M., Lehn J.-M., *Coord. Chem. Rev.,* **1993**, 123, 201.

[15] *The Absorption and Fluorescence Spectra of Rare Earth Ions in Solution,* Carnell W. T., in *Handbook on the Physics and Chemistry of Rare Earths* eds. Gschneider Jr. K. A., Eyring L., North Holland Publishing Company: Amsterdam, 1979.

[16] Alpha B., Ballardini R., Balzani V., Lehn J.-M., Perathoner S., Sabbatini N., *Photochem. Photobiol.*, **1990**, 52, 299.

[17] Werts M. H. V., Hofstraat J. W., Geurts F. A. J., Verhoeven J. W., *Chem. Phys. Lett.*, **1997**, 276, 196.

[18] Weissman S. I., J. Chem. Phys., **1942**, 10, 214.

[19] Crosby G. A., Whan R. E., Alire R. M., *J. Chem. Phys.*, **1961**, 34, 743.

[20] Tanaka M., Yamaguchi G., Shiokawa J., Yamanaka C., *Bull. Chem. Soc. Japan,* **1970**, 43, 549.

[21] Crosby G. A., Kasha M., *Spectrochimica Acta*, **1958**, 10, 377.

[22] Kleinerman M., *J. Chem. Phys.*, **1969**, 51, 2370.

[23] Parker D., Senanayake K., Williams J. A. G., *J. Chem. Soc. Chem. Commun.*, **1997**, 1777.

[24] Parker D., Senanayake K., Williams J. A. G., *J. Chem. Soc. Perkin Trans. 2*, **1998**, 2129.

[25] *Excited State Lifetime Measurements*, Demas J. N., Academic Press, 1983, New York.

[26] Kropp J. L., Windsor M. W., *J. Chem. Phys.*, **1965**, 42, 1599.

[27] Kropp J. L., Windsor M. W., *J. Chem. Phys.*, **1963**, 39, 2769.

[28] Haas Y., Stein G., *J. Phys. Chem.*, **1971**, 75, 3668.

[29] Stein G., Wurzberg E., *J. Chem. Phys.*, **1975**, 62, 208.

[30] Haas Y., Stein G., *J. Phys. Chem.*, **1972**, 76, 1093.

[31] Aime S., Batsanov A. S., Botta M., Dickins R. S., Faulkner S., Foster C. E., Harrison A., Howard J. A. K., Moloney J. M., Norman T. J., Parker D., Royle L., Williams J. A. G., *J. Chem. Soc., Dalton Trans.*, **1997**, 3623.

[32] Aime S., Botta M., Parker D., Senanayake K., Williams J. A. G., Batsanov A., Howard J. A. K., *Inorg. Chem.*, **1994**, 33, 4696.

[33] Beeby A., Clarkson I. M., Dickins R. S., Faulkner S., Parker D., Royle L., de Sousa A. S., Williams J. A. G., Woods M., *J. Chem. Soc., Perkin Trans. 2*, **1999**, 493.

[34] Wang Z., Choppin G. R., Bernado P. D., Zanonato P. L., Portonova R., Tolazzi M., *J. Chem. Soc., Dalton Trans.*, **1993**, 2791.

[35] Ermolaev V. S., Sveshnikova E. B., *Chem. Phys. Lett.*, **1973**, 23, 379.

[36] Horrocks W. De W., Sudnick D. R., *Acc. Chem. Res.*, **1981**, 14, 384.

[37] Beeby A., Faulkner S., *Chem. Phys. Lett.*, **1997**, 266, 116.

[38] Beeby A., Dickins R. S., Faulkner S., Parker D., Williams J. A. G., *Chem. Commun.*, **1997**, 15, 1401.

[39] Oude Wolbers M. P., van Veggal F. C. J. M., Snellink-Ruël B. H. M., Hofstraat J. W., Guerts F. A. J., Reinhoudt D. N., *J. Am. Chem. Soc.*, **1997**, 119, 138.

[40] Oude Wolbers M. P., van Veggal F. C. J. M., Snellink-Ruël B. H. M., Hofstraat J. W., Guerts F. A. J., Reinhoudt D. N., *J. Chem. Soc., Perkin Trans. 2*, **1998**, 2141.

[41] Scandola F., Balzani V., *J. Chem. Educ.*, **1983**, 60, 814.

[42] *Modern Molecular Photochemistry*, Turro N. J., University Science Books, Sausalito, California, 1991.

[43] Forster Th., *10th Spiers Memorial Lecture*, 7.

[44] Forster Th., *Ann. Physik*, **1948**, 2, 55.

[45] Dexter D. L., *J. Chem. Phys.*, **1953**, 21, 836.

Chapter 2

Structural and Luminescence Studies of Lanthanide Containing Reverse Micelle Systems

Chapter 2

Structural and Luminescence Studies of Lanthanide Containing Reverse Micelle Systems

This chapter describes the preparation and characterisation of lanthanide containing surfactant salts of the type Ln(AOT)3 (Ln = Tb, Nd, Eu, AOT = bis-(2-ethylhexyl) sulfosuccinate). Small angle neutron scattering experiments have been used to determine the size and shape of reverse micelles formed by these surfactants in water/cyclohexane microemulsions. The luminescence lifetimes of the lanthanide ions have been used to investigate the solvation environment within reverse micelle systems as a function of water content.

2.1 Introduction

2.1.1 Surfactants, Micelles and Reverse Micelles

Surfactants, or surface active agents, are amphiphilic molecules, that is, they possess both a hydrophobic and hydrophilic part.

Cationic Surfactants	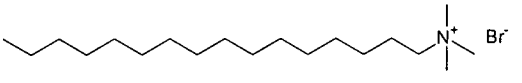 Cetyltrimethylammonium bromide 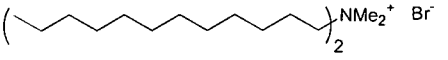 Didodecyldimethylammonium bromide
Anionic Surfactants	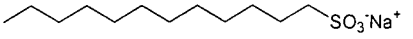 Sodium dodecylsulfate 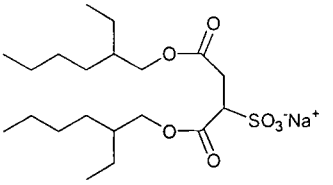 Aerosol OT
Non-ionic Surfactants	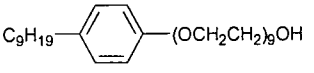 Nonoxynol-9

Table 2.1 Examples of common surfactants

The hydrophilic head group is usually ionic or polar and the hydrophilic part is usually made up of a straight or branched hydrocarbon tail or tails. Examples of anionic, cationic and non-ionic surfactants are shown in Table 2.1.

Surfactants are ambiphilic molecules that are active at the interface between two phases, for example, the interface between aqueous and hydrocarbon phases. In polar and non-polar solvents surfactant molecules can group together to form clusters of molecules see Table 2.2. In aqueous systems these are called normal micelles, in which the hydrophobic tails aggregate together with the polar head groups on the outside of the cluster. Micelle formation minimises the unfavourable interactions between the hydrophobic tail and the water molecules of the bulk phase, namely the disturbance of the strong hydrogen bonding in the bulk water by the long hydrocarbon tails. The unfavourable electrostatic interactions between the polar head groups are reduced by the incorporation of any counterions between them. In a non-polar solvent, such as a hydrocarbon, the reverse happens; the polar head groups cluster together with the hydrocarbon tails extending out into the bulk medium. These aggregates are known as reverse micelles.

Micelle and reverse micelle formation is determined by a number of factors. The shape of the surfactant molecule is important as this governs how well the molecule will pack around the central core of the normal or reverse micelle. For normal micelles a cone shape is required with a large hydrophilic head attached to a thinner hydrophobic tail. The opposite is required for reverse micelle formation where a truncated cone shape is needed with the hydrophobic tail or tails being wider than the hydrophilic head group[1]. This is shown diagrammatically in Table 2.2.

Surfactant shape	Cone	Truncated Cone
Surfactant + oil + water	oil water Micelle	water oil Reverse Micelle

● = polar head group ∿∿∿ = non-polar tail

Table 2.2 Structure of normal and reverse micelles

Formation of micelles and reverse micelles only takes place above a certain concentration of surfactant, which is known as the critical micellar concentration (cmc). This is the concentration above which the loss in entropy for the surfactant molecule on formation of an ordered micelle is compensated for by the gain in free energy of micelle formation. Formation of micelles is also temperature dependent with micelles only forming above the Kraft temperature.

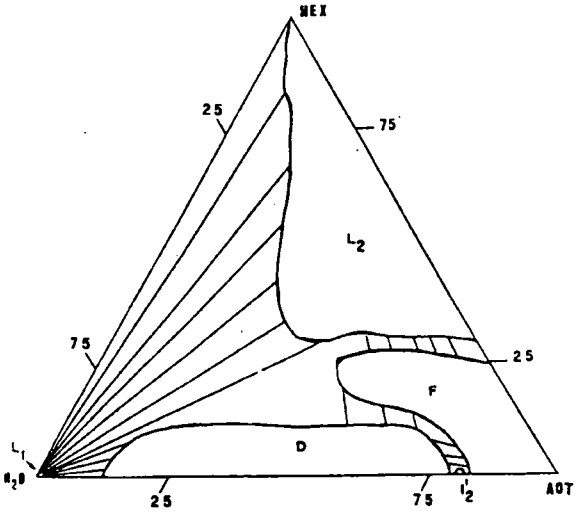

Figure 2.1 The phase diagram of a water-hexane-AOT system[2]

Figure 2.1 shows the phase diagram for a ternary system of Aerosol OT in water-hexane as determined by La Mesa *et al.*[2] The diagram shows the phase properties of the system

as the weight fraction of each component is varied. There is a small micellar region, L_1, indicating that Aerosol OT is only capable of dissolving small amounts of oil in water. The region of interest in this work is the reverse micellar region labelled L_2. Other regions shown include a lamellar phase, D, a viscous isotrophic phase I_2' and a reverse hexagonal phase, F.

2.1.2 Reverse Micelles

Surfactant molecules can form reverse micelles in non-polar solvents and any water present in these systems is solubilised in the polar cores of the reverse micelles. In cases where the surfactant-oil system contains no added water there is no well defined critical micellar concentration and the micelles are small and polydisperse; close packing of the polar head groups leads to a cavity which is filled with water of hydration. The addition of water swells the micellar core leading to larger well- defined micelles which may also be referred to as a microemulsion system. In the case of ionic surfactants, any counterions are contained within the micellar core.

The amount of water contained within a reverse micellar system is given by the water-surfactant molar ratio, *w*.

$$w = \frac{[\text{added water}]}{[\text{surfactant}]} \qquad \textbf{2.1}$$

The higher the water loading, *w*, of the reverse micellar system, the larger the micelle becomes, with the radius increasing linearly with *w*. The water within the micellar core becomes increasingly bulk-like as the core expands. FTIR measurements indicate this occurs at a *w* of approximately 6.[3] Efficient sensitised luminescence from lanthanides in reverse micelles has been observed using co-surfactants with organic chromophores. The efficiency of this process suggests that the sensitiser, naphth-2-yl acetic acid, remains associated with the lanthanide ion, that is, the lanthanide ions are located close to the ionic head groups of the surfactant molecules.[7]

The structures of reverse micelles formed by Aerosol OT have been investigated with various counterions using small angle neutron scattering[4]. It was found that at $w = 5$, the Aerosol OT salts of Na^+, K^+, Rb^+, Cs^+ and Ca^{2+} formed small spherical particles,

whilst the salts of Co^{2+}, Ni^{2+}, Cu^{2+} and Zn^{2+} formed cylindrical rods. This effect has been attributed to the size of the hydrated cations. The smaller counterions such as sodium can approach the SO_3^- headgroup more effectively than a larger counterion such as nickel. In the restricted water environment of the reverse micelle the larger cations will be less effective at screening the repulsive $SO_3^- \leftrightarrow SO_3^-$ interactions than the smaller ions. This causes a change in shape from a sphere to a cylinder on increasing the hydrated counterion radius because the packing in a cylindrical system is more planar than that for spherical systems.

2.1.3 Small Angle Neutron Scattering (SANS)

There are a number of methods available for structural characterisation of reverse micelle systems[5]. Use of electron microscopy or an ultracentrifuge can determine particle sizes down to about 5 nm. These techniques are often non-ideal as they involve perturbation of the sample. Dynamic light scattering from reverse micelle samples does not perturb the sample, but this technique can be unsuitable if the sample is opaque, the particle and solvent have similar refractive indices (no scattering), the particle size is less than $\lambda/100$ (5 nm for 500 nm light) or if one is interested in internal details of the particles. Small angle neutron or X-ray scattering methods are non-perturbative methods that are used to determine fine detail in reverse micelle systems. Neutron scattering is a major advantage over X-ray scattering due to the extra contrast available from isotopic H/D substitutions within the systems.

2.1.4 Neutron Contrast Variation

The strength of the signal in a scattering experiment depends on the interaction between the incident radiation and the sample. This can be quantified using a parameter called the scattering length density, ρ, which is the scattering length per unit volume. X-rays interact with electrons in the sample and ρ therefore scales with atomic number. This means that for systems such as the ones studied here which contain mainly C, H and O, ρ is virtually the same across the sample, and sample contrast is low.

Neutrons interact with the nuclei in the sample and therefore ρ is isotope dependent. Compounds and their deuteriated analogues have widely differing values of ρ, as shown

in Table 2.3. This increases the contrast between the different parts of a multi-component system relative to the contrast obtained for X-ray scattering.

Substance		$\rho / 10^{10}$ cm^{-2}
Water	H_2O	-0.56
	D_2O	+6.40
Hydrocarbon	C_8H_{18}	-0.53
	C_8D_{18}	+6.43
Surfactant	$C_{12}H_{25}OSO_3^-Na^+$	+0.387
	$C_{12}D_{25}OSO_3^-Na^+$	+6.704

Table 2.3 Selected values of the coherent scattering length density ρ at 25°C (Ref. 5)

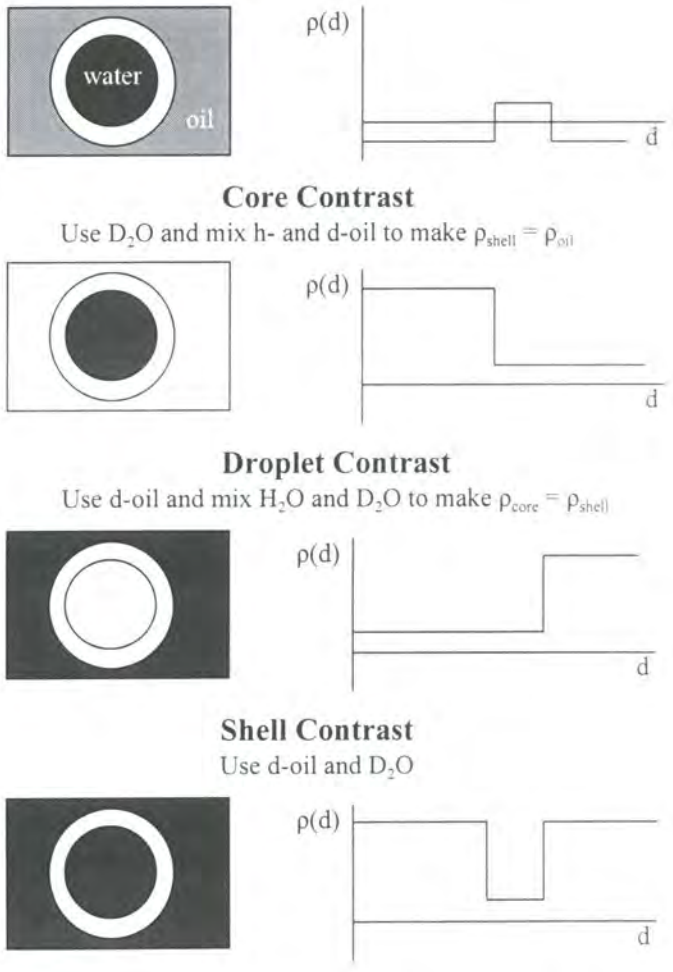

Figure 2.2 The use of contrast variation in SANS to elucidate the structure of water in oil microemulsion droplets. (Ref 5)

Figure 2.2 shows schematically how contrast enhancement is achieved. The scattering length density varies as a function of *d*, the distance from the centre of the droplet. The first part of the figure shows the situation before any deuteriation is introduced into the system, scattering can come from both the core and the shell of the droplet. By using a mixture of d-oil and h-oil to obtain a scattering density matched to that of the surfactant and using D_2O in the core the contrast on the droplet core can be increased. Similarly by using a mixture of H_2O and D_2O to obtain a scattering density matched to the surfactant and using fully deuteriated oil contrast can be increased between the droplet and the oil allowing the overall droplet size to be determined. Finally by making $\rho_{core} = \rho_{oil}$ the shell can be studied on its own.

2.2 Experimental

2.2.1 SANS

The SANS results presented in this thesis were obtained on the LOQ time-of-flight small-angle diffractometer at ISIS at the Rutherford Appleton Laboratories in Oxfordshire. In the ISIS spallation neutron source neutrons are produced by firing a pulsed beam of fast protons at a heavy metal target, such as uranium, tantalum or tungsten. Impact results in nuclear spallation as neutrons 'boil off' producing a pulsed (50 Hz) source of neutrons. A chopper in the beam path reduces the frequency to 25 Hz, thus eliminating the possibility of fast neutrons from a following pulse overlapping with slow neutrons from the first one. Collimation of the beam occurs prior to it being passed through the sample, held in a 2 mm pathlength quartz cell. Prior to entering the sample the incident beam flux and pulse structure was determined by a scintillator/photomultiplier tube. Scattered neutrons were detected by a ^3He-CF_4-filled detector positioned 4.5 m from the sample. The ionisation detector is both position and time sensitive with an active area of 64 x 64 cm^2. Simple geometry was used to work out the angle of scatter whilst the wavelength was determined by time-of-flight methods. Averaging of the signal over many pulses, typically 10^4, followed by fitting to mathematical models allowed determination of the parameters of interest associated with the scattering solution such as particle size and shape. The data interpretation for the systems studied in this thesis was carried out by Dr. Julian Eastoe of Bristol University and Richard Heenan of the Rutherford Appleton Laboratories.

2.2.2 Preparation of the Reverse Micelle Systems

Europium and terbium salts of AOT have been prepared previously[6,7,8] and their luminescence behaviour investigated. Preparation from NaAOT involved an ion exchange process. Analysis of the salts by fast atom bombardment mass spectroscopy (FAB-MS) gave peaks at m/z of 995, 986 and 1002 for the Eu, Nd and Tb salts respectively, corresponding to $Eu(AOT)_2^+$, $Nd(AOT)_2^+$ and $Tb(AOT)_2^+$. Elemental analysis (C and H) were consistent with the required compounds. Sodium content was determined by elemental analysis and was between 0.10 and 0.35% indicating that greater than 95% ion exchange had occurred.

The reverse micelle systems were prepared by adding aliquots of H_2O or D_2O to a cyclohexane solution of the lanthanide salt of AOT, [AOT] = 0.1 mol dm^{-3}, followed by sonication to give a clear solution. Reverse micelle systems for study by SANS were prepared using H_2O, h-AOT and C_6D_{12}. This mixture provides droplet contrast, that is, the contrast is between the micelle and the C_6D_{12} as illustrated in Figure 2.2.

2.3 Results

2.3.1 Small-Angle Neutron Scattering

The SANS experiment gives information about the angle through which neutrons have been scattered, and through time of flight measurements, it measures the momentum of these neutrons. Data from SANS experiments are expressed by the intensity of neutron scatter as a function of the scattering vector, Q. The term Q refers to the difference between the incident and scattered wave vectors and takes into account both the momentum and angle of scatter for the neutrons, equation 2.2.

$$Q = \frac{4\pi}{\lambda}\sin\left(\frac{\theta}{2}\right) \qquad \textbf{2.2}$$

The intensity data $I(Q)$ was described by equation 2.3. The form factor, $P(Q,R_i)$, describes the three-dimensional shape of the scattering particles. The data was fitted to various form factors. The data for the europium, terbium, neodymium and ytterbium

containing reverse micelle systems fitted best to a spherical model rather than ellipsoids, cylinders or disks for values of w greater than 1.

$$I(Q) = n\,(\rho_{mic} - \rho_{C6D12})^2\,[\Sigma_I\, V_i^2\, P(Q,R_i)\, X(R_i)] \qquad \textbf{2.3}$$

$I(Q)$	normalised SANS intensity
n	micelles unit volume
ρ_{mic}, ρ_{C6D12}	coherent scattering length densities for micelles and C_6D_{12}
V_i	micelle volume
R_i	micelle radius
$P(Q,R_i)$	form factor
$X(R_i)$	polydispersity

The polydispersity, $X(R_i)$, is a measure of the distribution of particle sizes in the system. In this work a Schultz distribution was used, which defines an average micelle radius, R_{av}, and a root mean square deviation, σ. During the modelling σ/R_{av} was fixed at 0.20; however in the range σ/R_{av} = 0.15 to 0.25 the values of R_{av} changed only by ±2 %. A consistency check on the data was performed by fitting the scale factor, S, equation 2.4. This factor was allowed to change during the fitting and compared to the known values for the sample composition.

$$S = n\, V_i\, (\rho_{mic} - \rho_{C6D12})^2 \qquad \textbf{2.4}$$

As the scale factor, polydispersity and form factors were all constrained, the only unknown parameter to be fitted was the mean micelle radius, R_{av}. Figure 2.3 shows typical experimental data and fitted curves for reversed micelles of $Eu(AOT)_3$ at three w values.

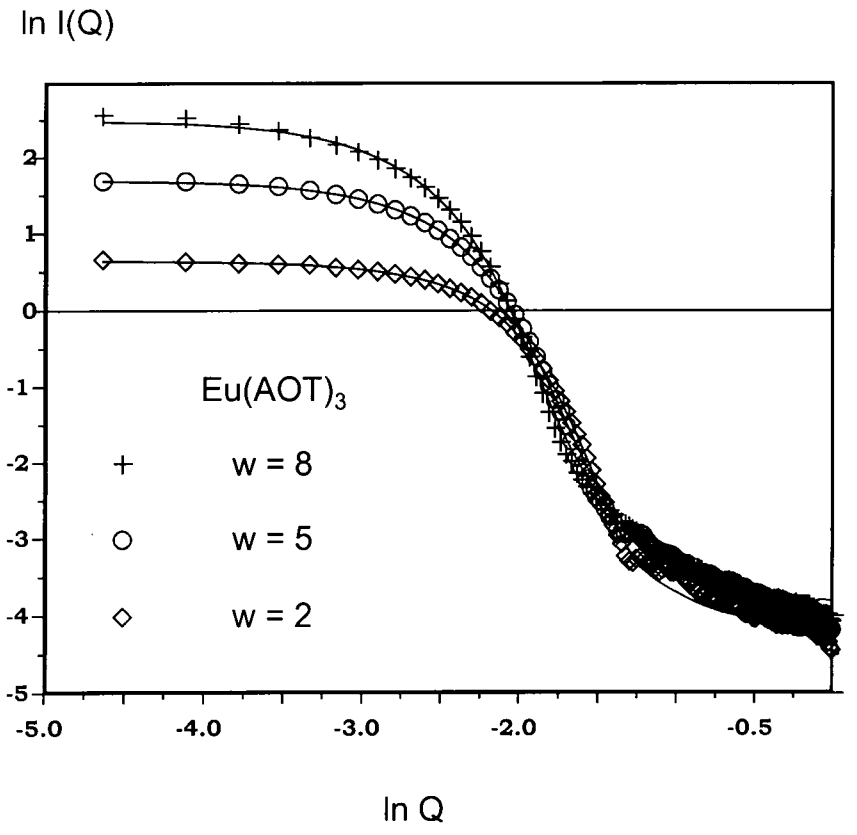

Figure 2.3 SANS data and model fits for $Eu(AOT)_3$ reversed micelles using H_2O-*h*-AOT-C_6D_{12}

	R_{av} / Å	
w	$Eu(AOT)_3$	$Nd(AOT)_3$
0.0		11.7
2.0	13.7	13.4
5.0	14.9	17.6
8.0	18.5	

Table 2.4 Experimentally determined radii of europium and neodymium AOT reverse micelles

Table 2.4 shows the fitted mean radii for the systems studied. For neodymium it can be seen that the radius is linear with respect to water loading, *w*, fitting to equation 2.5.

$$R_{av} \approx 11.5 + 1.2\,w \qquad \textbf{2.5}$$

2.3.2 Effect of Sodium

SANS experiments using mixed terbium and sodium AOT salts also showed the formation of spherical reversed micelles.

Sodium-terbium mixtures in the ratio 0 to 4 and w values of 0, 4 and 8 gave similar luminescent spectra and lifetimes. These results suggest that self-quenching of the lanthanide ions is negligible and that there is minimal interference from any residual sodium in the samples.

2.3.3 Luminescence Results

The variation of k_{obs} with w for reverse micelle systems containing Eu, Tb and Nd is shown in Figures 2.4 – 2.6.

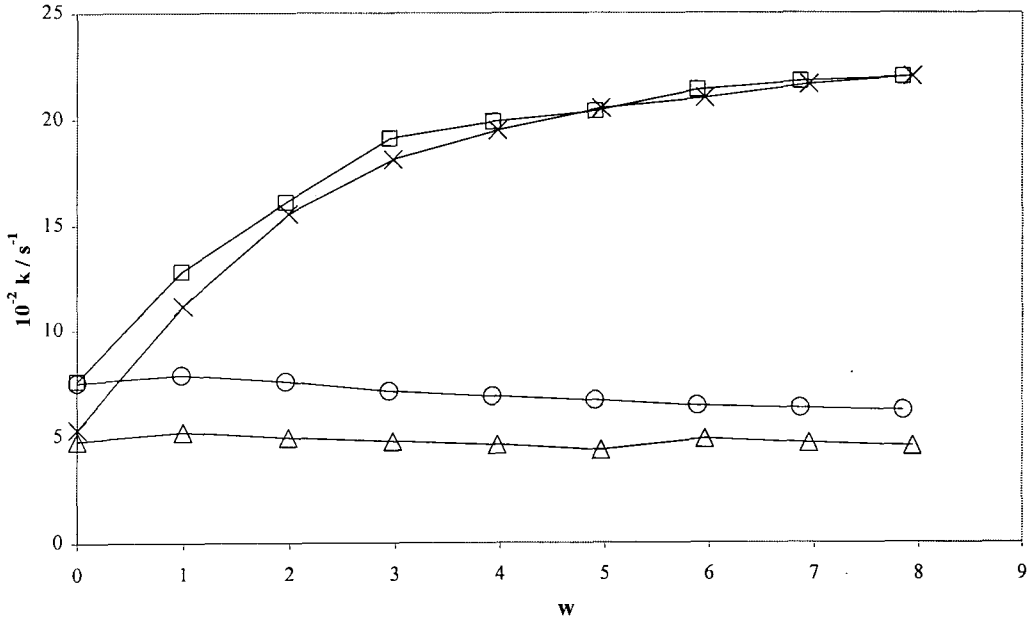

Figure 2.4 Variation in k_{obs} with w for $Tb(AOT)_3$ in cyclohexane.

□ = H_2O added (residual H_2O), x = H_2O added (residual D_2O),

○ = D_2O added (residual H_2O), Δ = D_2O added (residual D_2O).

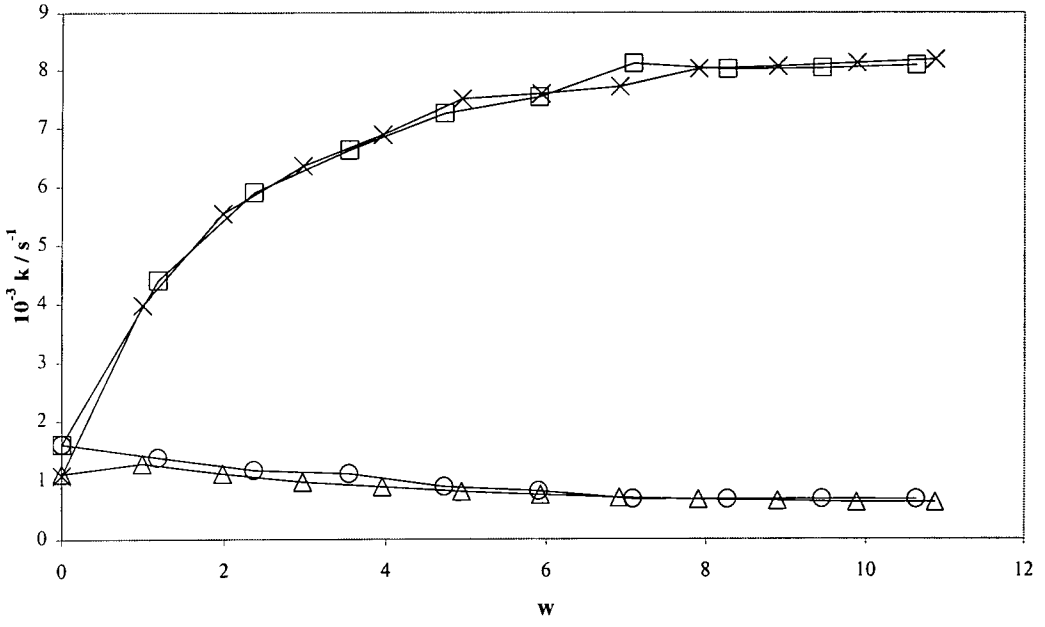

Figure 2.5 Variation in k_{obs} with w for $Eu(AOT)_3$ in cyclohexane.

□ = H_2O added (residual H_2O), x = H_2O added (residual D_2O),

○ = D_2O added (residual H_2O), Δ = D_2O added (residual D_2O).

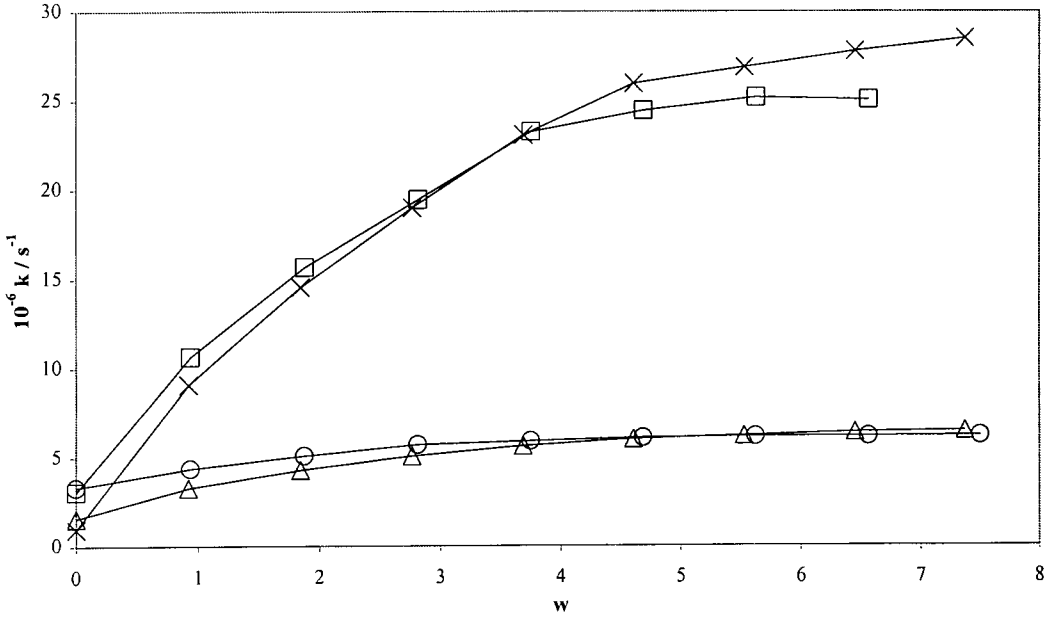

Figure 2.6 Variation in k_{obs} with w for $Nd(AOT)_3$ in cyclohexane.

□ = H_2O added (residual H_2O), x = H_2O added (residual D_2O),

○ = D_2O added (residual H_2O), Δ = D_2O added (residual D_2O).

A small, but significant, difference in k_{obs} was noticed at $w = 0$ depending on the method of sample preparation. Samples prepared using H_2O, as opposed to D_2O, had a higher value of k_{obs} at $w = 0$. This is attributed to the residual water of hydration of the lanthanide AOT salts, that is, water that cannot be removed by desiccation. Using this difference in k_{obs} for the systems prepared using H_2O and D_2O it can be estimated that there are 0.3 ± 0.1 water molecules per AOT, or one per metal ion.

As can be seen in Figures 2.4 – 2.6 addition of H_2O to the micelles causes a steady increase in k_{obs} until at high w it approaches that observed for the lanthanide aqua ion: $k_{obs} = 2.3 \times 10^3$, 8.3×10^3, 3.3×10^7 s^{-1} for Tb^{3+}, Eu^{3+} and Nd^{3+} respectively. Addition of D_2O to the solutions of Tb and Eu micelles brings about a decrease in k_{obs}while for $Nd(AOT)_3$, k_{obs} increases with D_2O concentration. In both cases the tendency at high w is toward the value for the lanthanide in D_2O solution where $k_{obs} = 2.9 \times 10^2$, 2.8×10^2 and 6.7×10^6 s^{-1} for Tb^{3+}, Eu^{3+} and Nd^{3+} respectively.

As discussed earlier lanthanide ions are very sensitive to the vibrational modes of their local ligands (chapter 1). When the energy gaps of local vibrational oscillators and/or their overtones match the electronic energy gaps of the excited ion, an energy transfer process can occur, resulting in deactivation of the luminescent state. Hydroxyl groups are particularly efficient at this, although other high frequency oscillators such as C-H and N-H are also effective.[9,10]

At low w values the water pool is expected to be strongly coordinated to the sulfonate headgroups of the surfactant molecules and solvation of the lanthanide ion will be limited.[11] Furthermore, in this restricted water environment it may be energetically favourable for the lanthanide ion to co-ordinate to the surfactant, either via the sulfonate, the two ester linkages, or as a combination of both. As w is increased, more water becomes available to satisfy the high charge density demand of the lanthanide ion and preferential solvation by water over these less strongly co-ordinating groups must occur. Evidence for this comes from the observed changes in luminescence lifetime with w (Figures 2.4 – 2.6). This hypothesis is supported by IR and Raman studies of

NaAOT in cyclohexane carried out by Moran *et al.* who observed shifts in the C=O stretching and the symmetric SO_3^- bands. [12,13]

First consider Nd^{3+}: when $w = 0$ the major contributors to the deactivation of the metal ion must arise from the C-H oscillators of the AOT^- to which the Nd^{3+} is bound and the residual H_2O/D_2O in the reverse micelles. As the H_2O and/or D_2O content of the micelle increases so does the degree of metal ion hydration, and its luminescence behaviour more closely resembles that observed in bulk solvent. Interestingly, the luminescence lifetime of the Nd^{3+} bound to the AOT^- is longer than that of the Nd^{3+} in bulk D_2O, suggesting that the C-H oscillators are less effective at deactivating the excited state of the Nd^{3+} than O-D groups. This is not surprising given that the overlap between higher harmonics of the C-H stretching bands and the Nd^{3+} energy levels is poor as opposed to the relatively good overlap with the second, third and forth overtones of the O-D stretch in D_2O. It should also be pointed out that the oscillator strength of the O-D band is much larger than that of the C-H.

As the lanthanides are chemically similar, Eu^{3+} and Tb^{3+} would be expected to follow a similar trend. However, addition of D_2O to reverse micelles containing europium and terbium causes an increase in the observed luminescence lifetimes. Here the deactivation of the metal ion by C-H oscillators is greater than that by O-D, although in absolute terms the deactivation processes in Eu^{3+} and Tb^{3+} are far less effective than those for Nd^{3+}. This is due to the fact that the excited states of Eu^{3+} and Tb^{3+} are isoenergetic with much higher vibrational levels of both X-H and X-D ($v \geq 5$), compared to Nd ($v = 2, 3$), and hence the Franck-Condon overlap is much smaller.

Mwalupindi *et al.* suggest that the lanthanide ion will be coordinated to the sulfonate head group within the reverse micelle and, hence, not be evenly distributed in the water pool.[14] This was deduced because the most effective energy transfer was obtained for analytes that adsorb at the oil/water interface, i.e., close to the AOT headgroups. The possibility of complexation of the lanthanide by the analyte at this interface was not considered. Although sulfonate is not widely recognised as a ligating species for lanthanide ions, coordination may occur due to the relatively high concentration of $-SO_3^-$ coupled with the restricted steric environment. Coordination to the sulfonate group will

allows less hydration around the metal, limiting the solvation of the ion compared to bulk water. This should also promote spherical micelle formation, which is observed, rather than cylinders.

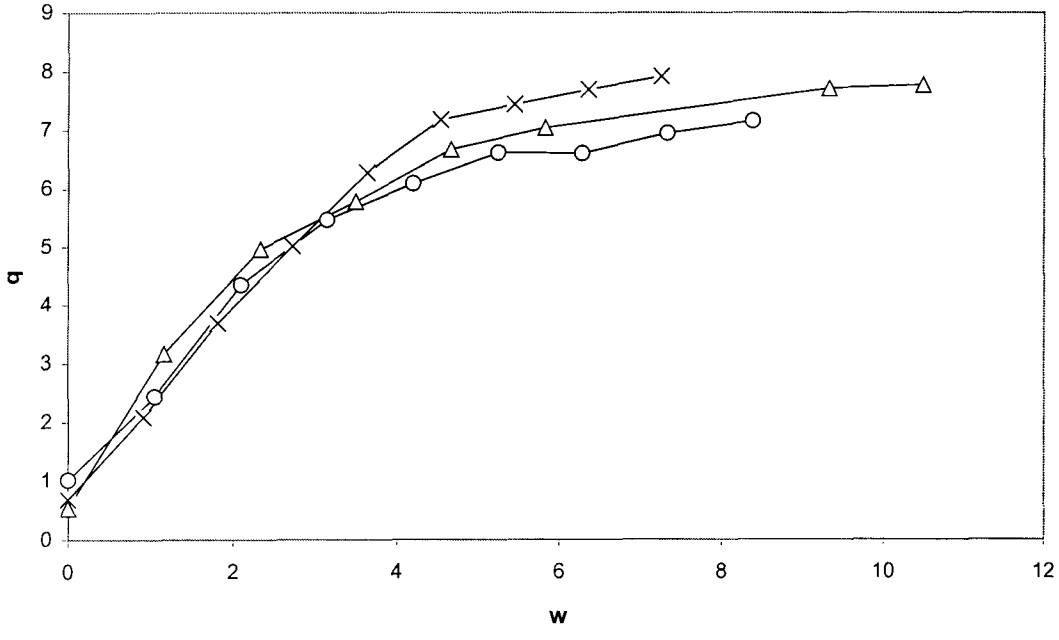

Figure 2.7 Variation in the apparent mean hydration number, q, with w.
o = $Tb(AOT)_3$, Δ = $Eu(AOT)_3$, x = $Nd(AOT)_3$.

Using the method of Horrocks and Sudnick, it is possible to calculate the apparent solvation of the ion q, and plots of q verses w are shown in Figure 2.7. As can be seen from these data all three lanthanides show very similar behaviour, and at $w = 0$, q is between 0.5 and 1. As w increases so too does q, reaching a maximum value of *ca.* 8. This must be compared to the value of 9 observed for the $Ln(aq)^{3+}$ ion in bulk water, providing further evidence that the ions are still partially complexing with the sulfonate groups at the upper limit of w imposed by this surfactant/hydrocarbon system. Further evidence for the water in these systems not being truly bulk like is has been provided recently by Fitzgerald[15]. The hypersensitive, $^5D_0 \rightarrow {}^7F_2$, transition in europium was studied. This transition is sensitive to the symmetry around the emitting ion. It was found that as the size of the water pool was increased the ratio of intensity of the hypersensitive $^5D_0 \rightarrow {}^7F_2$ peak (615 nm) to the intensity of the $^5D_0 \rightarrow {}^7F_1$ peak (590 nm) decreased from $\approx$ 2 at w = 0 to $\approx$ 0.7 for w =10. However this does not reach the value

observed in aqueous solution of $\approx$ 0.5 thereby confirming that the water within the reverse micelle approaches but does not become truly bulk like.

2.4 Conclusions

It has been shown that the lanthanide AOT salts and lanthanide sodium mixtures form spherical reverse micelles in cyclohexane solution. The photophysical properties indicate that with no added water the solvation of the lanthanide ion is restricted, resulting in reduced de-activation of the excited states by non-radiative processes, in particular those mediated by water. Addition of more water results in progressive hydration of the lanthanide ion shown by smooth changes in the luminescence lifetimes. These experiments demonstrate that these systems with a controlled water environment provide a facile means of modifying the photophysical properties of the lanthanides.

2.5 References for Chapter 2

[1] Langevin D., in *Structure and Reactivity in Reverse Micelles*, ed. Pileni M. P., Elsevier, 1989.

[2] La Mesa C., Coppola L., Ranieri G. A., Terenzi M., Chidichimo G., *Langmuir*, **1992**, 8, 2616.

[3] Moran P. D., Bowmaker G., Cooney R. P., Bartlet J. R., Woolfrey J. L., *Langmuir*, **1995**, 11, 738.

[4] Eastoe J., Robinson B. H., Towey T. F., Heenan R. K., *J. Phys. Chem.*, **1993**, 97, 1459.

[5] *Small-angle Neutron Scattering and Neutron Reflection*, Eastoe J., in Chapter 12 in *New Physico-Chemical Techniques for the Characterisation of Complex Food Systems*. ed. E.Dickinson, Blackie, Glasgow 1995

[6] Mwalupindi A. G., Blyshak L. A., Ndou T. T., Warner I. M., *Anal. Chem.*, **1991**, 63, 1328.

[7] Mwalupindi A. G., Ndou T. T., Warner I. M., *Anal. Chem.*, **1992**, 64, 1840.

[8] Mwalupindi A. G., Agbaria R. A., Warner I. M., *Applied Spectroscopy*, **1994**, 48, 1132.

[9] Parker D., Dickins R. S., DeSousa A. S., Williams J. A. G., *J. Chem. Soc., Chem. Commun.*, **1996**, 697.

[10] Beeby A., Clarkson I. M., Dickins R. S., Faulkner S., Parker D., Royle L., deSousa A. S., Williams J. A. G., Woods M., *J. Chem. Soc., Perkin Trans. 2*, **1999**, 493.

[11] Moran P. D., Bowmaker G., Cooney R. P., Bartlett J. R., Woolfrey J. L., *Langmuir*, **1995**, 11, 738.

[12] Moran P. D., Bowmaker G., Cooney R. P., Bartlett J. R., Woolfrey J. L., *Langmuir*, **1995**, 11, 738.

[13] Moran P. D., Bowmaker G., Cooney R. P., Bartlett J. R., Woolfrey J. L., *J. Mater. Chem.*, **1995**, 5, 295.

[14] Mwalupindi A. G., Ndou T. T., Warner I. M., *Anal. Chem.*, **1992**, 64, 1840.

[15] 'Investigation into the development of near infra-red liquid phase laser gain media', Simon Fitzgerald, Final year undergraduate report, University of Durham, May 1999.

Chapter 3

Time resolved luminescence microscopy and lifetime mapping using lanthanide complexes

Chapter 3

Time resolved luminescence microscopy and lifetime mapping using lanthanide complexes

This chapter describes the use of lanthanide complexes based on 1,4,7,10-tetraazadodecane bearing phenanthridine antennae in luminescence microscopy. Time resolved measurements have allowed time gating of the sample from a fluorescent background and lifetime mapping of the images.

3.1 Fluorescent microscopy

Fluorescence microscopy is a well-recognised technique for research in chemistry[1], cell physiology and cell biology[2,3,4]. Fluorescence imaging has been used to provide information as to the localisation of proteins and macromolecules during cellular processes and to image intracellular concentrations of ions such as Ca^{2+} or Cl^{-} [2]. Phillips *et al.*[5,6] have used fluorescence microscopy to study the localisation of agents such as zinc and aluminium phthalocyanines used as photosensitizers in photodynamic therapy. Chemical problems such as the photodegredation of naturally occurring polymers, dyeing of fibres of the measurement of glass transition temperature values[1] have also been studied using this technique.

One of the main problems with fluorescence microscopy for studying biological systems is interference with the signal from sample autofluorescence, and Raleigh and Raman scattering. Autofluorescence arises from short-lived emission (ns) from the sample due to the presence of biological chromophores such as ATP, flavanoids, pyrimidines and NAD/NADH.

Time-resolved measurements offer a solution to the problems of autofluorescence. If the luminescent reporter group has a lifetime significantly longer than the biological autofluorescence, the signal from the reporter can be monitored after the autofluorescence has decayed to zero. The ideal situation is to have a luminescent reporter group with a lifetime several orders of magnitude longer than the autofluorescence. Detection of the delayed emission leads to an increase in the

signal to noise ratio of the probe, thereby increasing image contrast and/or lowering the detection limit of the probe. Typically the lifetime of autofluorescence is < 10 ns, meaning that reporter groups should ideally have lifetimes of < 1 ms. Also if the reporter group emits light at a very different wavelength to the excitation then, by monitoring the signal well away from the excitation wavelength, scatter can be reduced. However time-resolved luminescence measurements are rarely made in cell biology because phosphorescent probes, such as the commonly used eosin, have a much lower quantum efficiency than the fluorescent probes. As these probes rely on delayed emission from the triplet state, and the triplet state of an organic molecule is effectively quenched by molecular oxygen, they must be used in oxygen free buffers, a condition incompatible with most studies on living cells. Time-resolved measurements and probes with large Stokes' shifts also solve the problem of Rayleigh and Raman scattering from samples, as both of these processes are instantaneous after excitation of the sample and are therefore easily time-gated out as for auto-fluorescence.

3.2 Lanthanide Complexes

Sensitized luminescence from lanthanide complexes is ideal for such measurements as they offer long lived luminescence and a large Stokes' shift of greater than 200 nm. In many cases they have good quantum efficiencies, a range of hydrophobicities/hydrophilicities, thermodynamic stability and low toxicity. The luminescence is also independent of sample aeration, solving the problem of quenching by molecular oxygen.

A wide variety of lanthanide complexes with long luminescent lifetimes have been synthesised in recent years following the recognition of their potential for use in bioassays and luminescence imaging. The use of time resolved assays, such as those marketed under the DELFIA™ (dissociation enhanced lanthanide fluoroimmunoassay), is well established[7,8]. These fluoroimmunoassays offer an effective alternative to the more widely used radioimmunoassays but offer a significant advantage in terms of increased safety and availability of reagents.

These features of lanthanide complexes have been exploited by a number of groups for time-resolved imaging purposes. Seveus *et al.*[9] used the luminescent europium chelate **4** conjugated to antisera and streptavidin to study the localisation of the antigen C242, associated with tumours, in the malignant mucosa of the human colon. They also studied the localisation of type II collagen mRNA in developing human cartilaginary growth plates and the detection of HPV type specific gene sequences in the squamous epithelium of the human cervix. They only use this system to monitor the signal after the short-lived fluorescence has occurred, thereby demonstrating the use of these complexes and time-gating to eliminate autofluorescence. Unfortunately the chelate was found to be unstable under the conditions of excitation used.

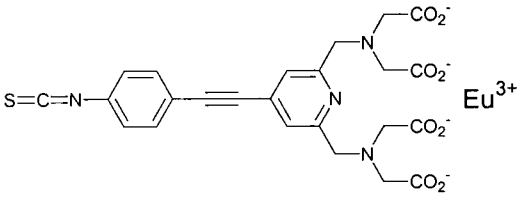

4

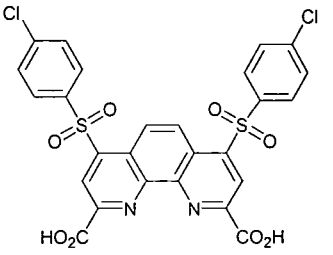

5

Marriott *et al.*[10] have used a used a streptavidin based macromolecular complex incorporating the europium complex of **5** to image living amoeba cells, the complex can be readily excited at 340 nm with sensitised emission being monitored at 612 nm. It was also shown that the system is more stable to ultraviolet excitation that the previous system of Serveus. The cells were also stained with the fluorescent dye lucifer yellow, contained in pinocytosed vesicles. Time-resolved measurements were used to effectively reject the strong fluorescence from the lucifer yellow. Measurements of the lifetime of the emission were also made for the probe within the cell including histogram plots of the range of lifetimes obtained.

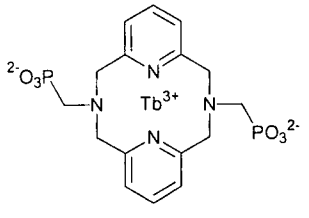

6

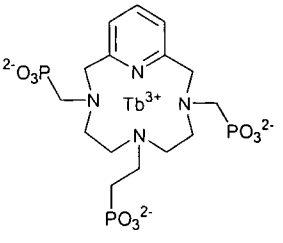

7

Hubbard *et al*[11]. describe the construction of a high resolution, fluorescence imaging endoscope and its use to image rat femur samples *in vitro* stained with the terbium complexes **6** and **7**. These complexes are known to accumulate in the bone tissue. These complexes were excited at 270 nm and the signal monitored at 550 nm by use of an interference filter. Reduction of any autofluorescence or scatter is purely from use of the large Stokes' shift, and time-resolved measurements were not taken. However through use of calibration measurements they are able to quantify the amount of complex present from the intensity information.

In further work[12] **7** is found to show a significant affinity for adenocarcinoma cells verses normal epithelial cells in Sprague Dawley rat large intestines. A millimolar solution of the complex was introduced by topical application, or lavage introduction, under endoscopy. Subsequent fluorescence detection and standard histological examination showed enhanced uptake by the adenocarcinoma cells. Improvements in signal/noise were only due to the large Stokes' shift (280 nm) and no investigations of lifetime or temporally resolved measurements were made. As in the previous work the strength of the luminescence signal was used to provide a semiquantitative method for determining the amount of **7** present.

3.3 Experimental

3.3.1 Microscope set-up

A schematic of the luminescence microscope that was used in this work is illustrated in Figure 3.1. The sample was irradiated using the third harmonic, 355 nm, of a Q-switched Nd:YAG laser (Continuum Power Lite) operating at 10 Hz delivering < 1 mJ at the sample with a pulse duration of 6 ns. The laser light was delivered to the microscope stage of the inverted microscope (Olympus IMT-2) via a 25 m length of 0.5 mm silica fibre optic (Thor Laboratories Inc.). The luminescence from the sample was collected by the same objective, passed through the dichroic mirror and imaged onto the gated image intensifier (Kentech Instruments). This device provided gate periods of up to 200 μs and a luminous gain of up to 1000.

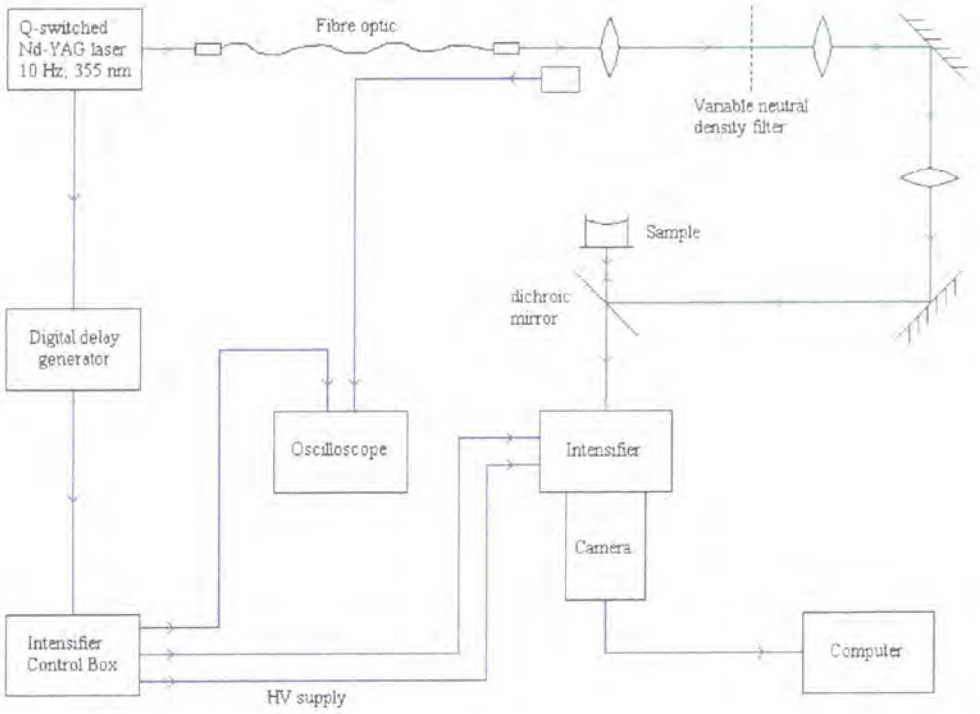

Figure 3.1 Schematic of the luminescence microscope

The intensifier was synchronised with the optical pulse using a digital delay generator (Stanford DG535). This intensified image was relayed to a CCD camera (Cohu 4910). This camera provides 8-bit resolution and is capable of on-chip integration for periods of tens of seconds at room temperature. The camera control and image acquisition was achieved using a frame grabber system (Oxford Framestore Applications). Each image was in the form of a string of unsigned byte integers, meaning that the intensity data for each pixel had a maximum value of 255 and a minimum value of 0.

Using this system the gate period could be varied in length and scanned across a wide range of delay times, including those which resulted in the intensifier being turned on before the arrival of the optical pulse at the sample. Fluorescence from the sample could be observed by selecting a negative delay time, ensuring that the laser pulse arrived during the intensifier gate period.

3.3.2 Image processing and lifetime mapping

Image manipulation and lifetime mapping was carried out using software written by the author in National Instruments LabView 5.0 (see appendix). Lifetime maps were obtained by acquiring images using a fixed gate period over a range of delay times. The program took each pixel in turn and determined its luminescence lifetime by fitting to a single exponential decay plus offset ($I(t) = A_0 + A_1e^{-kt}$) using a non-linear Levenberg-Marquardt iterative fitting technique. By obtaining a fit for each pixel, 3 images are constructed showing the lifetime, pre-exponential factor and the offset. In some cases image contrast was improved by 'filtering' the data. In essence the lifetime map viewing software searched through each data point, and if the pre-exponential factor was below a certain value, would set the same pixel in the lifetime map to black. This 'filtering' is justified as in these areas of the image there is no intensity from the particle and the program has fitted a lifetime based upon the background intensities, thus this value is not meaningful. The lifetime image was presented as a false colour image.

The scale of each image was obtained by taking an image of a graticule under the same microscope conditions.

3.3.3 Lanthanide Complexes used in Imaging Studies

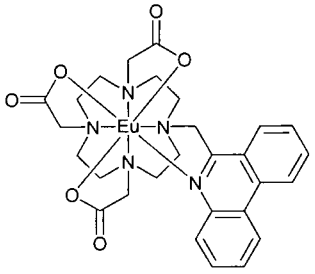

8

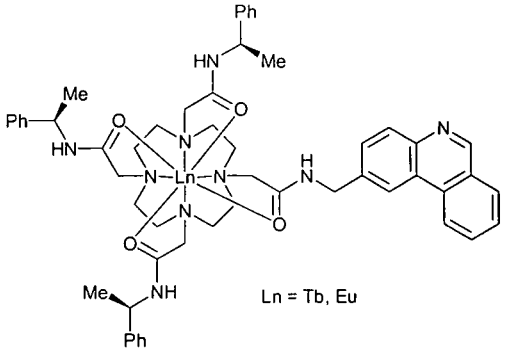

9 (Ln = Eu), 10 (Ln = Tb)

Three complexes were used based on the 1,4,7,10-tetraazacyclododecane macrocycle, each incorporating a phenanthridine substituted arm. The synthesis of the europium ligand, **8**, is described in chapter 6 along with some further photophysical detail. The europium and terbium complexes **9** and **10** were prepared

by Dr. Gareth Williams (University of Durham)[13]. The phenanthridine chromophore absorbs at 355 nm at physiological pH and is readily excited using the third harmonic of a Nd:YAG laser. Furthermore the use of 355 nm light allows conventional glass microscope optics to be used without significant losses due to absorbance by glass or fluorescence from the optics. The use of shorter wavelength radiation would require the use of reflective or rather expensive quartz optics.

3.4 Results

3.4.1 Silica Particles

The various complexes used adsorb readily onto the surface of small silica particles (30 – 60 μm). These particles provide an ideal substrate for initial experiments as they are easily prepared and visualised on the microscope. A number of particles were placed on a microscope slide and focussed images observed using transmission microscopy. Luminescence images were then obtained at various delay times between the firing of the laser and the triggering of the intensifier, using a constant intensifier gate time. This allowed the generation of a lifetime map of the particles. The particles were washed with water, methanol and dichloromethane and this had no effect on the image intensity indicating that the complex was strongly adsorbed to the silica surface.

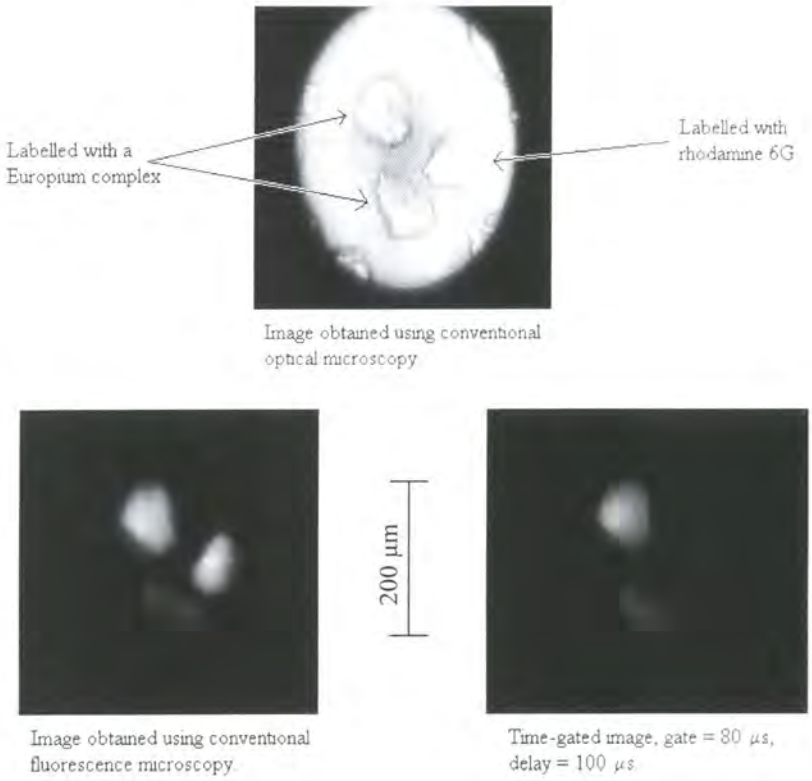

Figure 3.2 Silica particles labelled with **9** and rhodamine 6G showing the effect of variation of the delay time

To further demonstrate the effectiveness of time-gated measurements a more complex system was studied. A mixture of silica particles some labelled with the europium complex, **9**, and the rest labelled with Rhodamine 6G. Rhodamine 6G is a laser dye with a short luminescence lifetime ($\tau \approx 2.2$ ns), it absorbs and emits in the same spectral regions as the complex. Therefore it provides a model for the short-lived autofluorescence. Figure 3.2 shows three of these particles: the two on the left are labelled with the lanthanide complex, while the right hand particle is labelled with rhodamine 6G. The images obtained by transmission and fluorescence microscopy provide no discrimination between the three particles. However, when a delay time of 100 µs was applied to the image intensifier, the fluorescence of the

rhodamine labelled particle can no longer be seen, allowing the lanthanide particle to be distinguished.

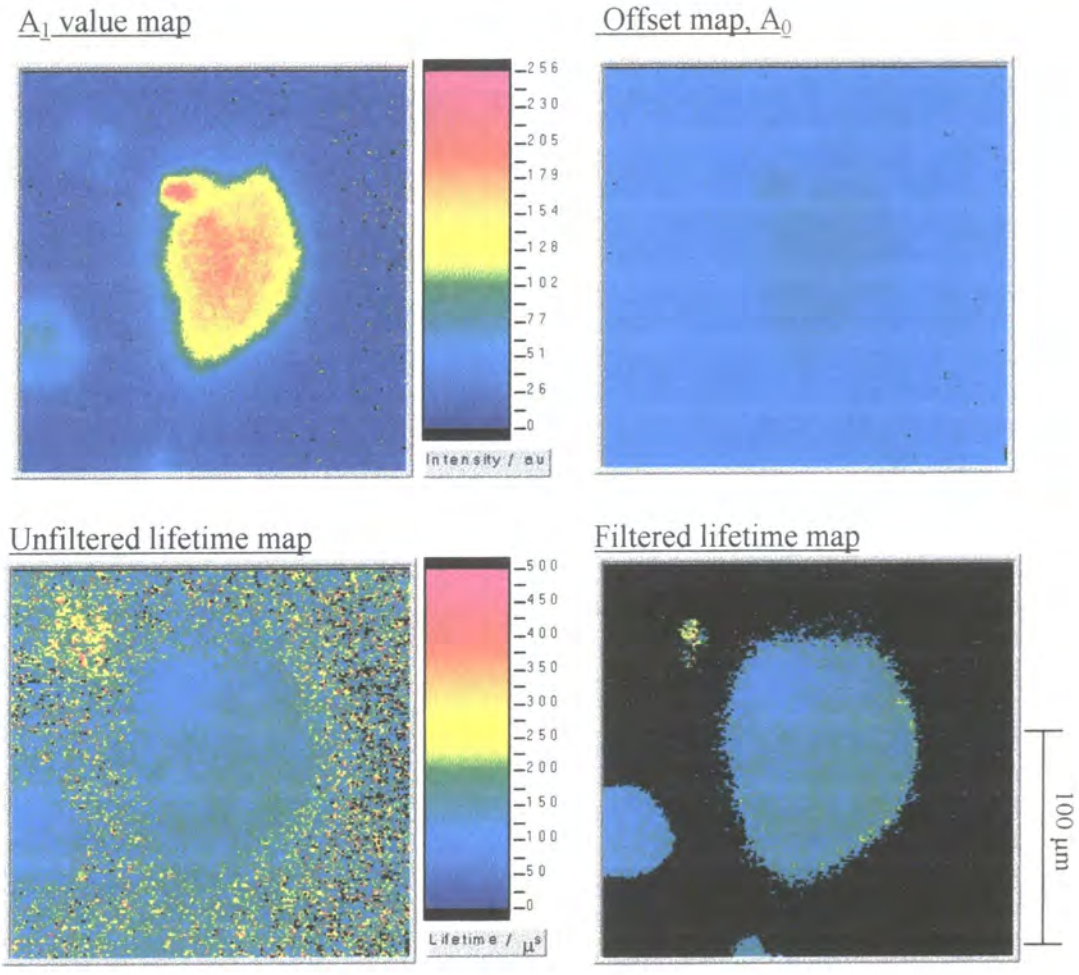

Figure 3.3 Complex **10** on silica showing the data 'filtering' technique.

Figure 3.3 demonstrates the lifetime mapping technique and the filtering technique. The images shown are for a silica particle labelled with the terbium complex **10**, the pre-exponential factor map shows the intensity of fluorescence to be most intense in the areas where the particle is located. The offset map shows that the data had a reasonably constant background level, this background being fitted with an offset of around 50 arbitrary units. In the unfiltered lifetime map it can be seen that the areas with no intensity have had lifetimes fitted to them, however as already mentioned these values are not meaningful and as such are filtered out by the software to yield the final filtered lifetime map. A filter value of 30 arbitrary units was used. A further addition to the lifetime mapping software allows a histogram of the lifetimes

to be generated. Figure 3.4 shows such a histogram for the sample shown in Figure 3.3, complex **10** on silica, it shows that the the particle has a lifetime of around 150 μs with the data having a full width half maximum of around 60 μs.

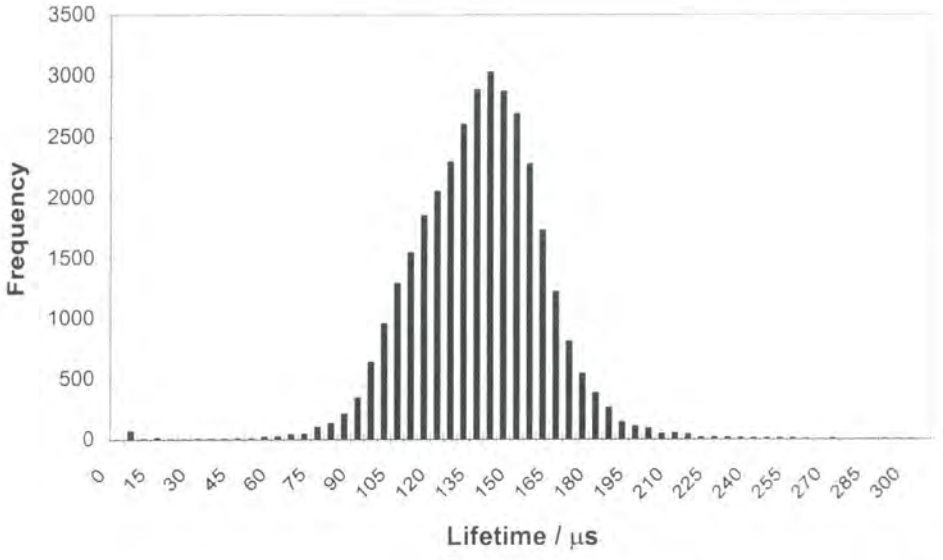

Figure 3.4 Histogram showing the distributions of lifetimes observed for complex **10** absorbed on a silica particle (Figure 3.3)

Figure 3.5 and Figure 3.7 show fluorescent images and lifemaps for complexes **8** and **9** respectively. The europium complex **8** has a lifetime of around 160 μs (FWHM 110 μs) and the europium complex **9** has a lifetime of around 800 μs (FWHM 600 μs). Figure 3.6 shows a typical fit for one of the pixels of the sample shown in Figure 3.5. It can be seen by inspection that the fit is good. Furthermore the importance of fitting to an exponential function with an offset can be seen. If this data had been fitted to a simple exponential function or using a logarithmic transform of the intensity data followed by linear regression, the lifetime obtained would have been substantially less accurate.

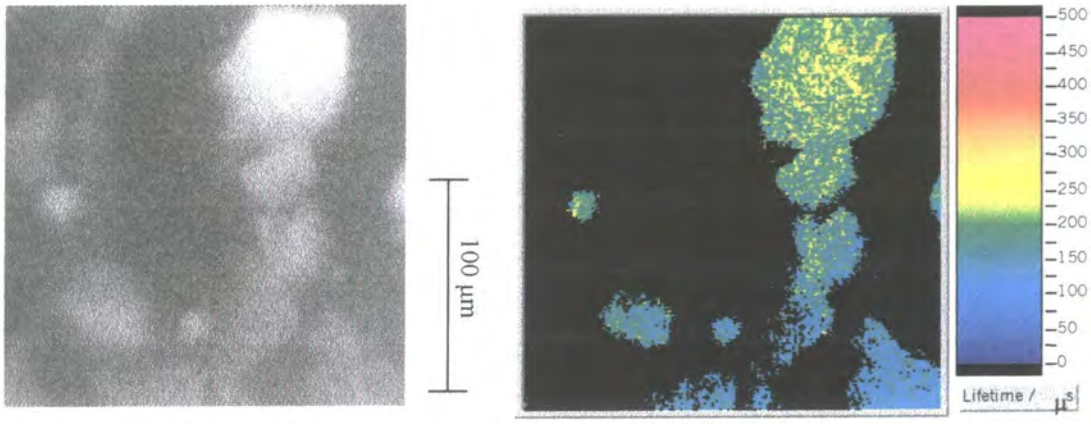

Fluorescence image Filtered lifetime map

Figure 3.5 Complex **8** on silica

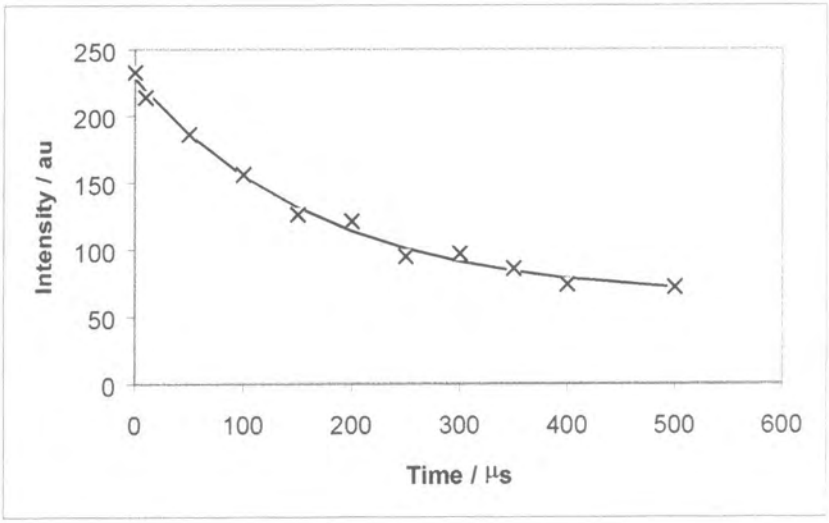

Figure 3.6 Typical data for a pixel from the image shown in Figure 3.5. $\tau = 170$ μs, $A_0 = 63$, $A_1 = 165$.

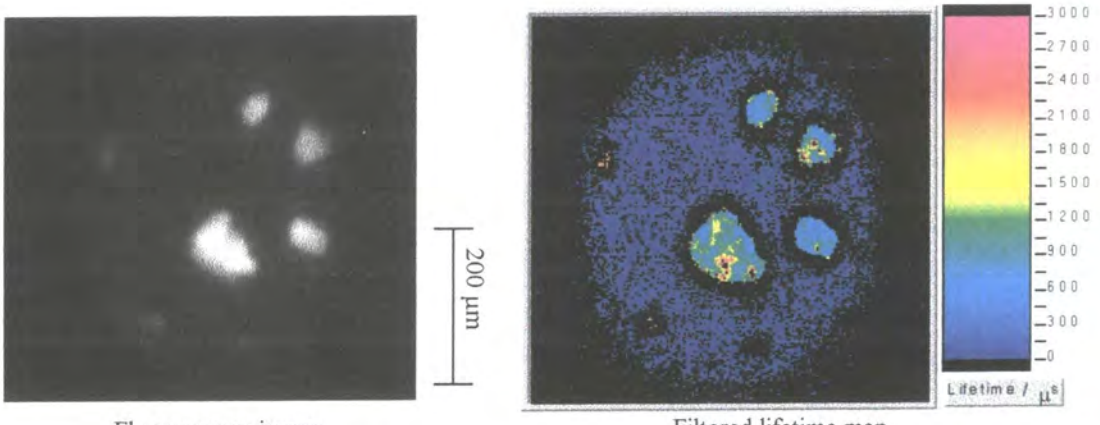

Fluorescence image Filtered lifetime map

Figure 3.7 Complex **9** on silica, $t_g = 200$ μs.

3.4.2 Onion Cells

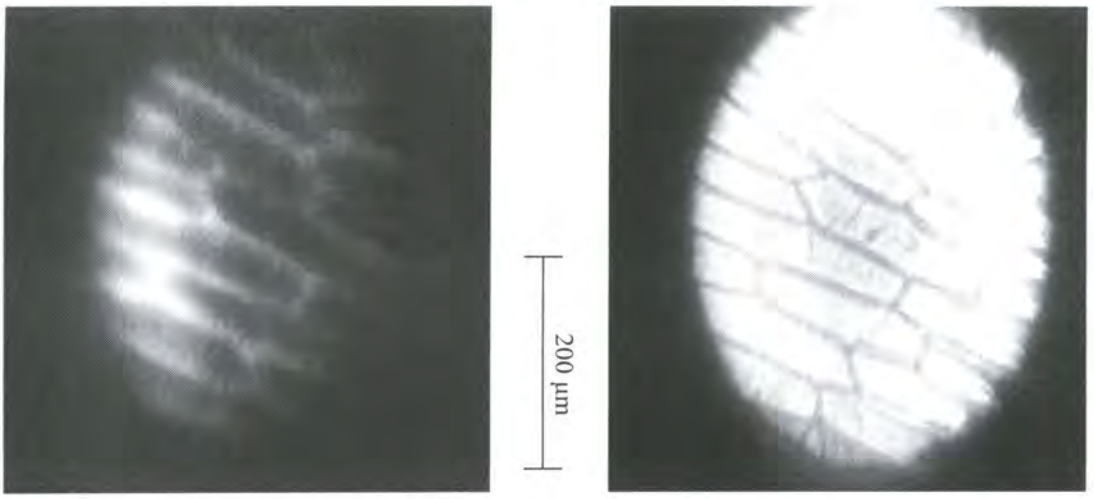

Time-gated image, gate = 100 μs
Delay = 100 μs

Transmission optical microscope image.

Figure 3.8 Onion cells stained with complex **9**

Europium complex **9** was also used to stain onion skin cells. The cells were immersed in a solution of complex in water for 15 min and then washed with water. Figure 3.8 shows that the complex stains the cell walls and its distribution could be seen after a time delay of 100 μs. Control experiments with unstained onion cells were performed, showing that the signal was due to the complex and not any constituent of the cells.

3.4.3 Animal Cells

A number of methods were attempted to load animal cells with all three lanthanide complexes. The cells used were guinea pig heart cells (provided by Prof. T. Powell, Oxford University) suspended in phosphate buffered saline (PBS; 137 mmol NaCl, 2.7 mmol KCl, 10 mmol phosphate buffer). Attempts to load the cells using the complex dissolved in DMSO and surfactants such as Triton-X were unsuccessful. Electroporation proved to be more successful. Electroporation involves discharging 100 V across a suspension of heart cells in a solution of complex. The cell membranes open momentarily allowing the complex to enter before closing again. The cell suspension was then centrifuged and the cells washed with PBS twice before imaging the cells under the microscope.

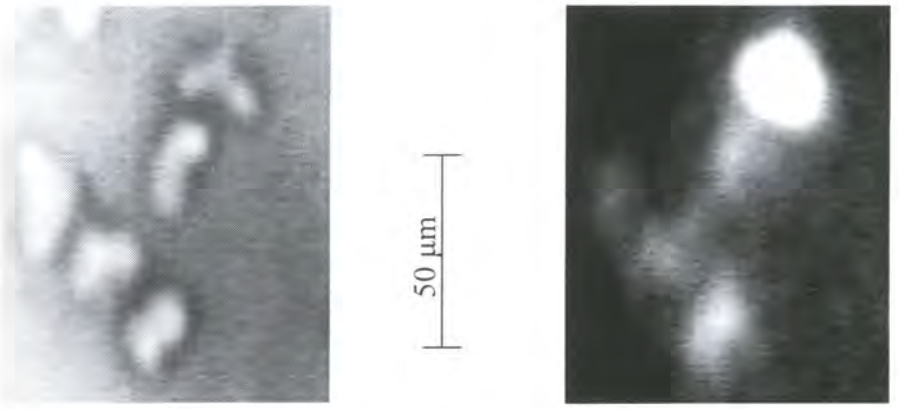

Image obtained using transmission optical microscopy.

Time-gated image, gate = 500 μs, Delay = 650 μs.

Figure 3.9 Complex **10** used to stain guinea pig heart cells by electroporation

Figure 3.9 shows a cluster of guinea pig heart cells imaged by both conventional transmission microscopy and a delayed image demonstrating that the complex is associated with the cells in some way. From the image it is not possible to ascertain whether the complex is localised within the cell or stuck to the external cell wall.

3.5 Conclusions

These results demonstrate that lanthanide complexes adsorbed onto silica particles can be used for time-gating imaging and mapping of surfaces. They have also proved that these complexes have potential for imaging both *in vivo* and *in vitro*. These types of measurement offer potential for use in combinatorial synthesis where lifetime and wavelength mapping could provide a way of identifying the reaction pathway of single beads or in cell imaging using complexes known to have a lifetime which is dependent on the concentration of biologically interesting molecules[13,14].

3.6 References for chapter 3

[1] Davidson R. S., *Chem. Soc. Rev.*, **1996**, 25, 241.

[2] Szmacinski H., Lakowicz J. R., Johnson M. L., *Meth. Enzymol.*, **1994**, 240, 723.

[3] *Fluorescent Labels for Confocal Microscopy,* Wells S., Johnson I., in *Three-Dimensional Confocal Microscopy: Volume Investigation of Biological Specimens,* eds. Stevens J. K., Mills L. R., Trogadis J. E., 1994, Academic Press Inc., San Diego, California.

[4] Singh A., Gopinathan K. P., *Current Science*, **1998**, 74, 841.

[5] Scully A. D., Ostler R. B., MacRobert A. J., Parker A. W., de Lara C., O'Neill P., Phillips D., *Photochem. Photobiol.*, **1998**, 68, 2, 199.

[6] Bech Ø., Phillips D., Moan J., MacRobert A. J., *J. Photochem. Photobiol. B. Biol.*, **1997**, 41, 1-2, 136.

[7] Elliot C. T., Francis K. S., McCaughy W. J., *Analyst*, **1994**, 119, 2565.

[8] Dickson E. F. G., Pollock A., Diamandis E. P., *J. Photochem. Photobiol. B. Biol.*, **1995**, 27, 3.

[9] Seveus L., Väisälä M., Syrjänen S., Sandberg M., Kuusisto A., Harju R., Salo J, Hemmilä I., Kojola H., Soini E., *Cytometry*, **1992**, 13, 329.

[10] Marriott G., Heidecker M., Diamandis E. P., Yan-Marriott Y., *Biophys. J.*, **1994**, 67, 957.

[11] Hubbard D. S., Houlne M. P., Kiefer G. E., McMillan K., Bornhop D. J., *Bioimaging*, **1998**, 6, 63.

[12] Bornhop D. J., Hubbard D. S., Houlne M. P., Adair C., Kiefer G. E., Pence B. C., Morgan D. L., *Anal. Chem.*, **1999**, 71, 2607.

[13] Parker D., Sennanayake P. K., Williams J. A. G., *J. Chem. Soc. Perkin Trans. 2,* **1998,** 2129.

[14] Parker D., Senanayake P. K., Williams J. A. G., *Chem. Commun.*, **1997**, 1777

Chapter 4

The effect of C-H/D on the luminescent lifetime of dota complexes of the lanthanide ions

Chapter 4

The effect of C-H/D on the luminescent lifetime of dota complexes of the lanthanide ions

This chapter describes the preparation and characterisation of deuteriated complexes of dota (1,4,7,10-tetraazacyclododecane-1,4,7,10-tetraacetic acid) with lanthanide ions. Selective deuteriation of both the ring and arm sites allows the relative quenching effects of C-H/D oscillators to be determined for various lanthanides in a structurally well defined molecule.

4.1 Introduction

The effect of ligand deuteriation on the quenching rate of the excited $^5D_0$ state of $[Eu(dota)]^-$ has been determined in some preliminary work for the acetate (NCH_2CO) arm positions[1]. It was found that a 90 % level of deuterium incorporation at these positions led to an increase in the rate constant for decay of the excited state in both H_2O and D_2O, corresponding to a contribution of 26 s^{-1} per C-H. The purpose of this chapter is to further investigate the effect of C-H oscillators in lanthanide complexes of dota to determine the effect of both the acetate arm and the ring C-H oscillators.

4.2 Syntheses of 1,4,7,10-tetraazacyclododecane

The key part of the synthetic work discussed in this chapter is the synthesis of the deuteriated $12N_4$ macrocycle. This compound was first synthesised in 1961 by Stetter and Mayer[2] (Scheme 4.1). The protected diamine, **11**, is alkylated with methyl bromoacetate, **12**, and the resulting diester, **13**, is hydrolysed in base and then converted to the diacid chloride, **14**, with thionyl chloride. Condensation with ethylenediamine, **15**, yields the cyclic diamide, **16**, in 68 % yield. Treatment with lithium aluminium hydride both reduces the amides and removes the tosyl protecting groups to give $12N_4$, **17**, in an overall yield of 15 %. It has since been shown that the cyclisation can be carried out using the methyl[3], ethyl[4] or the more reactive *N*-hydroxysuccinimide[5] diester.

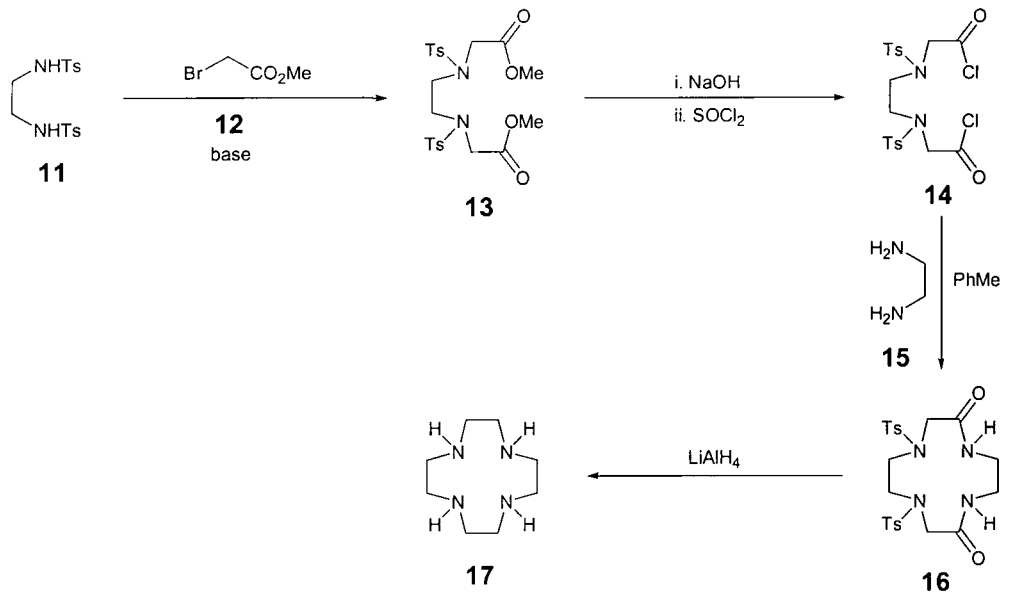

Scheme 4.1

The key step in the synthesis of $12N_4$ is the cyclisation step forming the macrocyclic polyamine. Many syntheses rely on an intermolecular reaction of a nitrogen nucleophile with a suitable electrophile. This is commonly effected using the dianion of a bis-toluenesulfonamide as the nitrogen nucleophile with attack onto a bis-tosylate or dihalo compound.

The toluenesulfonyl group has two purposes in these reactions: it both renders the secondary NH protons sufficiently acidic to permit salt formation and also functions as a nitrogen protecting group allowing only monoalkylation at the nitrogen. Schemes 4.2, 4.3 and 4.4 show that the cyclisations split broadly into two groups: those starting with the tetraamine, **18**, and those starting with the triamine, **22**. For the purposes of the syntheses outlined later in this report, the syntheses starting with the triamine are more suitable as they allow both of the cyclisation reactants to be produced from the same starting material.

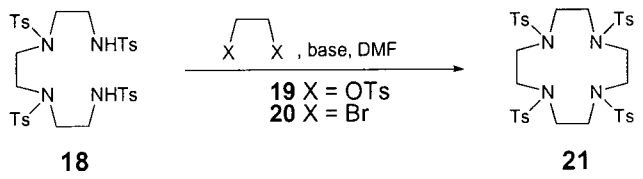

Scheme 4.2

Scheme 4.2 shows cyclisations starting from tosyl protected triethylenetetraamine, **18**. Reaction with the bis-tosylate, **19**, can be effected in DMF using either caesium carbonate[6], giving a 61 % yield, or sodium hydride[7] as the base. Using the dibromo compound, **20**, and finely divided potassium carbonate, Sherry *et al*[8] obtained a 61 % yield of the tetratosylamide, **21**.

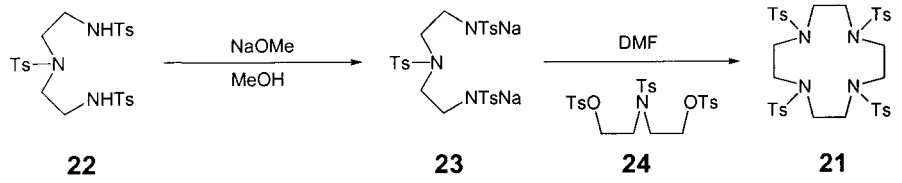

22 **23** **24** **21**

Scheme 4.3

Scheme 4.3 shows formation of the dianion of the *bis*-toluenesulfonamide, **23**, prior to reaction with the *bis*-tosylate[9], **24**. The sodium salt, **23**, is formed in 91 % yield followed by reaction with the *bis*-tosylate, **24**, to give an overall yield from the triamine of 61 %.

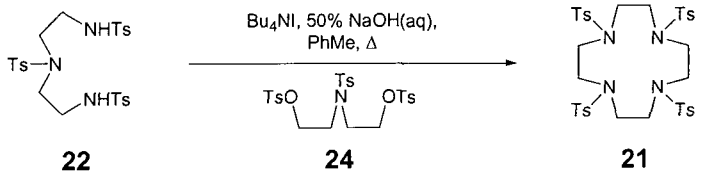

22 **24** **21**

Scheme 4.4

Scheme 4.4 shows a two phase reaction and offers a higher yield than the previous methods, in a reported yield of 90 %[10]. The tetrabutylammonium iodide acts as a phase transfer reagent. The sodium salt of the tosylamide, **22**, is formed in the aqueous phase and then reacts with the tosylate, **24**, effectively maintaining high dilution conditions, thereby minimising the formation of acyclic side products. Detosylation can be achieved in a number of ways the most common being the use of sodium in liquid ammonia[11,12] or sulfuric acid[13].

Scheme 4.5 shows a recent synthesis of $12N_4$ developed by Weisman. The two step synthesis involves the condensation of triethylenetetraamine, **25**, with dithiooxamide, **24**, followed by reduction using DiBAl-H.

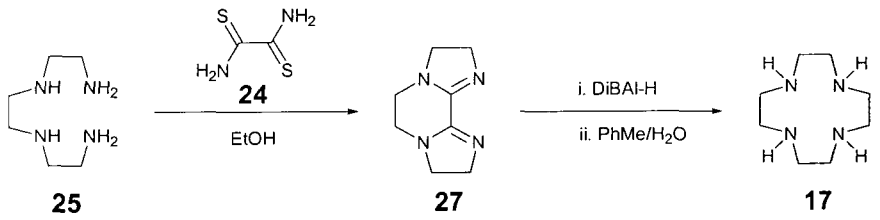

Scheme 4.5

Sandnes *et al.* have reacted glyoxal, **28**, with triethylenetetraamine, **25**, to template the ring closure reaction (Scheme 4.6)[14]. Free $12N_4$, **17**, was liberated by cleavage of the common bond between the 5 and 6-membered rings under acid hydrolysis. A similar technique but using butanedione has also been developed[15].

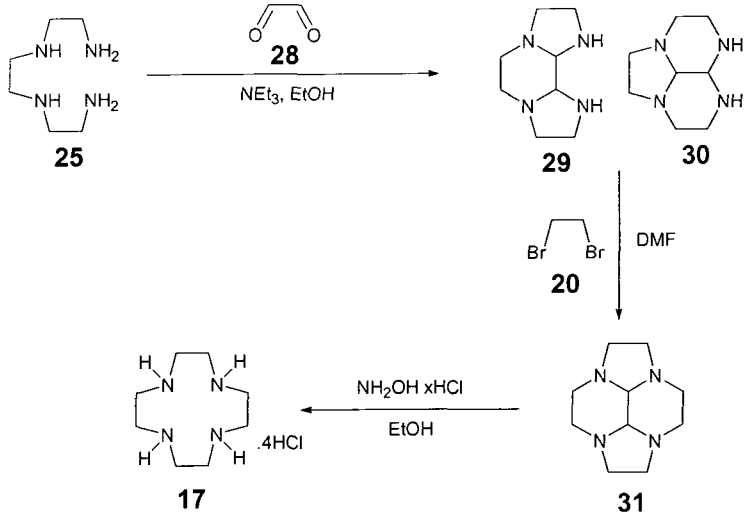

Scheme 4.6

The advantages of the methods shown in Scheme 4.5 and Scheme 4.6 are the low number of steps involved, relatively high yields and the absence of a final deprotection step.

4.3 Synthesis

The chosen synthesis of $12N_4$ involved the co-condensation of the protected triamine, **22**, with the ditosylate, **24**. Due to the expense of deuteriated solvents and reagents, the synthesis of the $12N_4$ ring was first repeated in concordance with literature procedures.

Scheme 4.7 shows the synthesis of the deuterated ditosylate, **37**. Iminodiacetic acid, **32**, was converted to **33** by reaction with tosyl chloride in sodium hydroxide followed by esterification in methanol under sulphuric acid catalysis to give the diester, **34**.

This diester, **34**, was deuteriated, exchanging the acidic protons $^{\alpha}$ to the ester carbonyl in d_4-methanol, with a catalytic quantity of sodium d_3-methoxide prepared *in situ* from the reaction of d_4-methanol with a small piece of freshly cut sodium. The reaction was followed by observing the disappearance of the ^{1}H nmr signal corresponding to the protons undergoing exchange (δ_H = 4.21 ppm). The sodium ions were then removed from the reaction mixture using a strongly acidic ion exchange resin, and the product obtained in yields of greater than 90% by removal of the methanol under reduced pressure. During the reaction transesterification took place to yield the trideuteriomethyl ester, **35**.

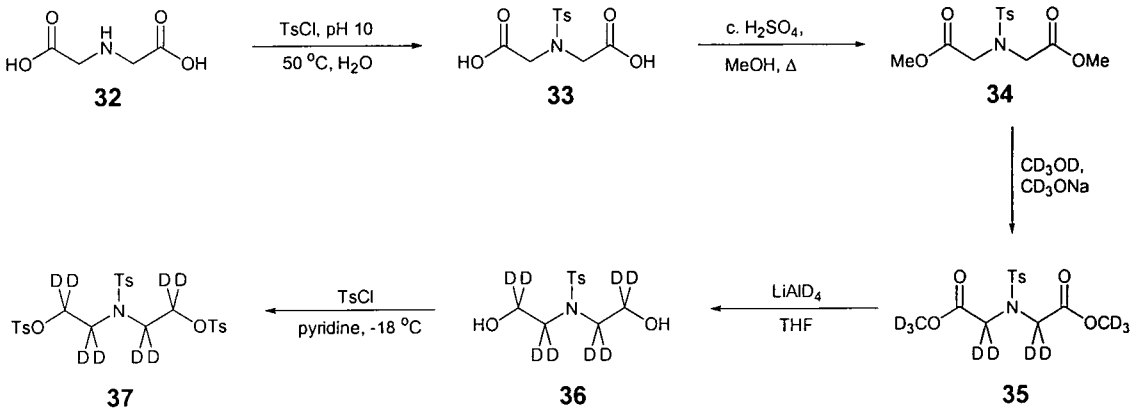

Scheme 4.7

Reduction of the diester, **35**, to the diol, **36**, using lithium aluminium deuteride gave near quantitative deuteriation in a 83 % yield. Tosylation of the resulting diol with tosyl chloride in pyridine yielded **37** as one of the component molecules necessary for the cyclisation. The tosylation reaction occurred with 82% yield: this compares to a yield of 84% for the related reaction for diethanolamine reported in the literature.

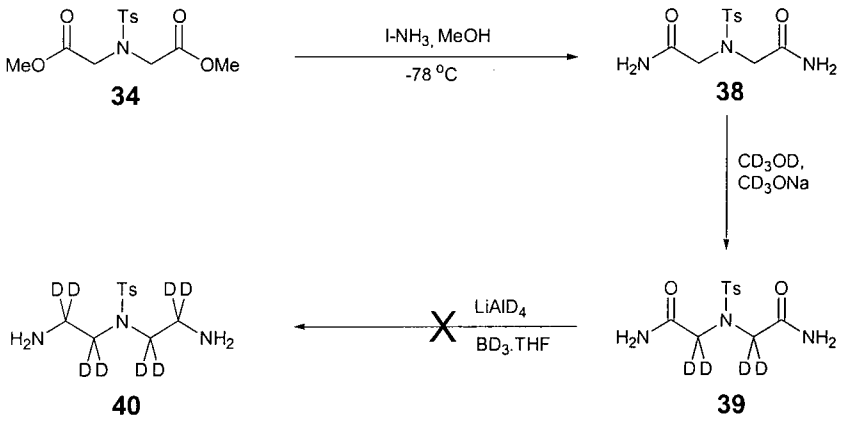

Scheme 4.8

Preparation of d_8-diethylenetriamine tristosylamide, **40**, proved more problematic. The initial strategy, shown in Scheme 4.8 was to make the amide, **38**, and exchange the $^{\alpha}$-protons in an analogous method to the ester, **35**, followed by reduction to the triamine using a deuteriated reducing agent. Treatment of the diester, **34**, with liquid ammonia gave a quantitative yield of the bis amide, **38**. Exchange of the $^{\alpha}$-protons was not as complete as in the case of the ester, ^{1}H NMR indicating an 80% level of deuterium incorporation. In spite of this problem, it was resolved to continue the synthesis, to check the validity of the remaining steps to the triamine, **40**. However attempts to reduce the amide using lithium aluminium deuteride or deuteroborane proved unsuccessful, starting material being recovered in both cases.

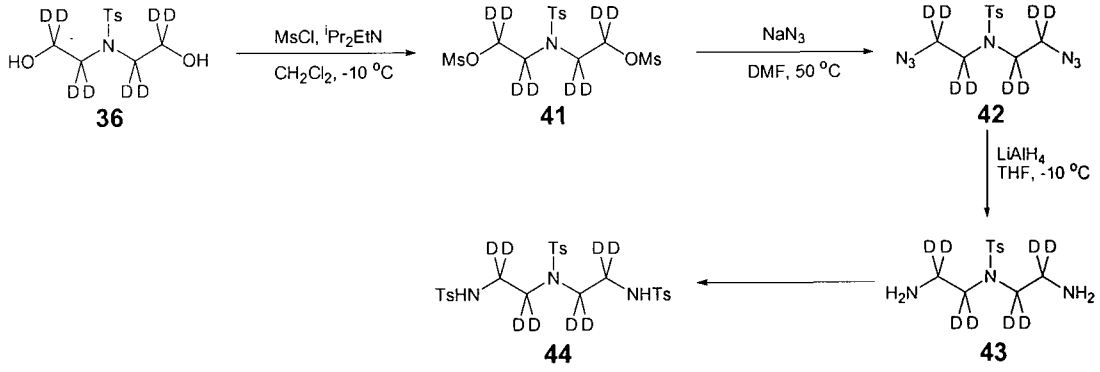

Scheme 4.9

A new strategy was developed, using the diol, **36**: for which the synthesis had proved uncomplicated. Conversion of the alcohol, **36**, to the azide, **42**, followed by

reduction to the amine, **43**, has been demonstrated by Bartsch *et* al.[16]. This strategy was applied to the deuteriated diol, **36**, Scheme 4.9. Conversion of the alcohol, **36**, to the mesylate, **41**, proceded in high yield (90-95%) using Hunig's base and mesyl chloride in CH_2Cl_2 at 0°C. Azide formation was carried out with a large excess of sodium azide in concentrated DMF solution and required heating to 50°C to initiate reaction. The observed yields (>90%) show a dramatic improvement on the literature procedure which uses phase transfer conditions (Aliquat 336 in water) to give a quoted 53% yield. The azide, **42**, was then reduced successfully using lithium aluminium hydride. Other reagents, including zinc/acetic acid and catalytic hydrogenation, did not yield the desired product. *N*-Tosylation to yield **44** was then carried out using tosyl chloride in aqueous sodium hydroxide solution.

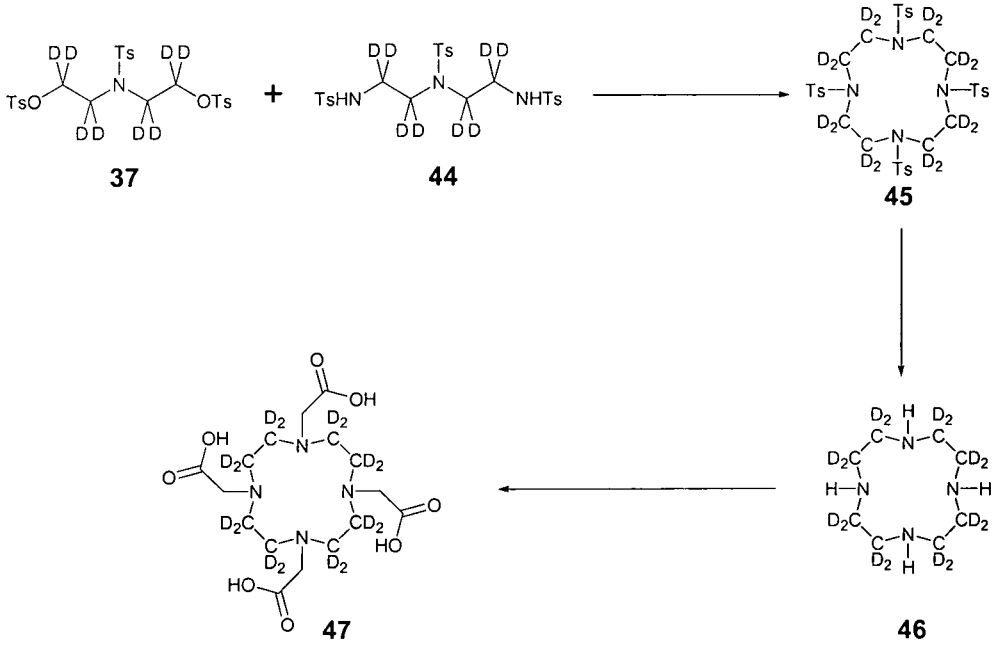

Scheme 4.10

The cyclisation proceeded according to literature conditions in 43 % yield followed by detosylation in concentrated sulfuric acid at 110 °C for 48 h. The tetraamine, **46**, was isolated in 93 % yield. Reaction of the deuteriated $12N_4$ with ethyl bromoacetate gave the ethyl ester of dota which was hydrolysed without further purification to give 'ring-deuteriated' dota, **47**.

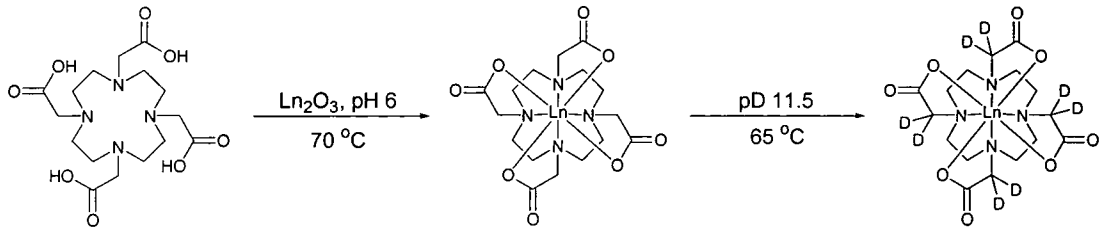

1 $h_{arms}h_{ring}$[Ln.1] $d_{arms}h_{ring}$[Ln.1]

Scheme 4.11

Complexes of both deuteriated and undeuteriated dota were made with ytterbium, terbium, neodymium and europium, by heating a suspension of the ligand and the lanthanide oxide in water at pH 6, Scheme 4.11. Excess lanthanide was removed by raising the pH to 9, whereupon excess lanthanide formed a precipitate of the hydroxide which was removed by filtration. The pH of the solution was then returned to 6. Deuteriation of the acetate methylene groups for both the deuterio- and protio- dota was achieved at 70 °C and a pD of 11.5[17]. Under these conditions enolisation of the bound carboxylate occurs readily, without competitive dissociation of the lanthanide, allowing exchange to occur in these arm positions.

4.4 Assessment of deuteriation levels

Deuteriation levels can be assessed by $^{1}H/^{2}H$ NMR and mass spectrometry. Proton NMR can be used to measure the intensity of residual protons in a molecule. By comparison with the signal intensities corresponding to non-deuteriated positions, an estimate of the extent of deuteriation can be obtained. The deuteriation levels of the dota complexes used in this work have all been assessed such by NMR techniques. For example, Figure 4.1 shows the proton NMR spectra for dota, and dota deuteriated on the ring positions. It can be seen that the signal corresponding to the ring protons at 3.1 ppm has been reduced in intensity to around 10 % of the value expected for the non-deuteriated dota, indicating a 90 % level of deuterium incorporation into these ring positions.

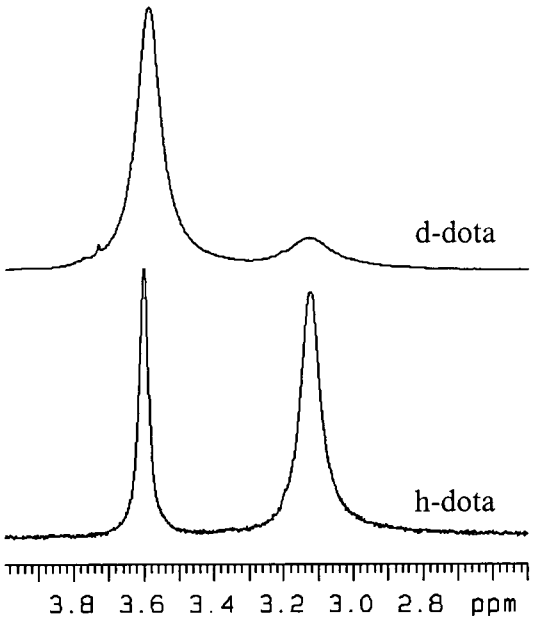

Figure 4.1 ^{1}H nmr spectra of dota deuteriated on the ring and undeuteriated

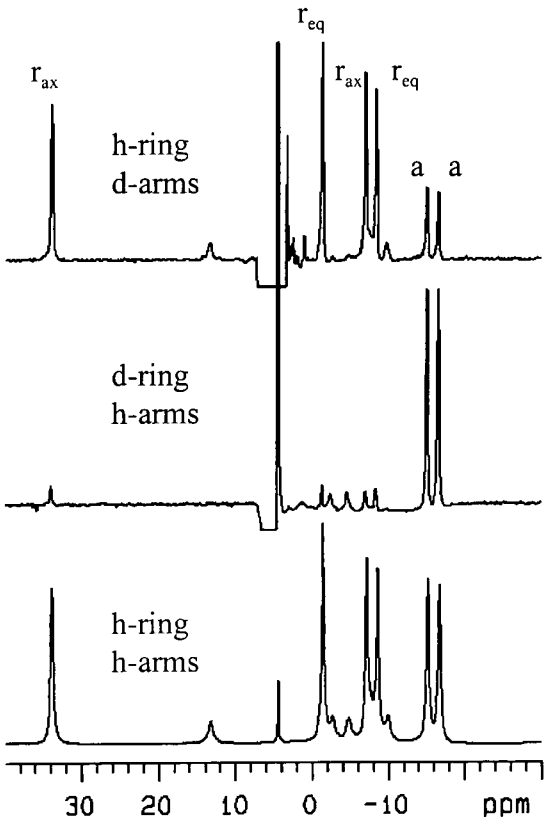

Figure 4.2 ^{1}H nmr spectra of europium(III) dota (200 MHz, pD = 6), 298 K

Figure 4.2 shows the proton NMR spectrum of $[Eu(dota)]^-$ (298 K, D_2O), undeuteriated and deuteriated in both the ring and arm positions. Due to the large

magnetic moment of the europium ion, a large paramagnetic shift is observed. The unpaired electrons cause large perturbations in the local magnetic fields, this leads to broadening of the lines usually causing a loss of any spin-spin splittings. The unpaired electrons also cause nuclear relaxation to occur. The other feature of interest in lanthanide NMR spectra are the large shifts in resonance frequencies. This phenomenon is known as the dipolar or pseudocontact shift and is due to the interaction of a lanthanide cation with an NMR active nucleus. The nucleus experiences a magnetic moment arising from the unpaired f-electrons, which leads to a shift in the NMR resonance frequency.

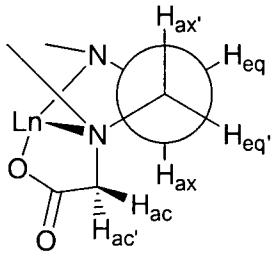

Figure 4.3

Figure 4.3 shows a Newman projection along one of the four equivalent ring carbon-carbon bonds. There are two pairs of anisochronous pseudo-axial and pseudo-equatorial ring protons which are labelled on the spectrum, along with the arm protons labelled 'a'. Only the major isomer which for $[Eu(dota)]^-$ is the square antiprism is labelled. The smaller peaks are due the twisted square antiprismatic minor isomer of dota. The ratio of major to minor isomer in D_2O is around 4:1 as observed by Aime *et al.*[18]. From peak integration the amount of incorporation of deuterium into the ring positions can be determined and was found to be 91 ± 2 %. The level of deuterium incorporation for the $[Ln(h_{ring}\text{-}d_{arms}\text{-}dota)]^-$ complexes is also determined from proton NMR data by comparison of the reduction in signal from the arm positions, with respect to the unlabelled ring positions. Deuterium NMR spectroscopy is used to determine the level of incorporation of deuterium into the arm positions in the $[Ln(d_{ring}\text{-}d_{arms}\text{-}dota)]^-$ complexes due to the lack of any major proton signals. The deuterium signal from the arm positions is compared to the signal from the 91 % deuteriated ring to give the level of arm deuteriation.

Deuteriation levels for the arm positions of the complexes used in this work are collected in Table 4.1.

	% arm deuterium incorporation	
Metal	Non-deuteriated ring	Deuteriated ring
Eu	64	83
Nd	9	-
Tb	42	27
Yb	39	68

Table 4.1 Deuterium incorporation levels for the complexes used in this work.

There is a large variation in the amount of deuterium incorporation into the arm positions. This may be due to small differences in the exchange conditions, for example even small differences in the pD of the solution could conceivably make a large difference to the amount of deuteriation. The systems were on average allowed to equilibrate for 3-4 days.

Mass spectrometry is also useful for determining the deuteriation levels of molecules particularly when high levels of deuterium incorporation have been attained. In these cases, NMR methods are unsuitable as the intensity of residual protons may be negligibly small and as such is subject to a large error. Systems where perdeuteriation has been accomplished present a further difficulty in that there is no internal proton reference and therefore mass spectrometry then provids the only method for assessing the deuteriation of these complexes. However, in this work, mass spectrometry was only used to determine deuteration levels in certain of the synthetic precursors to dota but not in the levels of incorporation into the complexes. This is for two reasons: firstly NMR is a more useful technique as it readily provides information about deuteriation levels at the different positions within the lanthanide dota complexes. Secondly, of the four lanthanides used in this work only terbium possesses a single isotope (^{159}Tb), europium has two naturally occurring isotopes (^{151}Eu, ^{153}Eu) with neodymium and ytterbium having seven. This makes interpretation of the mass spectra difficult due to the number of different isotopomers

that could contribute to each peak. Mass spectrometry does however provide an easy qualitative method to determine whether deuteriation has occurred as can be seen in Figure 4.4. The mass spectra could be compared with simulated spectra to obtain a best fit to obtain the level of deuteriation.

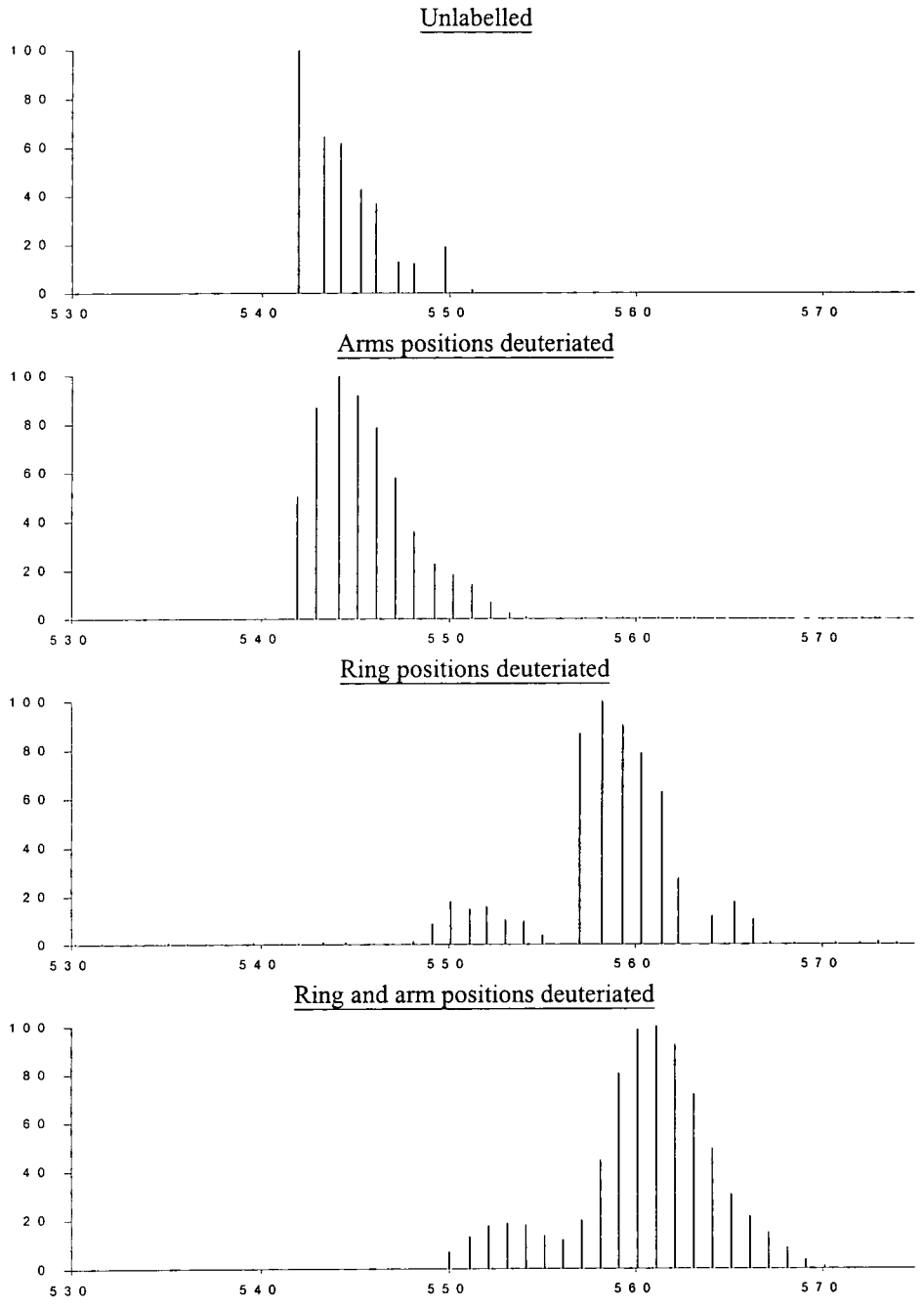

Figure 4.4 Electrospray mass spectra (negative ionization) of the labelled [Nd(dota)]$^-$

4.5 Lifetime measurements

Rate constants of luminescence were determined in both H_2O and D_2O for each of the labelled analogues of a given $[Ln(dota)]^-$ complex (Ln = Eu, Tb, Nd, Yb). All data was fitted to single exponential decay functions as described in chapter 1. These results are summarised in Table 4.2.

		k / s^{-1} (± 10 %, 293 K)			
		$h_{arms}h_{ring}$	$h_{arms}d_{ring}$	$d_{arms}h_{ring}$	$d_{arms}d_{ring}$
Nd	H_2O	1.31×10^7	1.27×10^7	1.31×10^7	1.20×10^7
	D_2O	3.14×10^6	2.39×10^6	3.00×10^6	2.17×10^6
Eu	H_2O	1.60×10^3	1.41×10^3	1.44×10^3	1.29×10^3
	D_2O	5.3×10^2	3.0×10^2	3.6×10^2	2.4×10^2
Tb	H_2O	5.7×10^2	6.0×10^2	6.0×10^2	5.4×10^2
	D_2O	3.5×10^2	4.0×10^2	3.4×10^2	3.3×10^2
Yb	H_2O	6.7×10^5	-	-	-
	D_2O	1.8×10^5	8.7×10^4	-	-

Table 4.2 Radiative rate constants for the decay of the excited states of Nd, Eu, Tb and Yb complexes of dota and its partially deuteriated analogues.

Unfortunately, only limited data is available about the ytterbium complexes as the optical parametric oscillator used to directly excite ytterbium ($2F_{5/2} \rightarrow 2F_{7/2}$ at 980 nm) was only available for a short period and has subsequently been 'out of action' and unavailable.

	$\Delta k / s^{-1}$			
	$h_{arms}h_{ring}$	$h_{arms}d_{ring}$	$d_{arms}h_{ring}$	$d_{arms}d_{ring}$
Nd	1.00×10^{7}	1.03×10^{7}	1.01×10^{7}	0.98×10^{7}
Eu	1.07×10^{3}	1.11×10^{3}	1.08×10^{3}	1.05×10^{3}
Tb	2.2×10^{2}	2.0×10^{2}	2.6×10^{2}	2.1×10^{2}
Yb	4.9×10^{5}	-	-	-

Table 4.3 Values of $k_{H_2O} - k_{D_2O}$ for $[Ln(dota)]^-$

Table 4.3 shows values of Δk, the difference between the rate constant for luminescent decay in H_2O and the rate constant for luminescent decay in D_2O. This factor is related to the number of co-ordinated water molecules, q, by Equation 4.1 (Chapter 1, p 11).

$$q = A (k_{H_2O} - k_{D_2O}) \qquad \textbf{4.1}$$

The values of Δk for each of the lanthanides are constant for each of their dota isotopomers indicating for each of the lanthanides that each isotopomer has the same number of water molecules associated with it in solution. Using the values of A for europium and terbium (Table 1.1, p 12) a value of q can be determined. In each case a q value of one was obtained as would be expected, for ytterbium the value is 0.5. It has been established for $[Yb(dota)]^-$, a mixture of eight (q = 0) and nine coordinate (q = 1) complexes exist in aqueous solution.

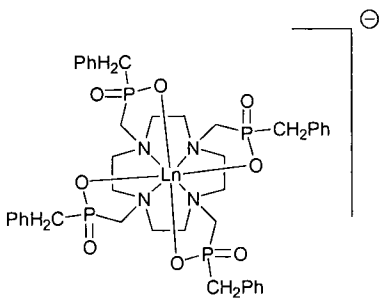

2

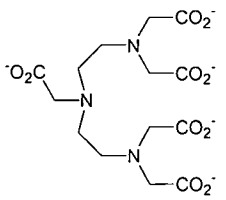

48

However for neodymium the literature value[19] of A gives a q value of 3.6. This is obviously too high. The Δk for the neodymium complex of diethylenetriaminepentaacetic acid, dtpa, **48**, a complex known to have one co-ordinated water has been determined to be $1.09 \times 10^7\ s^{-1}$. This value is the same as that determined for $[Nd(dota)]^-$, suggesting that the 'A' reported in the literature is not correct. This could be because the effect of quenching by water molecules not directly co-ordinated to the lanthanide molecule, *i.e.* 'outer sphere' water, may not have been taken into account. Europium, yttrium, gadolinium and ytterbium complexes of the relatively hydrophobic tetrabenzyl phosphinate, **2**, are known to have no 'inner sphere' co-ordinated water[20,21]. The neodymium complex of tetrabenzyl phospinate has a Δk of $3.25 \times 10^6\ s^{-1}$ providing a lower limit for the contribution by 'outer-sphere' water molecules. Using this value and assuming that both $[Nd(dota)]^-$ and $[Nd(dtpa)]^{2-}$ have one co-ordinated water molecule, a new estimate for 'A' can be made from Equation 4.2, where B is the rate constant for deactivation by 'outer-sphere' water molecules.

$$q = A\,[\,(k_{H_2O} - k_{D_2O}) - B\,] \qquad \textbf{4.2}$$

This treatment gives an estimate of the 'A' value to be 1.5×10^{-7} s.

The mean distances from the C-H oscillators to the lanthanide have been calculated from the reported X-ray structures[18,22,23] and are shown in Table 4.4. It can be seen that four of the arm hydrogen atoms are close to the lanthanide centre, around 3.7 Å, whereas the other set of four diastereotopic hydrogen atoms are more distant around 4.2 – 4.4 Å away. As a consequence of this increased distance, they are unlikely to cause significant quenching. The ring hydrogen atoms also consist of four sets of diastereotopic hydrogens. The pseudo axial, r_{Hax} and $r_{Hax'}$, are close to the lanthanide ion, around 3.7 Å, whilst the pseudo equatorial protons, r_{Heq} and $r_{Heq'}$, are further away. As for the case of the axial hydrogens, the closer, pseudo axial ring protons will give rise to the bigger quenching effect, compared to the more distant pseudo equatorial hydrogen atoms. These arguments result in the conclusion that the hydrogen atoms responsible for quenching in dota complexes are about 3.7 Å

whether or not they are in the ring or the arms. Therefore, it would be expected that the quenching effect of the ligand arm or ring hydrogens should be about the same. The values for quenching rate constants are quoted per C-H oscillator, taking into account for the ring protons only the 8 closest protons and for the arm it is the 4 proximate protons which are responsible for quenching.

Complex	r_{Hac}	$r_{Hac'}$	r_{Hax}	$r_{Hax'}$	r_{Heq}	$r_{Heq'}$
[Eu(dota)]$^-$	3.75[a]	4.39	3.74[b]	3.78	4.50	4.49
[Y(dota)]$^-$	3.68	4.23	3.68	3.72	4.35	4.39
[Lu(dota)]$^-$	3.65	4.18	3.65	3.70	4.31	4.32

[a] two shortest distances are3.48 and 3.52 Å

[b] two shortest distances are3.54 and 3.70 Å

Table 4.4 Mean distances between ligand hydrogen atoms and the lanthanide ion in lanthanide complexes of dota. The labels refer to those shown in Figure 4.3. From references 22,23,24.

The value of the quenching by ring C-H oscillators, k_{ring}, can be obtained by subtracting the value of the rate constant for the $h_{arms}d_{ring}$ complex from the value of the rate constant for the $h_{arms}h_{ring}$ complex, measured in the same solvent. It would be expected that this could also be measured in a similar way from the pair of complexes where the arms are both deuteriated, however in practice this cannot be achieved because the level of deuteriation in the arms in these pairs of complexes is not the same, as is found in the pair where the arms are undeuteriated. Similarly the value of quenching by arm C-H oscillators, k_{arms}, can be determined by subtraction of the rate constant value for the $d_{arms}h_{ring}$ complex from the value for the $h_{arms}h_{ring}$ complex or subtracting the value for the $d_{arms}d_{ring}$ from the value for the $h_{arms}d_{ring}$ complex. In all cases the values are then scaled appropriately to the level of deuterium incorporation to give values per C-H oscillator. The values obtained from this analysis are collected in Table 4.5.

	k_{arms} / s^{-1}	k_{ring} / s^{-1}
Nd	3.9×10^5	8.2×10^4
Eu	46	28
Tb	28	-5.4
Yb	-	1.3×10^4

Table 4.5 The rate constants for quenching per close C-H oscillator in lanthanide dota complexes

The value of the rate constant for quenching of europium luminescence by the arm hydrogen atoms is similar to the value of 26 s^{-1} previously obtained[1]. The quenching of the ring protons is a slightly smaller contribution but of the same order of magnitude. The larger value of rate constant for arm protons over ring protons may be because the closest proton in the europium structure are in the arm positions. The same pattern is observed for neodymium where the contribution of the arm protons is again larger than that for the ring protons.

In some of the terbium measurements obtained deuteriation increases the rate constant in others it decreased the constant. The results reported in Table 4.5, indicate that the overall effects are small and possibly lie within the limits of experimental error. If deuteriation of the terbium complex of dota did cause an increase in the rate constant for quenching it is possible that seventh harmonic of the C-D oscillator whilst, having a less favourable Franck-Condon overlap than the fifth harmonic of the C-H oscillator, actually possesses a better energy match with the terbium ion $^5D_4$ excited state.

4.6 Conclusions

Deuteriation of the C-H oscillators in dota complexes of europium, ytterbium and neodymium does decrease the rate constant for emission from the luminescent excited state. This effect has been quantified for both the ring and arm positions of the molecule and is most pronounced for the complexes of neodymium and ytterbium and is much less effective for terbium complexes. In the case of $[Eu(dota)]^-$ the per-

deuteriated complex (with 75 % deuterium incorporation overall) possessed a lifetime in D_2O of 4.1 ms, compared to 1.9 ms for the protiated analogue. Clearly, significant lifetime enhancement is possible using CH/CD exchange and is only limited in its scope by the presence of efficient OH quenching which still dominates the deactivation of the $^5D_0$ excited state. Therefore, for practical applications, CH/CD exchange in europium complexes is most desirable in complexes lacking any bound water molecules, such as the series of tetraphosphinate complexes[20].

4.7 References for chapter 4

[1] Dickins R. S., Parker D., de Sousa A. S., Williams J. A. G., *Chem. Commun.*, **1996**, 697.

[2] Stetter H., Mayer K. H., *Chem. Ber.*, **1961**, 94, 1410.

[3] Takenouchi K., Tabe M., Watanabe K., Hazato A., Kato Y., Shionoya M., Koike T., Kimura E., *J. Org. Chem.*, **1993**, 6895.

[4] Wei J. F., Zhou R. X., Yan G. P., Du P., *Chem. J. Chin. Uni.*, **1997**, 18, 658.

[5] McMurry T. J., Brechbiel M. W., Kumar K., Gansow O. A., *Bioconjugate Chem.*, **1992**, 2, 108.

[6] Parker D., *Aza Crowns in Macrocycle Synthesis* ed Parker D., Oxford University Press 1996, Chapter 1.

[7] Matsumoto N., Hirano A., Hara T., Ohyoshi A., *J. Chem. Soc. Dalton Trans.*, **1983**, 2405.

[8] Chavez F., Sherry A. D., *J. Org. Chem.*, **1989**, 54, 2990.

[9] Swinkels D. W., van Duynhoven J. P. M., Hilbers C. W., Tesser G. I., *Rec. Trav. Chim. Pays-Bas*, **1991**, 110, 124.

[10] Lukyanenko N. G., Basok S. S., Filonova L. K., *J. Chem. Soc. Perkin Trans.*, **1988**, 3141.

[11] Garrity M. L., Brown G. M., Elbert J. E., Sachleben R. A., *Tettrahedron Lett.*, **1993**, 5531.

[12] Cox J. P. L., Craig A. S., Helps I. M., Jankowski K. J., Parker D., Eaton M. A. W., Millican A. T., Millar K., Beely N. R. A., Boyce B. A., *J. Chem. Soc. Perkin Trans. 1*, **1990**, 2567.

[13] Hettich R., Schneider H.-J., *J. Am. Chem. Soc.*, **1997**, 119, 5638. Matsumoto N., Hirano A., Hara T., Ohyoshi A., *J. Chem. Soc. Dalton Trans.*, **1983**, 2405.

Lukyanenko N. G., Basok S. S., Filonova L. K., Kulikov N. V., Pastushok V. N., *Chem. Heterocycl. Compd. (Eng. Transl.)*, **1990**, 26, 346.

[14] Sandnes R. W., Gacek M., Undheim K., *Acta Chemica Scandinavica*, **1998**, 52, 1402.

[15] Hervé G., Bernard H., le Bris N., Yaouane J.-J., Handel H., Toupet L., *Tetrahedron Lett.*, **1998**, 39, 6861.

[16] Bartsch R. A., Chapoteau E., Czech B. P., Krzykawski J., Kumar A., Robison T. W., *J. Org. Chem.*, **1994**, 59, 616.

[17] Dickins R. S., Parker D., de Sousa A. S., Williams J. A. G., *Chem. Commun.*, **1996**, 697.

[18] Aime S., Botta M., Ermandi G., *Inorg. Chem.*, **1992**, 31, 4291.

[19] Beeby A., Faulkner S., *Chem. Phys. Lett.*, **1997**, 266, 116.

[20] Aime S., Batsanov A. S., Botta M., Dickins R. S., Faulkner S., Foster C. E., Harrison A., Howard J. A. K., Moloney J. M., Norman T. J., Parker D., Royle L., Williams J. A. G., *J. Chem. Soc., Dalton Trans.*, **1997**, 3623.

[21] Aime S., Botta M., Parker D., Senanayake K., Williams J. A. G., Batsanov A., Howard J. A. K., *Inorg. Chem.*, **1994**, 33, 4696.

[22] Spirlet M. R., Rebizant J., Loncin M. F., Desreux J. F., *Inorg. Chem.*, **1984**, 23, 4278.

[23] Dubost J. P., Leger M., Langlois M.-H., Meyer D., Schaefer M. C., *C. R. Acad. Sci., Ser. 2*, **1991**, 312, 349.

[24] Parker D., Pulukkody K., Smith F. C., Batsanov A. S., Howard J. A. K., *J. Chem. Soc., Dalton Trans.*, **1994**, 689.

Chapter 5

The distance dependence of energy transfer in lanthanide complexes

Chapter 5

The distance dependence of energy transfer in lanthanide complexes

This chapter describes investigations into the distance dependence of the energy transfer between aromatic chromophores and lanthanide ions. The synthesis of a model system for these studies is described along with some preliminary photophysical results.

5.1 Mechanisms of energy transfer

Electronic energy transfer is the simultaneous relaxation of a molecule in an excited state and the excitation of a molecule or ion in a lower-lying state. An electronic interaction between the two species is required, for which two different mechanisms have been proposed involving the Förster or the Dexter mechanism, as described in chapter 1.

5.2 System requirements

Investigations into the distance dependence of energy transfer between a donor aryl triplet and an acceptor lanthanide ion require a model system to be synthesised, in which the distance between the aromatic donor and lanthanide acceptor can be easily varied, over a controlled range of distances. A schematic of such a system is shown in Figure 5.1.

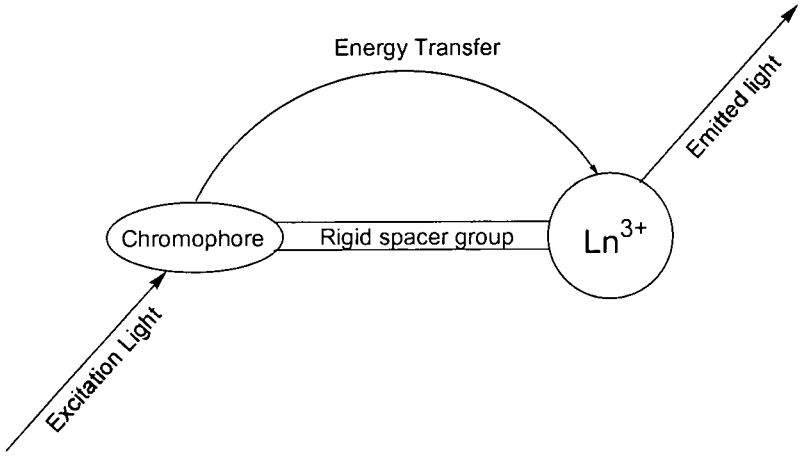

Figure 5.1 Schematic of the model system for distance dependence studies.

The chromophore must be an effective sensitiser for the lanthanide. This is dependent on the energy difference between the triplet state and the luminescent level of the lanthanide: the closer the two states in energy the more efficient the energy transfer. However, to prevent back energy transfer from the lanthanide to the triplet state of the sensitiser this gap must be at least 1500 cm^{-1} (at 298 K, kT is *ca.* 208 cm^{-1}), and the rate of such a thermally activated process is dependent upon $e^{-\Delta E/kT}$.

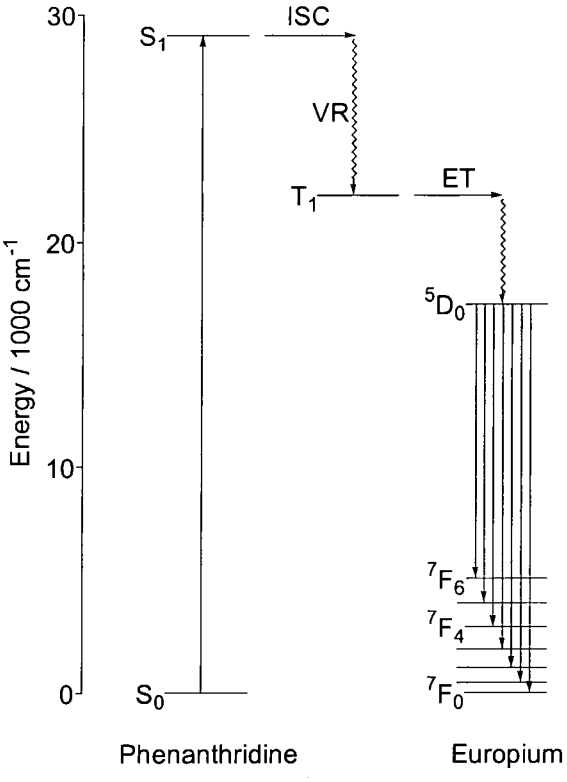

Figure 5.2 Jablonski diagram showing sensitised luminescence

A system based on the transfer of energy from a phenanthridine triplet state to a europium ion, separated by a rigid peptide spacer group, is well suited for these measurements. Figure 5.2 shows excitation of the ground state phenanthridine to the first excited singlet state (S_1). Intersystem crossing (ISC) followed by vibrational relaxation (VR) yields the first excited triplet state (T_1). Energy transfer (ET) from this triplet state populates the excited state of the europium ion. As can be seen in Figure 5.2, phenanthridine has a singlet energy[1] of about 28600 cm^{-1} and a triplet energy[1] of 22100 cm^{-1}, 4800 cm^{-1} above the luminescent $^5D_0$ level of europium. This system is well documented in the literature for sensitising emission from europium[2,6].

The spacer group should be non-conjugated and rigid so that in solution a preferred conformer is populated. Thus a reasonably well defined distance is engendered between the chromophore and the lanthanide ion. Oligomeric peptides are ideal for use as spacer groups and have been used in the literature to investigate the mechanism of the singlet-singlet energy transfer between naphthyl (donor) and dansyl groups (acceptor)[3]. Oligomers of poly-L-proline for example allow the donor and acceptor to be separated by distances from 12 – 46 Å.

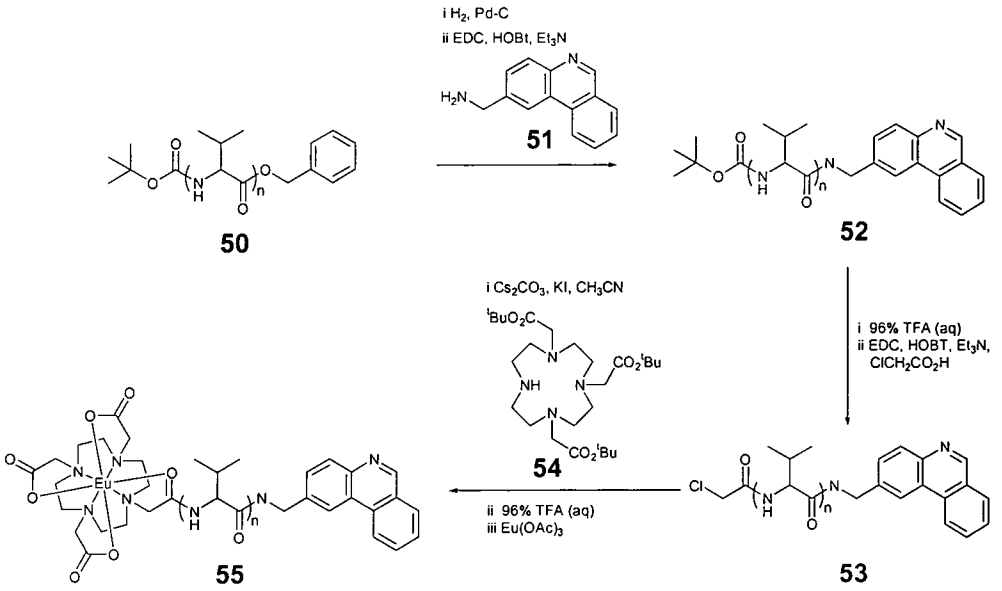

Scheme 5.1 Proposed synthetic scheme for **55**

The target molecule, **55**, is shown in Scheme 5.1. The target contains a rigid, non-conjugated spacer group separating the phenanthridine donor and the lanthanide ion acceptor. The lanthanide ion is complexed by an octadentate polyazamacrocycle with three appended acetate arms giving a charge neutral complex. The synthesis involved the production of diprotected oligomers of L-valine, followed by the chromophore or the lanthanide being selectively introduced in the final steps. Orthogonal protecting groups such as BOC (^{t}butoxycarbonyl) to protect the amine and a benzyl ester to protect the acid are used to allow independent deprotection of either the acid or amine functionality. 2-(Aminomethyl)-phenanthridine, **51**, was used as the phenanthridine unit and was attached to the carboxy terminus.

Deprotection of the acid using hydrogenation under heterogeneous catalysis, followed by use of standard peptide coupling techniques[8], allowed linkage of this phenanthridine unit, **51**. Removal of the BOC group using trifluoroethanoic acid followed by coupling with chloroethanoic acid gave the amide **53**. The lanthanide complexing unit was based on the tris(t-butyl ester), **54**, synthesised according to the method of Woods[4]. This triester may be coupled via its secondary amine position to the α-chloroamide **53**. After removal of the t-butyl esters using TFA, the protonated free ligand was formed. Complexation with europium(III) acetate in methanol yielded the neutral complex, **55**, which was purified on neutral alumina. This synthesis is advantageous as it allows easy variation of the donor and acceptor lanthanide groups in the final stages of the synthesis.

5.3.1 Synthesis of 1-(6'-phenanthridylmethyl)-4,7,10-tris(carboxymethyl)-1,4,7,10-tetraazadodecane

The synthesis of 1-(6'-phenanthridylmethyl)-4,7,10-tris(carboxymethyl)-1,4,7,10-tetraazadodecane is shown in Scheme 5.2. Phenanthridine was methylated in the 6-position using two equivalents of methyl lithium in THF. The reaction was carried out at 0 °C and then allowed to warm to room temperature for completion. This reaction leads to reduction of the central phenanthridine ring; re-aromatisation was achieved using manganese dioxide. Purification on silica gel gave the desired product, **57**, in 77 % yield.

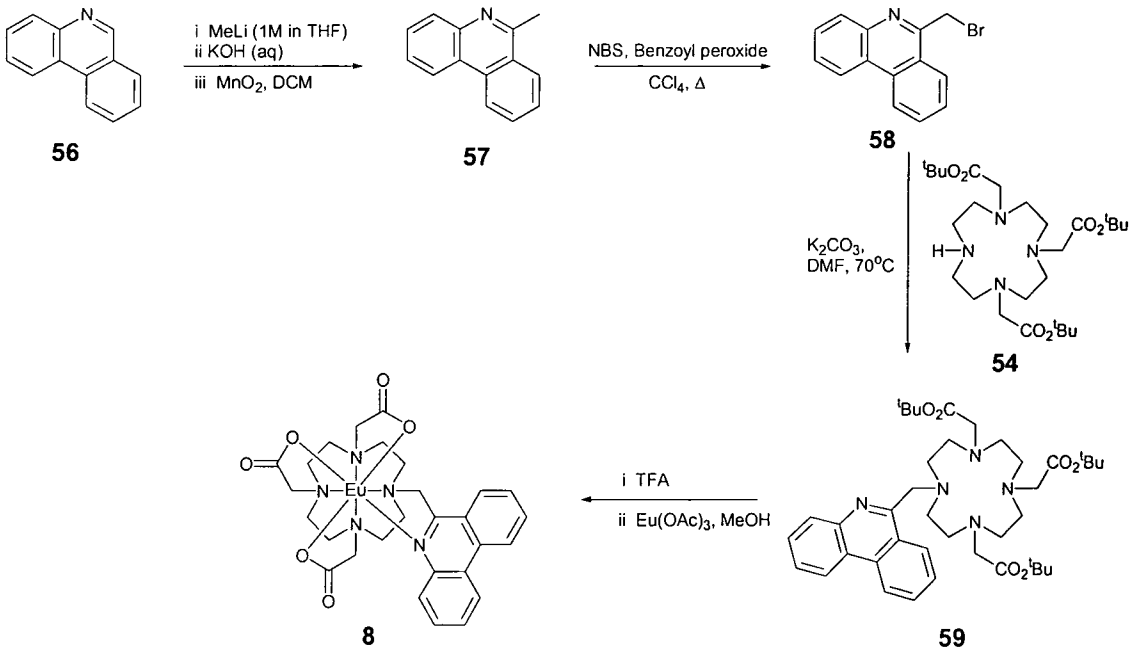

Scheme 5.2

Bromination of the methyl group using *N*-bromosuccinimide in boiling carbon tetrachloride, with a trace of benzoyl peroxide as a radical initiator, gave the desired product as an easily handled off-white solid. Heating 2-bromomethylpyridine, **60**, in a non-polar solvent has also been shown to form the pyrazine derivative, **61**, by a dimerisation reaction[5]. ^{1}H NMR provided evidence (appearance of a doublet at 9.4 ppm and the second order AB pattern for the central methylene group at 5.2 ppm indicative of the dimer, **62**) that the bromomethyl compound, **58**, had partially reacted to give the dimer, **62**, as around 10 % of the reaction mixture.

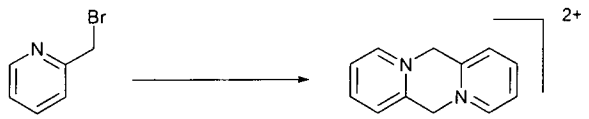

Scheme 5.3

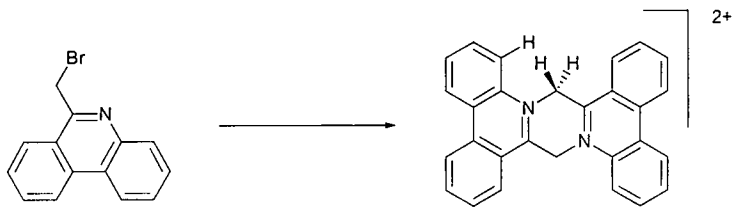

Scheme 5.4

Reaction with the triester, **54**, under standard conditions gave the *t*-butyl ester protected ligand, **59**, in 54 % yield after chromatography on silica. Removal of the *t*-butyl esters proceeded in quantitative yield using trifluoroethanoic acid to give the free ligand. The ligand was used without further purification to make the europium complex, **8**. This was achieved by heating the complex and europium (III) acetate in methanol under reflux. The complex was found to bind rather too strongly to silica or alumina to allow easy separation. Purification was therefore achieved using reverse phase chromatography on silica gel, eluting with ethanol.

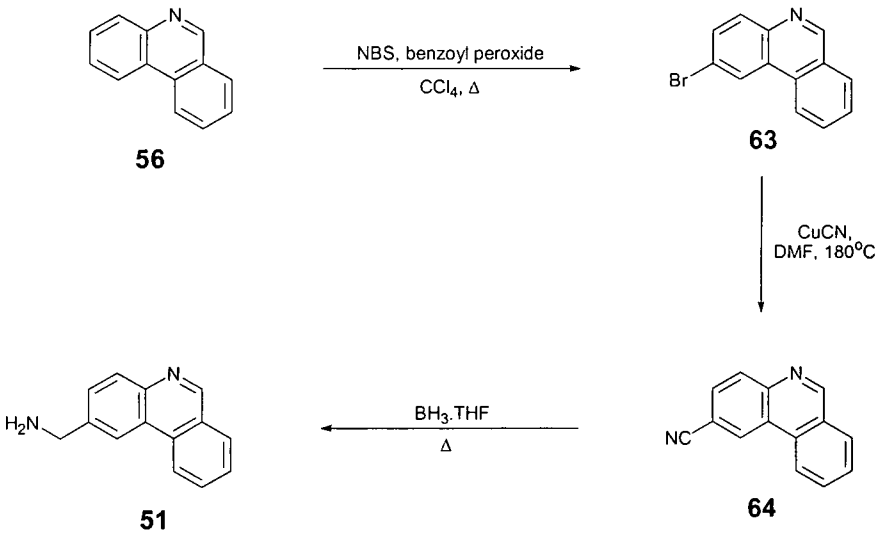

Scheme 5.5

5.3.2 Synthesis of 1-{N-[1-((2'-Phenanthridylmethyl)-carbamoyl)-2-methyl-propyl]-carbamoylmethyl}-4,7,10-tris(carboxymethyl)-1,4,7,10-tetraazadodecane, 70

2-Aminophenanthridine, **51**, was synthesised according to a literature procedure[6,7], as shown in Scheme 5.5. Phenanthridine was brominated using *N*-bromosuccinimide[7] in carbon tetrachloride with a trace of benzoyl peroxide present as a radical initiator. Cyanation was carried out using copper(I) cyanide in hot DMF, giving a disappointing yield of 27 % compared with the literature value of 68 %. Reduction of the nitrile, **64**, using borane·THF[6] at reflux took place slowly over the course of a week, the progress of the reduction was followed by observing the disappearance of

the nitrile band in the infra-red spectrum (2224 cm^{-1}). The amine, **51**, was obtained in 74 % yield, slightly less than the reported yield of 87%.

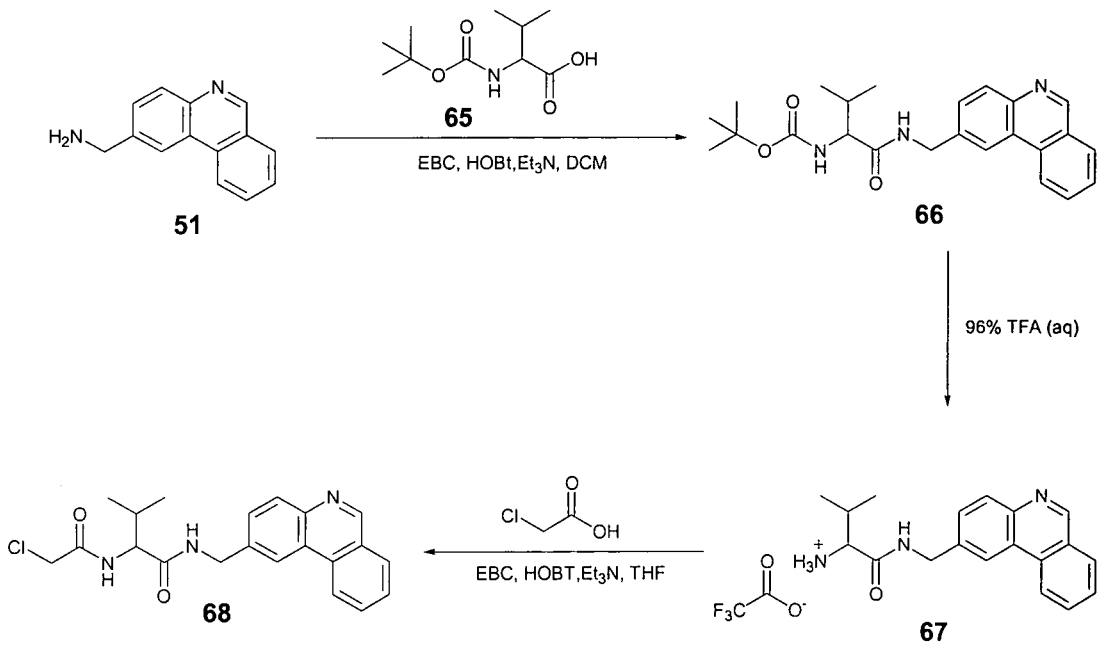

Scheme 5.6

Coupling of the amine, **51**, to BOC-L-valine, **65**, followed by column chromatography gave **66** in 76 % yield. Standard coupling reagents[8] were used 1-[3-(dimethylamino)propyl]-3-ethylcarbodiimide hydrochloride (EDC), 1-hydroxybenzotriazole (HOBT) and triethylamine in dichloromethane. Subsequent removal of the BOC protecting group using 96 % trifluoroethanoic acid in water gave the amine salt, **67**, in quantitative yield. Coupling of this salt to chloroethanoic acid using standard peptide coupling reagents proceeded with a disappointing yield of 32 %. The coupling reaction was performed in dry THF for solubility reasons.

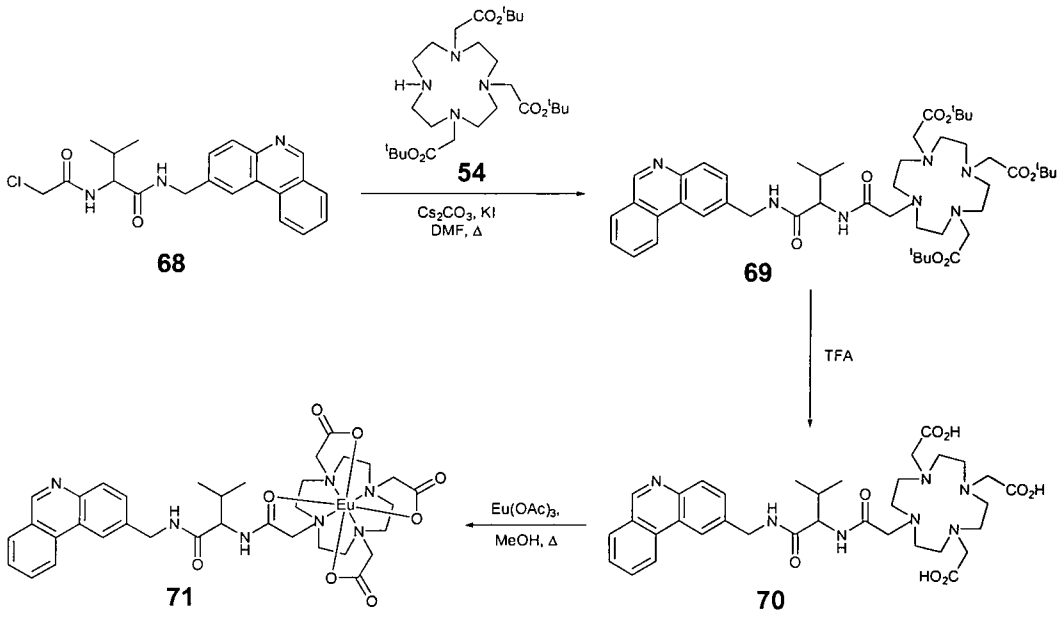

Scheme 5.7

Coupling of the tris(ᵗbutyl ester), **54**, with **68** using caesium carbonate and potassium iodide in dry acetonitrile gave the ᵗbutyl ester protected ligand, **69**, in 90 % yield after column chromatography. The ᵗbutyl esters were removed in quantitative yield giving the target ligand, **70**. This ligand was used without further purification for the complexation step, as the complex was more amenable to chromatographic purification than the ligand itself. Complexation with europium was achieved using europium(III) acetate in methanol under reflux, and the complex, **71**, was purified by preparative thin layer chromatography on alumina.

5.4 Photophysical Studies on the Europium Complexes 8, 71, 73, 74, 75

The complexes investigated in this work included not only **8** and **71** but also some related complexes available from co-workers, thanks to Dr. Linda Govenlock (**73**), Céline Mathieu (**74**) and Dr. Kanthi Senanayake (**75**).

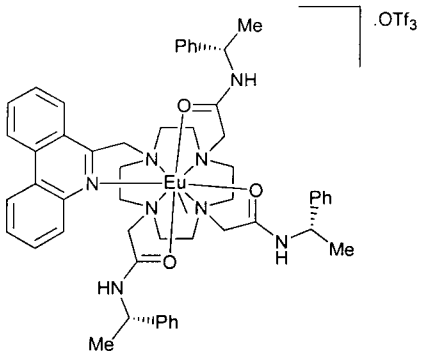

73

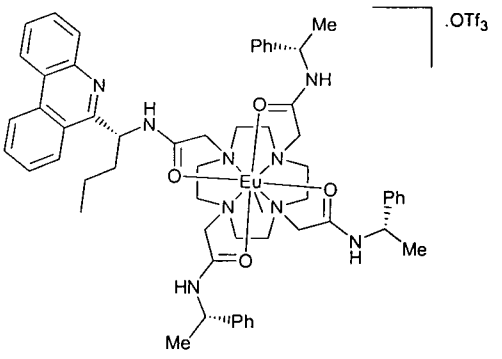

74

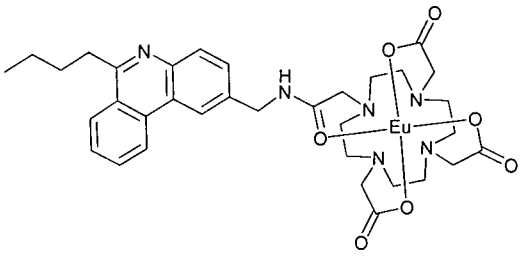

75

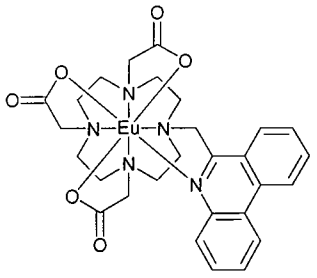

8

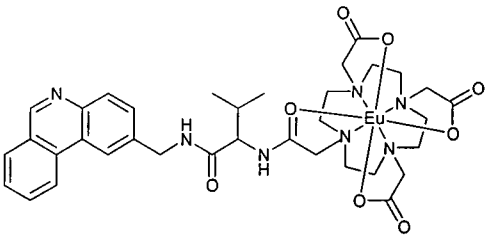

71

Complex **75** directly relates to **8** and **71** as they both possess the same pendant arm groups. It provides an example of a complex with an intermediate distance between europium and the phenanthridine moiety, compared to **8** and **71**. The complexes **73** and **74** have different arm groups to **75**, **8** and **71**. However **73** has the phenanthridine unit in a similar position to **8**, and **74** has the phenanthridine in a similar position to that found in **75**, making them useful for comparative purposes.

Complexes of europium and terbium based on a phenanthridine sensitiser have been investigated previously[6]. The photophysical properties were found to depend on the extent of protonation of the phenanthridine ring nitrogen. The complexes used in this work were all in their unprotonated form, as was confirmed by observing the absorption spectrum for each sample of complex. Protonation of the nitrogen has been shown to shift the absorption spectrum to the red, allowing the extent of protonation to be assessed by comparing absorbance values at 320 and 365 nm.

The overall quantum yield for metal-based luminescence of each of these complexes following excitation at 270 nm was measured in both H_2O and D_2O. The quantum yield of a process is defined as the number of photons due to a specific process that are emitted as a fraction of number of absorbed photons. In practice, this measurement is made by comparing compounds with unknown quantum yield to those with known yields[9]. A suitable standard must absorb light at the same wavelength as the compound of interest and should also emit over a similar range. The standards used in this work satisfy these criteria: they were cresyl violet and rhodamine 101[10]. The emission spectra of these standards and the spectrum of one of the complexes, **8**, are shown in Figure 5.3 and Figure 5.4. Full experimental details of this procedure are reported in chapter 6.

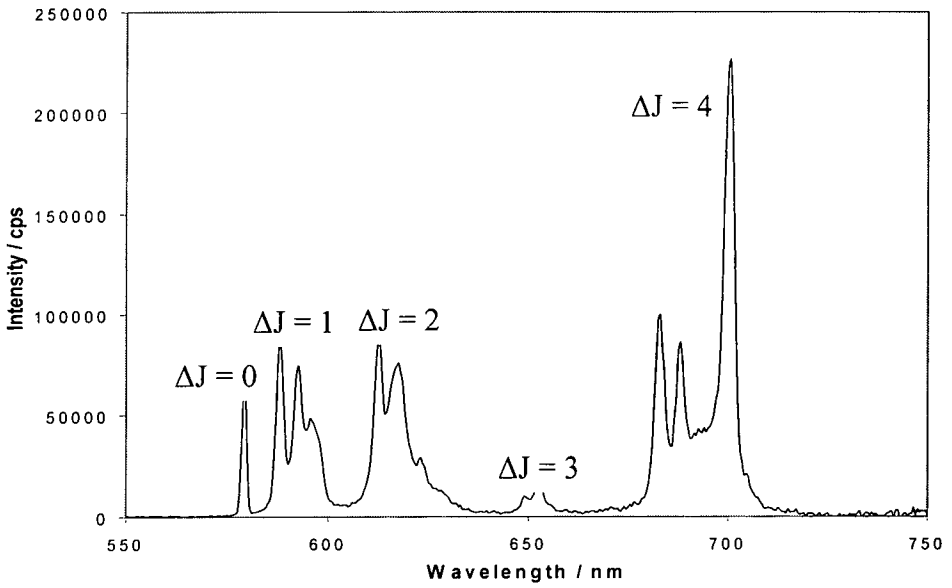

Figure 5.3 Corrected emission spectrum of **8**. (H_2O, 293 K, λ_{ex}=350 nm, 400 nm cut-off filter used.)

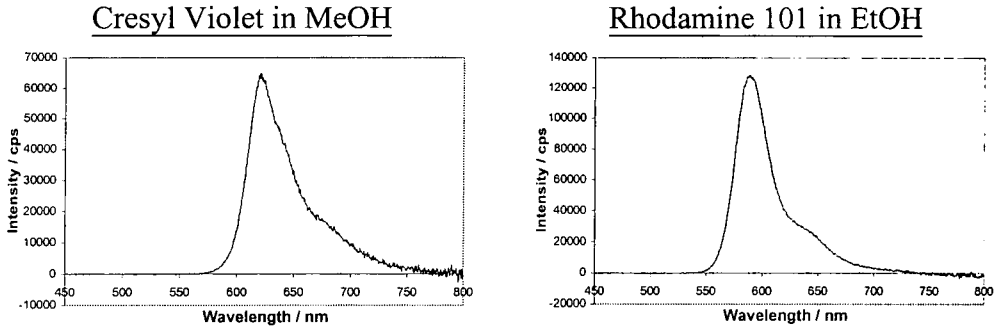

Figure 5.4 Corrected emission spectra of rhodamine 101 and cresyl violet. λ_{ex}=270 nm, 410 nm cut-off filter used.

The lifetimes for each of the complexes in H_2O and D_2O were also measured. In each case, the phenanthridine donor was excited at 270 nm and the emission was monitored at both 594 nm ($^5D_0 \rightarrow {}^7F_1$) and 615 nm ($^5D_0 \rightarrow {}^7F_2$). These results and the quantum yield data are collected in Table 5.1.

Complex	Φ (H_2O)	Φ (D_2O)	k (H_2O) / ms^{-1}	k (D_2O) / ms^{-1}	q^{Eu}
8	0.063	0.191	1.57	0.45	1.04
71	0.0038	0.012	1.63	0.61	0.84
73	0.039	0.130	1.52	0.47	0.71
74	0.0077	0.034	1.76	0.43	0.94
75	0.014	0.055	1.48	0.41	0.90

Table 5.1 Quantum yields and radiative decay constants for europium complexes (pH 6, 293 K). λ_{ex} = 270 nm, measured relative to cresyl violet and rhodamine 101. Values of q were determined using the equation $q^{Eu} = 1.2 (k_{H_2O} - k_{D_2O} - 0.25)$. An additional correction of –0.075 ms^{-1} was applied per NH oscillator, for those complexes bearing proximate amide groups.

The rate constants of emission allow the calculation of a value for the number of co-ordinated water molecules, *q*. For each case this is close to unity, indicating that each complex has one co-ordinated water molecule. It is important that the

complexes used throughout this work have the same q values as the quantum yield depends on all the available deactivation pathways and therefore on the number of co-ordinated water molecules. To determine the effect of varying the donor-acceptor distance the q value must therefore remain constant.

As expected, the quantum yield for europium luminescence is bigger in D_2O than in H_2O, with the trends in one solvent reflecting the trend in the other solvent. The quantum yield in D_2O was a factor of 3 to 4 times bigger than in H_2O consistent with the presence of a quenching bound water molecule in the latter case, which serves to competitively deactivate the europium $^5D_0$ state. The largest quantum yield is found for complex **8** followed by complex **73**. These are the two complexes in which the phenanthridine donor is closest to the europium ion as the phenanthridyl nitrogen is directly bound. The complexes are very similar, different only in the carboxy versus carboxamide ligation of three of the four pendant donors. The acetate arm containing compound has a higher quantum yield than the amide arm containing complex. Complexes **74** and **75** both have the phenanthridine moiety held the same number of atoms away from the macrocyclic polyaza ring binding the europium ion. Again, the complex with the acetate arms has a larger quantum yield than the amide arm containing ligand. In this case the comparison is not as fair as in the previous case as the orientation and substitution pattern of the phenanthridine moiety is different. Finally, the complex **71** with the phenanthridine ligand held the furthest away exhibits the lowest quantum yield, as expected.

Assuming a Förster mechanism, a more quantitative treatment can be attempted for the complexes with acetate arms. The efficiency of energy transfer, η_{ET} can be related to the donor-acceptor distance, R_{DA}, and the distance at which energy transfer is 50 % efficient[11], R_0 by equation 5.1, wherein the efficiency of energy transfer can be obtained from equation 5.2.

$$\eta_{ET} = \frac{1}{\left[1+\left(\frac{R_{DA}}{R_0}\right)^6\right]} \qquad \textbf{5.1}$$

$$\Phi_{em} = \Phi_T \cdot \eta_{ET} \cdot k_0 \cdot \tau_{obs} \qquad \textbf{5.2}$$

In Equation 5.2, Φ_{em} is the measured quantum yield of europium emission, Φ_T is the quantum yield of triplet formation, k_0 is the natural radiative rate constant of the metal and τ_{obs} is the observed lifetime of the metal. The natural radiative lifetime of europium has been calculated[12] to be 9.67 ms which corresponds to a k_0 value of 0.103 ms^{-1}. The quantities Φ_{em} and τ_{obs} have been measured. The triplet quantum yield for phenanthridine has not been reported. However for phenanthrene, at room temperature, in a polar solvent, the value is 0.73[1].

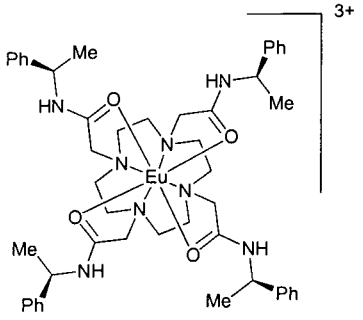

77

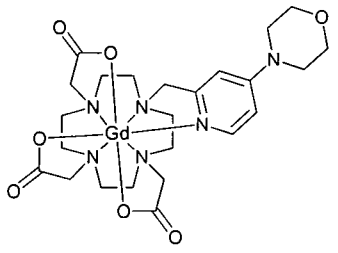

76

The donor-acceptor distances for the complexes in solution need to be estimated. This can be done by analysis of the crystal structures of analogous complexes. The crystal structure of the gadolinium complex of **76** has been solved[13] and the pyridyl N-Gd bond was found to be 2.53 Å. This provides a good estimate for the phenanthridyl N-Eu bond in complex **8**. The complex, **77**, has a distance from the lanthanide to the edge of the phenyl group of around 5.2 Å providing a reasonable estimate for **75** where the phenanthridine moiety is in a similar position[14]. Assuming that the spacer group in **71** is a linear peptide, there are three extra bonds in length compared to the spacer group in **75**. A 1 Å increase in length is assumed for each bond in a linear peptide chain and this gives an approximate donor-acceptor distance of 8.2 Å.

Using these values the efficiencies of energy transfer can be calculated, however use of these numbers leads to a calculated efficiency of energy transfer for complex **8** of greater than one. No process in this sequence can be greater than 100 % efficient, therefore some of the assumptions made must be erroneous.

The problem could be the assumption of the quantum yield of triplet formation for phenanthridine being the same as that for phenanthrene. In the case of napthalene (Φ_T = 0.8), quinoline (Φ_T = 0.31) and isoquinoline (Φ_T = 0.21) the quantum yields differ considerably on nitrogen substitution, at room temperature in a polar solvent[1]. Also this value may be expected to change depending upon whether the phenanthridine nitrogen is co-ordinating or not to the heavy lanthanide ion. Therefore, the approximation of the quantum yield of phenanthridine being the same as that of phenanthrene may not be reasonable.

The efficiency is also proportional to the natural radiative lifetime (equation 5.2). This calculated value may be too high at 9.67 ms. The longest known europium emission lifetime reported in D_2O is that of the europium complex of perdeuterio dota at 4.2 ms. Therefore, a more reasonable approximation for k_0 (in the complex) may be around 5 ms. Using this value for k_0 and the assumed value for Φ_T, values for the efficiency of energy transfer can be calculated and are displayed in Table 5.2.

Complex	R_{DA} / Å	η_{ET}
8	2.5	59 %
75	5.2	16 %
71	8.2	3.4 %

Table 5.2 Efficiencies of energy transfer for complexes **8**, **75** and **71** in D_2O (298 K, pH 6)

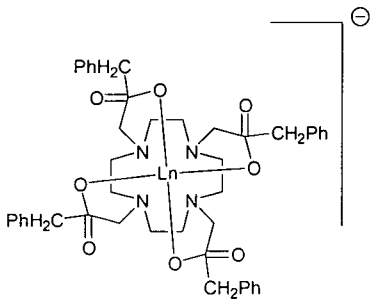

2

For complex **8** the efficiency of energy transfer is 59 % this gives a value of 2.66 Å for R_0. However, use of this value gives the efficiency of energy transfer for complexes **75** and **71** to be 1.8 % and 0.1 % respectively. The value of R_0 is also small compared to the previously calculated value[11] of 3.88 Å for the tetrabenzyl phosphinate complex, **2**. Therefore, for complex **8**, a different mechanism may be in

operation perhaps the Dexter mechanism. Values of R_0 can also be calculated for complexes **75** and **71** and they are 3.9 Å and 4.7 Å respectively, this suggests that for these complexes with the donor slightly further away that the Förster mechanism may be in operation with an R_0 between these limits.

5.5 Conclusions

The synthetic groundwork of a system suitable for studying the distance dependence of energy transfer between phenanthridine and europium has been successfully laid. It has been shown that the quantum yield of emission decreases with the distance between the donor and acceptor. The complex with the directly bound phenanthridine nitrogen undergoes relatively efficient energy transfer possibly via the Dexter mechanism while the two complexes with more distant donors, exhibit behaviour which suggests that a Förster mechanism may operate with an R_0 value of around 4 Å.

5.6 References for chapter 5

[1] *Handbook of Photochemistry 2nd ed.*, Murov S. L., Carmichael I., Hug G. L., Dekker, 1993, New York.

[2] Parker D., Senanayake K., Williams J. A. G., *J. Chem. Soc. Chem. Commun.*, **1997**, 1777.

[3] Stryer L., Haugland R. P., *Proc. Natl. Acad. Sci. USA*, **1967**, 58, 720.

[4] Woods M., PhD thesis, University of Durham, 1998.

[5] Bryce M. R., Eaves J. G., Parker D., Howard J. A. K., Johnson O., *J. Chem. Soc., Perkin Trans. 2*, **1985**, 433.

[6] Parker D., Senanayake K., Williams J. A. G., *J. Chem. Soc., Perkin Trans. 2*, **1998**, 2129.

[7] Gilman H., Eisch J., *J. Am. Chem. Soc.*, **1955**, 77, 6359.

[8] *The Practice of Peptide Synthesis 2nd ed.*, Bodanszky M., Bodanszky A., Springer-Verlag, Berlin, 1994.

[9] Demas J. N., Crosby G. A., *J. Phys. Chem.*, **1971**, 75, 8, 991.

[10] *Handbook of Organic Photochemistry*, Scaiano J. C., CRC Press, 1989, Boca Raton, Florida.

[11] Murru M., Parker D., Williams, G., Beeby A., *J. Chem. Soc., Chem. Commun.*, **1993**, 1116.

[12] *The Absorption and Fluorescence Spectra of Rare Earth Ions in Solution*, Carnell W. T., in *Handbook of the Physics and Chemistry of Rare Earths*, eds. Schneider K. A. G., Eyring L., North Holland, 1979.

[13] Aime S., Batsanov A. S., Botta M., Howard J. A. K., Lowe M. P., Parker D., *New J. Chem.*, **1999**, 23, 669.

[14] Dickins R. S., Howard J. A. K., Maupin C.L., Moloney J. M., Parker D., Riehl J. P., Siligardi G., Williams J. A. G., *Chem. Eur. J.*, **1999**, 5, 1095.

Chapter 6

Experimental

Chapter 6

Experimental

6.1 General Experimental

Reactions requiring an inert atmosphere or anhydrous conditions were carried out under a dynamic atmosphere of argon using standard Schlenk line techniques. Solvents were dried from an appropriate drying agent when required and water was purified by the "Purite$_{STILL}$ plus" system.

Thin layer chromatography was carried out using neutral aluminium oxide plates (Merck Art 5550) or silica plates (Merck Art 5554), both of these being fluorescent on irradiation at 254 nm. Preparative column chromatography was carried out using silica (Merck silica gel 60, 230-400 mesh).

IR spectra were recorded with a Perkin-Elmer 1600 FT-IR spectrophotometer operating with GRAMS Analyst software using a 'Golden Gate' accessory.

Mass spectra (CI) were recorded using a VG autospec 7070E spectrometer using ammonia as the impingent gas. Electrospray mass spectra were recorded using a VG Platform II spectrometer (Fisons Instruments) with methanol as the carrier solvent.

Proton NMR spectra were recorded on a Varian VXR 400 (65.26 MHz), Varian VXR 200 (199.99 MHz), Varian Gemini 200 (199.99 MHz), Varian Mercury 200 (199.99 MHz) or Varian Unity 300 (299.91 MHz). Carbon NMR spectra on Varian Mercury 200 (50.29 MHz), Varian Unity 300 (75.41 MHz), Varian VXR 400 (100.58 MHz) and a Bruker AMX 500 spectrometer (125.77 MHz). Deuterium NMR spectra were recorded on a Bruker AMX 500 spectrometer (76.77 MHz). Spectra were referenced to solvent residual proton resonances. All chemical shifts (δ) are reported in ppm and coupling constants are reported in Hz.

Melting points were measured using a Reichart Köfler block and are uncorrected.

Optical rotations were measured on a Bellingham and Stanley Ltd. P20 polarimeter and are calculated according to equation 6.1.

$$[\alpha]_D = \frac{100 \times \theta}{cl} \qquad \textbf{6.1}$$

Where θ = observed rotation in degrees

c = concentration in g/100mL

l = cell pathlength in dm.

Elemental analyses were determined on an Exeter Analytical CE440 Elemental Analyser.

6.2 Photophysical Measurements

6.2.1 Instrumentation

Ultraviolet absorbance spectra were recorded on a Unicam UV/Vis spectrometer UV2 operating with Unicam Vision software. Extinction co-efficients were calculated using the Beer-Lambert law (equation 6.2)

$$A = \varepsilon cl \qquad \textbf{6.2}$$

Where A = absorbance

ε = extinction co-efficient in $dm^3\ mol^{-1}\ cm^{-1}$

c = concentration in mol dm^{-3}

l = cell pathlength in cm.

Two spectrometers were used during this work for recording luminescence spectra and luminescent lifetimes, a Perkin Elmer LS 50B and an Instruments SA Fluorolog 3-11 equipped with a Spex 1934D3 phosphorimeter.

The light source for the **LS 50B** is a xenon flash tube which produces a short duration pulse of radiation with a full width at half maximum intensity of less than 10 μs. The excitation wavelength is then selected using a single grating monochromator. The light emitted from the sample is focused onto the entrance slit

of the single grating emission monochromator and the intensity is measured using a Hamamatsu R928 photomultiplier tube.

The **Fluorolog** can operate either as a fluorimeter or phosphorimeter depending on the excitation source. For spectra a 450 W high pressure xenon lamp is used. As with the LS 50B the excitation and emission wavelengths are selected using single grating monochromators with the intensity being measured using a Hamamatsu R928 photomultiplier tube. For time resolved measurements a xenon flash tube is used which produces a pulse of radiation with a full width at half maximum intensity of 3 μ_s.

6.2.2 Spectra

Gratings, detectors and other components in a spectrometer have characteristic wavelength dependent responses. These characteristics are superimposed on spectra, yielding a potentially misleading spectrum. To ensure that spectra are indicative of the actual properties of the sample raw spectra must be corrected. This is especially important for such measurements as quantum yield determinations where accurate intensity comparisons are required. Correction is usually carried out by use of a correction spectrum which takes into account the wavelength-dependent responses of the instrument and scales the collected signal accordingly.

Other effects that require correction in luminescence spectra include correcting for a non-zero baseline and second order diffraction effects. The first of these may be corrected by running a blank sample and subtracting this from the obtained spectra. Second order diffraction effects occur when scattered light from a sample is transmitted by the monochromator at double the wavelength of the excitation light. For instance a sample excited at 355 nm has an apparent emission at 710 nm. This is corrected by using a cut-off filter to remove the scattered light before it enters the emission monochromator, for the above example a 380 nm cut-off filter would be used.

6.2.3 Europium and Terbium Lifetime Measurements

Excited state lifetime measurements for europium and terbium were made on either the Perkin Elmer LS 50B (using *Phlemming* data acquisition written by Dr. A. Beeby, University of Durham) or the Instruments SA Fluorolog (using DataMax for Windows v2.1). Lifetimes were measured by excitation of the sample by a short pulse of light (355 nm for terbium, 397 nm for europium) followed by monitoring the integrated intensity of light (545 nm for terbium, 594 nm or 619 nm for europium) emitted during a fixed gate time, t_g, a delay time, t_d, later, this is shown in Figure 6.1. At least 20 delay times were used covering 3 or more lifetimes. Typically gate times of between 100 and 250 μs were used, and the excitation and emission slits were set to 5-15 nm bandpass. The obtained decay curves were fitted to equation 6.3 using either Grafit 3.0 (Erithacus software) or Microsoft Excel.

$$I = A_0 + A_1\exp(-kt) \qquad \textbf{6.3}$$

where I = intensity at time t after the flash

A_0 = intensity after the decay has finished

A_1 = pre-exponential factor

k = rate constant for decay of the excited state.

The excited state lifetime, τ, is the inverse of the rate constant, k.

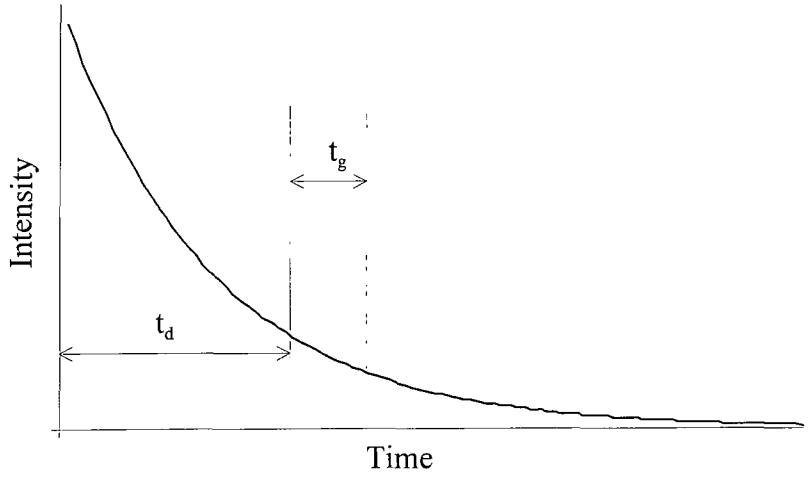

Figure 6.1 Measured parameters for lifetime measurements

6.2.4 Neodymium Lifetime Measurements

Neodymium lifetimes were measured using a home built ns-laser pumped fluorimeter. A schematic of the system is shown in Figure 6.2.

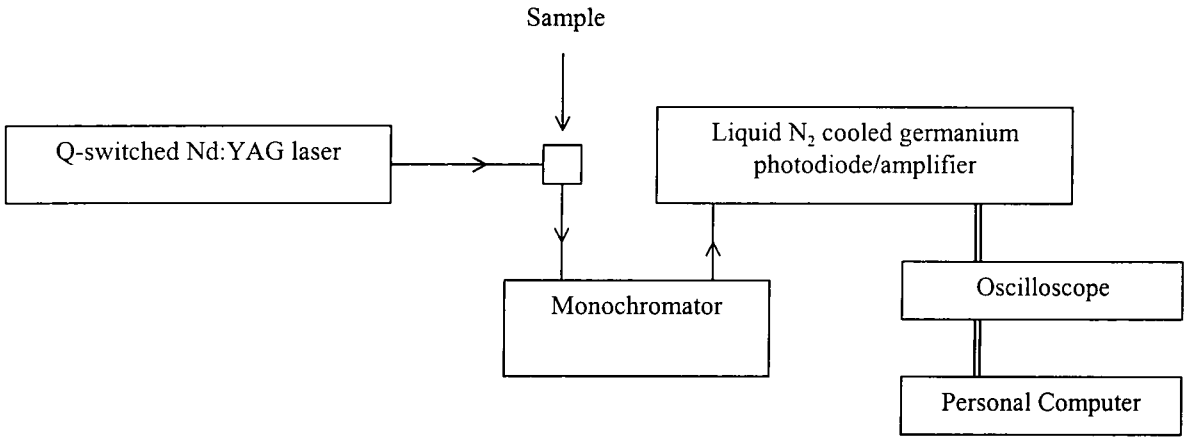

Figure 6.2 Schematic of a ns-laser pumped fluorimeter

The frequency tripled output of a Q-switched Nd:YAG laser (Spectra Physics GCR-150-10) operating at 10 Hz was focussed onto the samples contained in a 1 cm quartz fluorescence cuvette. Typical pulse energies at the sample were between 0.1 and 2 mJ with a pulse duration of around 6 ns. Residual 1064 and 532 light in the excitation beam was avoided by using optical filters. The luminescence was collected at 90° and focussed onto the entrance slits of a 320 mm focal length monochromator (SPEX Triax 320) set to 1055 nm. The bandpass of the monochromator was in the range 1-5 nm FWHM. The selected radiation was focused onto the active area of a liquid nitrogen cooled germanium diode/amplifier (North Coast EO-817P) operating in high speed mode, this has a rise time *c.a.* 200 ns and a FWHM of 400 ns. The luminescence signal was captured and averaged by a digital storage oscilloscope (Tektronix TDS320) and transferred to a PC for analysis.

6.2.5 Ytterbium Lifetime Measurements

For direct excitation of the ytterbium ion the output from a Nd:YAG driven optical parametric oscillator was used, producing photons at 970 nm. Emission from the sample was observed in the low energy tail of the emission profile by use of a 1050

nm interference filter with a 40 nm bandpass. A polariser was used to reduce scattered light from the laser. Lifetimes were obtained either through iterative re-convolution or fitting the tail of the data to an exponential decay function.

6.2.6 Convolution, Deconvolution and Reconvolution

The observed decay function, I(t), recorded for neodymium and ytterbium samples is a convolution of the response of the instrument, F(t), and the response of the system under study, G(t).

$$I(t) = F(t) \otimes G(t) \qquad \textbf{6.4}$$

F(t), the instrument response function (IRF), is obtained by using a scatterer or a near-IR fluorophore with a very short lifetime. In this work the laser dye DCM (4-dicyanmethylene-2-methyl-6-(*p*-dimethylaminostyryl)-4H-pyran) in methanol is used. This has a fluorescence lifetime of 2.2 ns. The temporal response of this solution will be approximately the same as that of the laser pulse, this response gives the instrument response function. Knowing the IRF it should then be possible to extract the sample response from the observed decay by deconvolution. In practice this is difficult so the method of iterative reconvolution followed by least squares fitting is used. In this method the response of the system, G(t), is modelled by a decay function (usually a single exponential decay) this function is then convolved with the known IRF to give a calculated response function, typical examples of these functions can be seen in figure 6.3. The variables of this calculated function can then be varied iteratively until the best fit with the experimentally determined I(t) is obtained.

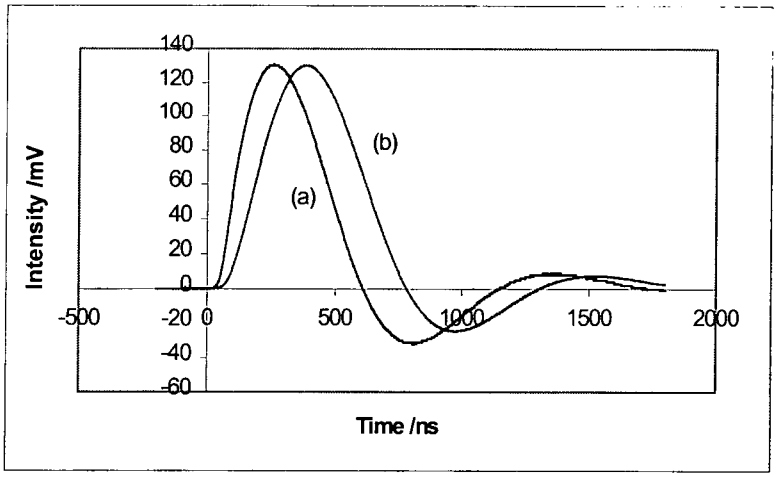

Figure 6.3 The convolution of the IRF (a) with a single exponential decay (b), τ = 150ns

This fitting was done using the solver function on Microsoft Excel to minimise the sum of the squares of the differences between the actual and calculated data. The quality of the fit can be judged by examining the randomness of the residuals.

6.2.7 Quantum Yield Determination

The quantum yield for a given process is defined as the total number of photons emitted by that process divided by the total number of photons absorbed. The techniques and equipment necessary to make an absolute determination of quantum yields are not generally available. Therefore the usual method is to determine a relative quantum yield where the compound of unknown yield is compared to a compound of known yield[1]. The unknown quantum yield can then be calculated using the following equation.

$$\Phi_x = \Phi_r \cdot \frac{A_r}{A_x} \cdot \frac{E_x}{E_r} \cdot \frac{I_r}{I_x} \cdot \frac{n_x^2}{n_r^2} \qquad \textbf{6.5}$$

Where *r* and *x* refer to reference and unknown respectively

A = absorbance at λ_{ex}

E = corrected integrated emission intensity

I = corrected intensity of excitation light

(as all of the measurements were taken using identical excitation conditions this term can be ignored)

n = refractive index of solution.

In practice the measurement was made relative to two known standards. For europium complexes these were Rhodamine 101 in ethanol (Φ = 1) and cresyl violet in methanol (Φ = 0.54)[2]. These standards were chosen as they emit in a similar spectral window to europium. For each of the standards and the unknown, five solutions with absorbances between 0.02 and 0.1 were used. For each of these solutions the absorbance at the excitation wavelength and the total integrated emission was determined. A plot of total integrated emission against absorbance gives a straight line with slope E/A. The unknown quantum yield can thus be calculated from the following equation.

$$\Phi_x = \Phi_r \cdot \frac{slope_x}{slope_r} \cdot \left(\frac{n_x}{n_r}\right)^2 \qquad \textbf{6.6}$$

Errors in quantum yield determinations can arise due to the inner filter effect or errors in the amount of absorbed light. The first of these can be very important when using references such as Rhodamine 101 and cresyl violet as these are both strongly absorbing in the emission region. This effect can be minimised by only using samples with absorbances below 0.2. Errors in the amount of light absorbed by each sample can be minimised by choosing the excitation wavelength to be on a relatively flat area of the absorption curve and by using a small bandpass for excitation.

6.3 Experimental for Chapter 2

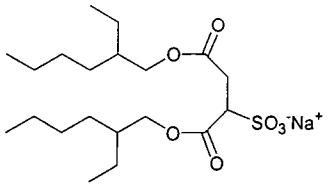

Aerosol OT

$Ln(AOT)_3.xH_2O(D_2O)$

Aliquots of $Ln(NO_3)_3$ in either H_2O or D_2O (25 mL, 0.5 mol dm^{-3}), NaAOT in ethanol (25 mL, 0.3 mol dm^{-3}) and ether (25 mL) were thoroughly mixed resulting in a Winsor-II microemulsion. Additional ether (25 mL) was then added to induce phase separation. The organic layer was extracted and washed with portions of either H_2O or D_2O (5 x 25 mL). The solvent was then removed under reduced pressure and the resulting waxy solid dried under vacuum at 40°C for 48 h before use.

$Eu(AOT)_3$

m/z (FAB) 995 ($Eu(AOT)_2^+$).

Found C, 50.2; H, 7.98; Na, 0.35%. $C_{60}H_{111}O_{21}S_3Eu.H_2O$ requires C, 50.2; H, 7.96 %.

$Nd(AOT)_3$

m/z (FAB) 986 ($Nd(AOT)_2^+$).

Found C, 49.2; H, 7.93; Na, 0.12%. $C_{60}H_{111}O_{21}S_3Nd.H_2O$ requires C, 50.5; H, 8.01 %.

$Tb(AOT)_3$

m/z (FAB) 1002 ($Tb(AOT)_2^+$).

Found C, 48.0; H, 7.95; Na, 0.23%. $C_{60}H_{111}O_{21}S_3Tb.H_2O$ requires C, 50.0; H, 7.93 %.

Water in Cyclohexane Microemulsions

The microemulsions were prepared by the addition of aliquots of H_2O or D_2O to a cyclohexane solution of the $Ln(AOT)_3.xH_2O(D_2O)$ complex and sonicated to give clear solutions. The concentration of AOT^- was always 0.1 mol dm^{-3}. For all the

lanthanide salts the maximum water solubilisation, w_{max}, was 12.0 $\pm$ 1.0 at 25 °C. The effect of co-dissolved sodium ions was investigated by sonication of aliquots of 0.1 mol dm^{-3} NaAOT in cyclohexane with 0.033 mol dm^{-3} $Tb(AOT)_3$ solutions. Water was then added to vary *w*.

6.4 Experimental for Chapter 4

N-p-Tolylsulfonyl-3-azapentan-1,5-dioic acid, 33

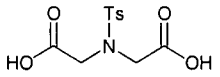

Iminodiacetic acid (40 g, 301 mmol) and tosyl chloride (60 g, 314 mmol) were stirred at 50°C in water (300 mL) with the pH maintained at 10 by addition of aqueous sodium hydroxide solution (2 mol dm^{-3}). After 20 h, the pH was adjusted to 5 and the resulting white precipitate collected. Drying under vacuum gave a white solid (76 g, 265 mmol, 88 %).

Mp 190 °C (lit.[3] 191 °C).

$\delta_H(D_2O)$: 2.56 (s, 3H, Ar-CH_3), 3.86 (s, 4H, -CH_2-), 7.28 (d, 2H, Ar, J=8.2 Hz), 7.58 (d, 2H, Ar, J=8.2 Hz).

Dimethyl-N-*p*-tolylsulfonyl-3-azapentane-1,5-dioate, 34

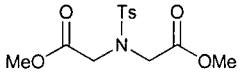

A solution of the acid **33** (20 g, 69.7 mmol) and concentrated sulphuric acid (8 mL) in methanol (150 mL) was stirred at reflux under argon for 24 h. The reaction mixture was then neutralised with potassium carbonate and the solvents removed under reduced pressure. The resulting solids were partitioned between water (100 mL) and dichloromethane (100 mL), the dichloromethane layer was washed with water (100 mL), dried over anhydrous potassium carbonate and the solvents removed under reduced pressure to yield a white solid (16.7 g, 53.0 mmol, 76%).

Mp 97-98 °C (lit.[4] 100-101 °C).

$\delta_H(CDCl_3)$: 2.42 (s, 3H, Ar-CH_3), 3.66 (s, O-CH_3), 4.20 (s, 4H, -CH_2-), 7.30 (d, 2H, Ar, J=8.0 Hz), 7.72 (d, 2H, Ar, J=8.4 Hz).

Bis(trideuteriomethyl) N-p-tolylsulfonyl-5-aza-2,2,4,4-tetradeuteriopentane-1,5-dioate, 35

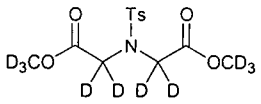

An excess of d_4-methanol (30 mL) was added to the ester, **34**, (1.46 g, 4.63 mmol) and freshly cut sodium metal (10 mg, 0.43 mmol, cat.). The resulting solution was stirred under argon with occasional heating for two h. DOWEX 50 Ion exchange resin was then added and stirring continued for 20 min. The solution was filtered while hot and the solvents removed under reduced pressure to give a white crystalline solid (1.54 g, 4.46 mmol, 96%).

Mp 96-98 °C.

$\delta_H(CDCl_3)$: 2.42 (s, 3H, Ar-CH_3), 7.59 (d, 2H, Ar, *J*=8.1 Hz) ,7.31 (d, 2H, Ar, *J*=8.1 Hz).

$\delta_D(CHCl_3)$: 3.62 (s, 6D, O-CD_3), 4.17 (s, 4D, -CD_2-).

$\delta_C\{^1H\}(CDCl_3)$: 15.2 (s, -CH_3), 47.5 (p, -CD_2-, *J*=21 Hz), 51.5 (nonet, -CD_3, *J*=21 Hz), 127.3 (s, Ar), 129.5 (s, Ar), 136.4 (s, Ar), 143.8 (s, Ar), 169.1 (s, *C*=O).

m/z (CI): 326 (M^+ + 1); found 343.1748; $C_{13}H_7D_{10}NO_6S + NH_4^+$ requires 343.1755.

ν/cm^{-1}:1496m, 1595m,1743s (C=O), 2081w, 2182w, 2263w, 2361w.

Found C, 47.6; H, 5.31; N, 4.09. $C_{13}H_7D_{10}NO_6S$ requires C, 48.0; H, 5.22; N, 4.30%.

N-p-Tolylsulfonyl-1,1,2,2,4,4,5,5-octadeuterio-3-azapentane-1,5-diol, 36

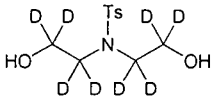

Lithium aluminium deuteride (0.275 g, 8.3 mmol) was added gradually to a solution of the deuteriated ester, **35**, (1.0 g, 3.07 mmol) in THF (50 mL) with stirring under argon and the mixture was heated to reflux for 2 h. The resulting yellow-green suspension contained excess lithium aluminium deuteride which was quenched by careful addition of water (10 mL). The solvents were removed under reduced pressure and the resulting solids partitioned between hydrochloric acid (2 M, 50 mL) and diethyl ether (50 mL). The aqueous layer was extracted with ether (3 x 50mL) and the combined ether extracts were dried over anhydrous magnesium sulphate and

the solvents removed under reduced pressure to yield a white crystalline solid (0.68 g, 2.55 mmol, 83%).

Mp 90-91 °C.

$\delta_H(CDCl_3)$: 2.44 (s, 3H, Ar-CH_3), 7.34 (d, 2H, Ar, J=8.6 Hz), 7.71 (d, 2H, Ar, J=8.3 Hz).

$\delta_D(CHCl_3)$: 3.23 (s, 4D), 3.83 (s, 4D).

$\delta_C\{^1H\}(CDCl_3)$: 21.5 (s), 52 (m), 61 (m), 127.3 (s), 129.8 (s), 135.2 (s), 143.7 (s).

m/z (CI) 268 ($M^+ + 1$), 285 ($M + NH_4^+$).

ν/cm^{-1}: 1336s, 1490w, 1596m, 2086w, 2200w, 2236w (C-D), 3232br,m (O-H).

Found C, 49.4; H, 6.49; N, 5.08. $C_{11}H_9D_8NO_4S$ requires C, 49.1; H, 6.32; N, 5.20%.

N-p-Tolylsulfonyl-1,5-bis(p-tolylsulfonyloxy)-3-aza-1,1,2,2,4,4,5,5-octadeuteriopentane, 37

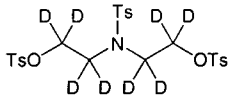

A solution of the deuteriated diol, **36**, (0.46 g, 1.72 mmol) and toluene-4-sulfonyl chloride (2.6 g, 13.6 mmol) in pyridine (15 mL) under argon was kept at -18 °C for 3 weeks. Water (15 mL) was then added resulting in formation of a precipitate, which was collected and dried under vacuum to give a white solid (0.813 g, 1.41 mmol, 82%).

Mp 75-77 °C.

$\delta_H(CDCl_3)$: 2.43 (s, 3H, Ar-CH_3), 2.46 (s, 6H, Ar-CH_3), 7.29 (d, 2H, Ar, J= 8.2 Hz), 7.36 (d, 4H, Ar, J= 8.1 Hz), 7.61 (d, 2H, Ar, J= 8.6 Hz), 7.76 (d, 4H, Ar, J= 8.4 Hz).

$\delta_D(CHCl_3)$: 3.33 (s, 4D), 4.08 (s, 4D).

ν/cm^{-1} (gg): 3066w, 2956w, 2916w, 2161w, 2034w, 1596m, 1494w, 1340s, 1163s, 971s.

Found C, 52.2; H, 4.92; N, 2.57. $C_{25}H_{21}D_8NO_8S_3$ requires C, 52.2; H, 5.04; N, 2.43%.

N-p-Tolylsulfonyl-1,5-bis(methylsulfonyloxy)-3-aza-1,1,2,2,4,4,5,5-octadeuteriopentane, 41

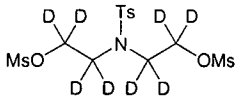

A solution of diisopropylethylamine (0.474 mL, 6.12 mmol) in dichloromethane (25 mL) was added to a stirred solution of deuteriated diol, **36**, (0.75 g, 2.79 mmol) and methanesulfonyl chloride (1.07 mL, 6.12 mmol) in dichloromethane (25 mL) at 0 °C, under an atmosphere of argon over a period of 15 min. When the addition was complete the reaction mixture was washed with saturated sodium carbonate solution (30 mL) then hydrochloric acid (1M, 30 mL). The organic layer was dried over anhydrous potassium carbonate and the solvents removed under reduced pressure to yield a light yellow oil. Crystallisation was encouraged by addition of methanol to yield a light yellow crystalline solid (1.14 g, 2.70 mmol, 97%).

Mp 61-62 °C.

$\delta_H(CDCl_3)$: 2.44 (s, 3H, Ar-CH_3), 3.06 (s, 6H, SO_2-CH_3), 7.36 (d, 2H, Ar, J=8.0 Hz), 7.71 (d, 2H, Ar, J=8.3 Hz).

$\delta_D(CHCl_3)$: 3.46 (s, 4D), 4.38 (s, 4D).

$\delta_C\{^1H\}(CDCl_3)$: 21.5, 37.4, 127.2, 130.0, 134.8, 144.3.

m/z (ES+): 424 (M^+ + 1) 5 %, 446 (M^+ + Na) 100%.

ν/cm^{-1} (gg): 3030w, 2939w, 2364w, 1597w, 1326s, 1171s, 960s, 815s, 669s, 522s.

Found C, 37.2; H, 5.15; N, 3.10. $C_{13}H_{13}D_8NO_8S_3$ requires C, 36.9; H, 4.96; N, 3.31%.

N-p-Tolylsulfonyl-1,5-diazido-3-aza-1,1,2,2,4,4,5,5-octadeuteriopentane, 42

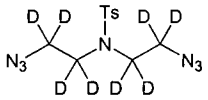

To a solution of deuteriated bis(mesylate), **41**, (0.25 g, 0.60 mmol) in dimethylformamide (5 mL) was added sodium azide (1.5 g, 23 mmol). The resulting suspension was stirred under argon at 40 °C for 12 h. The reaction mixture was diluted with ether (100 mL) and washed with water (8 x 25 mL). The organic layer

was then dried over anhydrous potassium carbonate and the solvents removed under reduced pressure to yield a white crystalline solid (0.18 g, 0.58 mmol, 95%).

Mp 40-42 °C.

$\delta_H(CDCl_3)$: 2.45 (s, 3H, Ar-CH_3), 7.35 (d, 2H, Ar, J=8.1 Hz), 7.72 (d, 2H, Ar, J=8.2 Hz).

$\delta_D(CHCl_3)$: 3.27 (s, 4D), 3.51 (s, 4D).

$\delta_C\{^1H\}(CDCl_3)$: 21.6 (s), 48.2 (m), 50.0 (m), 127.2 (s), 130.0 (s), 135.8 (s), 144.1 (s).

m/z (CI): 318 ($M^+ + 1$) , 335 ($M + NH_4^+$).

ν/cm^{-1} (gg): 601s, 677s, 1168s, 1280s, 1339s, 1489m, 1593m, 2093s (azide), 2195w, 2362w, 2552w, 2922w, 3058w, 3362w.

Found C, 42.0; H, 4.88; N, 29.9. $C_{11}H_7D_8N_7O_2S$ requires C, 41.6; H, 4.73; N, 30.9%.

N-p-Tolylsulfonyl-3-aza-1,1,2,2,4,4,5,5-octadeuteriopentane-1,5-diamine, 43

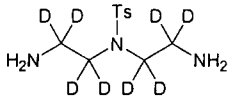

A solution of deuteriated diazide, **42**, (1.05 g, 3.31 mmol) in THF (10 mL) was added dropwise to a stirred suspension of lithium aluminium hydride (0.314 g, 8.28 mmol) in THF (10 mL) under an argon atmosphere at -10 °C. After complete addition the temperature was raised to 10 °C for 30 mins. Sodium hydroxide solution (5 %, 0.7 mL) was added and the reaction mixture stirred for 18 h. The resultant precipitate was filtered and the solvents removed under reduced pressure to yield a light yellow oil (0.87 g, 3.28 mmol, 99%). The hydrochloride salt was prepared, for elemental analysis, by bubbling HCl gas through a solution of the amine in ether, the salt precipitating out as a colourless solid.

$\delta_H(CDCl_3)$: 2.38 (s, 3H, Ar-CH_3), 7.26 (d, 2H, Ar, J=8.2 Hz), 7.65 (d, 2H, Ar, J=8.4 Hz).

$\delta_D(CHCl_3)$: 2.84 (s), 3.09 (s).

$\delta_C\{^1H\}(CDCl_3)$: 21.5 (s), 40.3 (p, J=21 Hz), 51.8 (p, J=21 Hz), 127.2 (s), 129.8 (s), 136.1 (s), 143.4 (s).

m/z (CI): 266 ($M^+ + 1$).

ν/cm^{-1} (as HCl salt, gg): 2989 br s, 1598m, 1482m, 1342m.

Found C, 38.7; H, 6.32; N, 12.0. $C_{11}H_9D_8N_3SO_2.2HCl$ requires C, 39.0; H, 6.26; N, 12.4 %.

1,3,5-Tris(p-tolylsulfonyl)-3-aza-1,1,2,2,4,4,5,5-octadeuteriopentane-1,5-diamine, 44

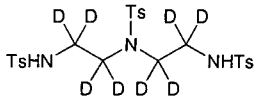

Deuteriated diamine, **43**, (0.73 g, 2.75 mmol) and tosyl chloride (1.31 g, 6.88 mmol) were stirred at 50°C in water (25 mL) with the pH maintained at 10 by addition of aqueous sodium hydroxide solution (2 mol dm^{-3}). After 20 h the pH was adjusted to 5 and the resulting white precipitate collected and washed with cold water (3 x 10 mL). Drying under vacuum gave a white solid (0.97 g, 1.69 mmol, 62 %).

Mp 171-172 °C.

$\delta_H(CDCl_3)$: 2.38 (s, 3H, Ar-CH_3), 7.26 (d, 2H, Ar, J=8 Hz), 7.62 (d, 2H, Ar, J=8 Hz).

$\delta_D(CHCl_3)$: 3.11 (s).

$\delta_C\{^1H\}(CDCl_3)$: 21.8 (-CH_3), 127.4 (2Ts), 127.5 (1Ts), 130.0 (2Ts), 130.2 (1Ts), 134.9 (1Ts), 136.9 (2Ts), 143.8 (2Ts), 144.4 (1Ts).

m/z (FAB, glycerol): 682 (M^+ + 1).

Found C, 51.9; H, 5.45; N, 7.24. requires C, 52.3; H, 5.40; N, 7.32.

1,4,7,10-Tetrakis(p-tolylsulfonyl)-2,2,3,3,5,5,6,6,8,8,9,9,11,11,12,12-hexadecadeutero-1,4,7,10-tetraazacyclododecane, 45

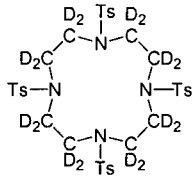

A suspension of deuteriated ditosylate, **37**, (0.43 g, 0.75 mmol), deuteriated tosylated triamine, **44**, (0.45 g, 0.75 mmol) and caesium carbonate (0.49 g, 1.5 mmol) in DMF (3 mL) was heated at 60 °C for 48 h, 70 °C for a further 48 h and finally 95 °C for 12 h. The solvents were then removed under reduced pressure and the resulting solids partitioned between dichloromethane (10 mL) and water (10 mL). The

aqueous layer was further extracted with dichloromethane (2 x 10 mL). The combined organic layers were dried over anhydrous potassium carbonate and the solvents were removed under reduced pressure to give a white solid (0.26 g, 0.323 mmol, 43 %).

Mp > 250 °C.

$\delta_H(CDCl_3)$: 2.44 (s, 12H, Ar-CH_3), 3.43 (br, 1H, residual CHD), 7.33 (d, 8H, Ar, J = 8 Hz), 7.69 (d, 8H, Ar, J = 8 Hz).

$\delta_D(CHCl_3)$: 3.45 (s).

$\delta_C\{^1H\}(CDCl_3)$: 21.5 (s), 50-53 (m), 127.7 (s), 129.9 (s), 133.9 (s), 143.9 (s)

2,2,3,3,5,5,6,6,8,8,9,9,11,11,12,12-Hexadecadeutero-1,4,7,10-tetraazacyclododecane, 46

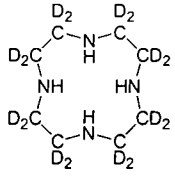

A solution of deuteriated tetratosylated tetraamine, **45**, (324 mg, 0.43 mmol) in conc. sulphuric acid (0.7 mL) was heated under argon at 110°C for 48 h. The resulting dark solution was cooled to 0°C, water (2 mL) added and the pH adjusted to 13 using KOH pellets. Ethanol (10 mL) was added and the suspension was filtered, the residual solids being washed with further ethanol (3 x 10 mL). The solvents were removed under reduced pressure to give a yellow solid. This solid was dissolved in the minimum quantity of hydrochloric acid (0.1 mol dm^{-3}, 1-2 mL) and this aqueous layer was washed with dichloromethane (3 x 5mL). The pH of the aqueous layer was raised to >13 by addition of KOH pellets and the further extracted with chloroform (5 x 5 mL). The combined organic extracts were dried over anhydrous potassium carbonate and then solvents were removed under reduced pressure to yield a colourless solid (0.075 g, 0.40 mmol, 93 %).

Mp 100-102 °C.

$\delta_D(CHCl_3)$: 2.69 (s).

$\delta_C\{^1H\}(CDCl_3)$: 46.0 (pent, J = 21 Hz).

1,4,7,10-Tetrakis(ethoxycarboxymethyl)-2,2,3,3,5,5,6,6,8,8,9,9,11,11,12,12-hexadecadeuterio-1,4,7,10-tetraazacyclododecane, 77

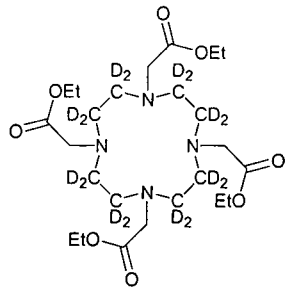

A suspension of deuteriated tetraamine, **46**, (59 mg, 0.31 mmol), ethyl bromoacetate (0.141 mL, 1.27 mmol), potassium iodide (10 mg, 60 mmol) and caesium carbonate (564 mg, 1.73 mmol) in DMF (20 mL) was stirred under argon at 80 °C for 18 h. The solvent was removed under reduced pressure and the residue suspended in dichloromethane (20 mL) and filtered through Celite which was thoroughly washed with dichloromethane (2 x 10 mL) and chloroform (2 x 10 mL). The combined filtrates were evaporated under reduced pressure to give a colourless solid (0.145 g, 0.26 mmol, 84 %) which was hydrolysed without further purification.

$\delta_H(CDCl_3)$: 1.27 (t, 12H, -C*H*$_3$, J = 7.2 Hz), 3.19 (br s, 8H, C*H*$_2$CO), 4.19 (q, 8H, C*H*$_2$O, J = 7.2 Hz).

$\delta_C\{^1H\}(CDCl_3)$: 14.0 (-*C*H$_3$), 47.8 (br), 51.5 (br), 54.9 (*C*H$_2$CO), 61.1 (*C*H$_2$O), 173.5 (*C*=O).

m/z (ES+): 555 ($M^+ + 1$).

1,4,7,10-Tetrakis(carboxymethyl)-2,2,3,3,5,5,6,6,8,8,9,9,11,11,12,12-hexadecadeuterio-1,4,7,10-tetraazacyclododecane, 47

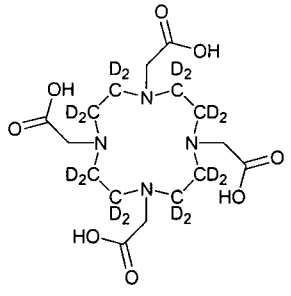

The tetra-ethyl ester, **77**, (145 mg, 0.26 mmol) was dissolved in sodium hydroxide solution (1 mol dm^{-3}, 3 mL) and left at room temperature for 1 h. Hydrochloric acid (1 mol dm^{-3}, 3.1 mL) was added to give a solution pH of *ca.* 2.5. The volume of this

solution was reduced until a crystalline solid began to form which was separated by filtration to give a colourless solid (99 mg, 0.23 mmol, 88 %). Crystallographic analysis of the ligand obtained under similar crystallisation conditions revealed that the solid was the oxonium salt of the [monodeprotonated (on carboxy group) dihydrochloride salt][5].

δ_H(pD 5): 3.24 (br s, 1H residual C*H*D), 3.61 (s, 8H).

δ_D(pD 5): 3.06.

$\delta_C\{^1H\}$(D_2O, pD 5): 48.8 (pent, *C*D_2N), 56.9 (*C*H_2CO), 178.6 (*C*=O).

N-p-Tolylsulfonyl-3-aza-pentanediamide, 38

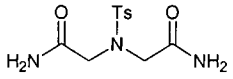

A suspension of the diester, **34**, (4.0g, 12.7 mmol) in methanol was stirred with liquid ammonia at –78 °C for 4 h. The ammonia was removed by allowing the reaction mixture to warm to room temperature followed my removal of the solvents under reduced pressure to yield a white solid (3.6 g, 12.6 mmol, 99 %).

δ_H(d_6-DMSO): 2.42 (s, 3H, Ar-C*H*$_3$), 3.78 (s, 4H, -C*H*$_2$-), 7.25 (br s, 2H, -N*H*$_2$), 7.44 (d, 2H, Ar, J = 8.2 Hz), 7.73 (d, 2H, Ar, J = 8.2 Hz), 8.06 (br s, 2H, -N*H*$_2$).

N-*p*-Tolylsulfonyl-3-azapentane-1,5-diol, h-36

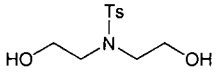

The title compound was prepared following the method described for N-p-tolylsulfonyl-1,1,2,2,4,4,5,5-octadeuterio-3-azapentane-1,5-diol, **36**.

Mp 96 °C (lit.[6] 100-101 °C).

δ_H($CDCl_3$): 2.46 (s, 3H, Ar-C*H*$_3$), 3.19 (s, -C*H*$_2$-, 4H), 3.88 (s, -C*H*$_2$-, 4H), 7.37 (d, 2H, Ar, *J*=8.5 Hz), 7.79 (d, 2H, Ar, *J*=8.5 Hz).

N-p-Tolylsulfonyl-1,5-bis(methylsulfonyloxy)-3-azapentane, h-41

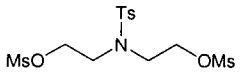

The title compound was prepared following the method described for N-p-tolylsulfonyl-1,5-bis(methylsulfonyloxy)-3-aza-1,1,2,2,4,4,5,5-octadeuteriopentane, **41**.

Mp 61-62 °C (lit.[7] 63-63.5 °C).

$\delta_H(CDCl_3)$: 2.45 (s, 3H, Ar-CH_3), 3.07 (s, 6H, SO_2-CH_3), 3.50 (t, 4H, J=5.7 Hz), 4.41 (t, 4H, J=5.8 Hz), 7.36 (d, 2H, Ar, J=8.2 Hz), 7.71 (d, 2H, Ar, J=8.3 Hz).

N-p-Tolylsulfonyl-1,5-diazido-3-azapentane, h-42

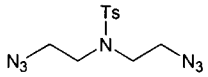

The title compound was prepared following the method described for *N-p*-tolylsulfonyl-1,5-diazido-3-aza-1,1,2,2,4,4,5,5-octadeuteriopentane, **42**.

$\delta_H(CDCl_3)$: 2.44 (s, 3H, Ar-CH_3), 3.31 (t, 4H, J=6.3 Hz), 3.13 (t, 4H, J=6.5 Hz), 7.31 (d, 2H, Ar, J=8.2 Hz), 7.70 (d, 2H, Ar, J=8.2 Hz).

m/z (ES+): 310 (M^+ + 1).

ν/cm^{-1}: 2085s (N_3), 1593m, 1491m, 1440m.

N-p-Tolylsulfonyl-3-azapentane-1,5-diamine, h-43

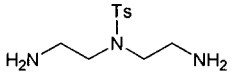

The title compound was prepared following the method described for N-p-tolylsulfonyl-3-aza-1,1,2,2,4,4,5,5-octadeuteriopentane-1,5-diamine, **43**.

$\delta_H(CDCl_3)$: 2.42 (s, 3H, Ar-CH_3), 2.87 (t, 4H, J=5.7 Hz), 4.41 (t, 4H, J=5.8 Hz), 7.36 (d, 2H, Ar, J=8.2 Hz), 7.71 (d, 2H, Ar, J=8.3 Hz).

1,3,5-Tris(*p*-tolylsulfonyl)-3-azapentane-1,5-diamine, h-44

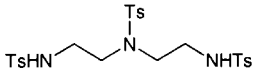

The title compound was prepared following the method described for 1,3,5-tris(p-tolylsulfonyl)-3-aza-1,1,2,2,4,4,5,5-octadeuterio-pentane-1,5-diamine, **44**.

Mp. 163 °C (lit.[8] 168-170 °C)

$\delta_H(CDCl_3)$: 2.42 (s, 9H, Ar-CH_3), 3.24 (s, 8H), 7.22 (d, 6H, Ar, J=8.1 Hz), 7.45 (d, 6H, Ar, J=8.1 Hz).

1,4,7,10-Tetrakis(*p*-tolylsulfonyl)-1,4,7,10-tetraazacyclododecane, h-45

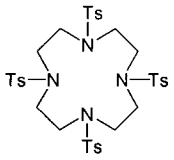

The title compound was prepared following the method described for 1,4,7,10-tetrakis(p-tolylsulfonyl)-2,2,3,3,5,5,6,6,8,8,9,9,11,11,12,12-hexadecadeuterio-1,4,7,10-tetraazacyclododecane, **45**.

Mp. > 250°C.

$\delta_H(CDCl_3)$: 2.44 (s, 12H, Ar-CH_3), 3.43 (s, 16H), 7.33 (d, 8H, Ar, J=8.0 Hz), 7.69 (d, 8H, Ar, J=8.0 Hz).

1,4,7,10-Tetraazacyclododecane, h-46

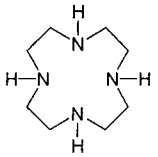

The title compound was prepared following the method described for 2,2,3,3,5,5,6,6,8,8,9,9,11,11,12,12-hexadecadeuterio-1,4,7,10-tetraazacyclododecane, **46**.

Mp 100 °C (lit. 113-114°C).

$\delta_H(CDCl_3)$: 2.58 (s).

1,4,7,10-Tetrakis(ethoxycarboxymethyl)-1,4,7,10-tetraazacyclododecane, h77

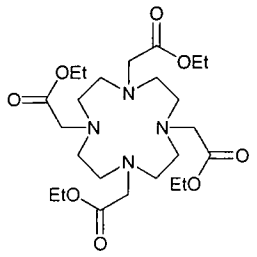

The title compound was prepared following the method described for 1,4,7,10-tetrakis(ethoxycarboxymethyl)-2,2,3,3,5,5,6,6,8,8,9,9,11,11, 12,12-hexadecadeuterio-1,4,7,10-tetraazacyclododecane, **77**.

$\delta_H(CDCl_3)$: 1.19 (t, 12H, -C*H*$_3$, J = 7.0 Hz), 4.11 (q, 8H, -OC*H*$_2$-, J = 7.0 Hz), 2.3 (br s, 16H, ring), 3.2 (br s, 8H, C*H*$_2$-CO).

$\delta_C\{^1H\}(CDCl_3)$: 14.0 (-*C*H$_3$), 48.6 (br), 52.6 (br), 55.1 (*C*H$_2$CO), 61.2 (*C*H$_2$O), 173.5 (*C*=O).

m/z (ES+): 539 (M + Na^+).

1,4,7,10-Tetrakis(carboxymethyl)-1,4,7,10-tetraazacyclododecane, 47

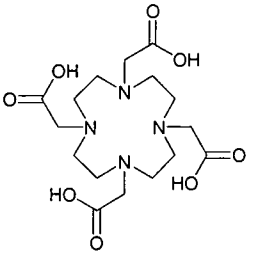

The title compound was prepared following the method described for 1,4,7,10-tetrakis(carboxymethyl)-2,2,3,3,5,5,6,6,8,8,9,9,11,11,12,12-hexadecadeuterio-1,4,7,10-tetraazacyclododecane, **47**.

$\delta_H(D_2O)$: 3.13 (br s, 16H, ring -C*H*$_2$-), 3.60 (br s, 8H, C*H*$_2$-CO-).

Complexations

The complexes were made according to a standard procedure[9]. A suspension of equimolar quantities of the ligand and the metal oxide in water (2 mL) was taken to pH 2 using hydrochloric acid (0.1 mol dm^{-3}). This suspension was heated at 70 °C for 18 h followed by adjustment of the pH to 6 by addition of aqueous sodium

hydroxide (0.1 mol dm^{-3}) and further heating for 3 h. The pH was then altered to pH 9, forming a precipitate of non-complexed lanthanide ion this was removed by filtration. The solution pH was readjusted to 6 followed by removal of the solvent by lyophilisation to give the complex.

The exchange of the arm protons was achieved by heating a solution of the ligand in D_2O (2 mL) at pD 11.5, 70 °C for 3 days monitoring the course of the isotopic substitution by changes in the ^1H spectrum. A suspension of lanthanide hydroxide formed which was removed by filtration. The resulting solution was adjusted to pD 5 using DCl (0.1 mol dm^{-3}) followed by lyophilisation to give the complex.

h_{ring}-h_{arms}-Eu(dota)

δ_H(D_2O, 200 MHz): -16.67 (M, a), -15.16 (M, a), -9.88 (m, r), -8.57 (M, r), -7.10 (M, r), -4.75 (m, a), -2.61 (m, a), -1.38 (M, r), 13.27 (m, r), 33.94 (M, r). M/m = 4.0.

m/z (ES-): 551 (95 %, M^-, ^{151}Eu), 553 (100 %, M^-, ^{153}Eu).

d_{ring}-h_{arms}-Eu(dota)

δ_H(D_2O, 200 MHz): -16.53 (M, a), -15.01 (M, a), -8.27 (M, r), -6.90 (M, r), -4.46 (m, a), -2.36 (m, a), -1.19 (M, r), 34.08 (M, r). M/m = 6.1. $\%d_{ring}$ = 92 %.

m/z (ES-): 565 (5 %), 567 (100 %), 568 (60 %), 569 (45 %), 570 (10 %).

h_{ring}-d_{arms}-Eu(dota)

δ_H(D_2O, 200 MHz): -16.52 (M, a), -15.06 (M, a), -9.78 (m, r), -8.42 (M, r), -7.00 (M, r), -4.62 (m, a), -2.51 (m, a), -1.33 (M, r), 13.41 (m, r), 33.98 (M, r). M/m = 4.2. $\%d_{arms}$ = 64 %.

m/z (ES-): 552 (8 %), 553 (12 %), 554 (32 %), 555 (65 %), 556 (92 %), 557 (100 %), 558 (90 %), 559 (60 %), 560 (30 %), 561 (10 %).

d_{ring}-d_{arms}-Eu(dota)

$\delta_D\{^1H\}$ (H_2O, 76.7 MHz): -16.28 (M, a), -14.80 (M, a), -8.22 (M, r), -6.95 (M, r), -1.26 (M, r), 33.65 (M, r). $\%d_{ring}$ = 92 %. $\%d_{arms}$ = 83 %.

m/z (ES-): 570 (10 %), 571 (13 %), 572 (45 %), 573 (95 %), 574 (100 %), 578 (92 %), 576 (33 %), 577 (12 %).

h_{ring}-h_{arms}-Tb(dota)

δ_H(D_2O, 65 MHz): -409.92 (M, r), -243.42 (m, r), -101.32 (M, r), -97.34 (M, r), -88.79 (m, a), -73.38 (m, r), 65.70 (m, a), 86.29 (M, a), 141.37 (M, r), 267.01 (M, a). M/m = 10.6.

m/z (ES-): 559 (M^-)

d_{ring}-h_{arms}-Tb(dota)

δ_H(D_2O, 65 MHz): -408.41 (M, r), -102.29 (M, r), -98.13 (M, r), -85.09 (m, a), 63.55 (m, a), 84.63 (M, a), 138.67 (M, r), 264.82 (M, a). M/m = 13.2. %d_{ring} = 91 %.

h_{ring}-d_{arms}-Tb(dota)

δ_H(D_2O, 65 MHz): -407.6 (M, r), -240.10 (m, r), -101.36 (M, r), -97.55 (M, r), -72.67 (m, r), -64.02 (m, a), 84.96 (M, a), 139.93 (M, r), 265.50 (M, a). M/m = 12.1. %d_{arms} = 42 %

m/z (ES-): 559 (6 %, M^-, d_0), 560 (25 %, M^-, d_1), 561 (68 %, M^-, d_2), 562 (97 %, M^-, d_3), 563 (100 %, M^-, d_4), 564 (71 %, M^-, d_5), 565 (30 %, M^-, d_6), 566 (10 %, M^-, d_7), 567 (2 %, M^-, d_8).

d_{ring}-d_{arms}-Tb(dota)

δ_D(H_2O, 46 MHz): -401.04 (M, r), -100.16 (M, r), -96.14 (M, r), 83.95 (M, a), 136.80 (M, r), 261.34 (M, a). %d_{ring} = 91 %. %d_{arms} = 27 %.

m/z (ES-): 573 (4 %, M^-, d_{14}), 574 (37 %, M^-, d_{15}), 575 (63 %, M^-, d_{16}), 576 (100 %, M^-, d_{17}), 577 (88 %, M^-, d_{18}), 578 (50 %, M^-, d_{19}), 579 (18 %, M^-, d_{20}), 580 (3 %, M^-, d_{21}).

h_{ring}-h_{arms}-Nd(dota)

δ_H(D_2O, 400 MHz, 277 K): -24.21 (m, r), -8.81 (M, r), -2.08 (r), 5-8, 9.40 (M, a), 11.65 (m, r), 14.74 (M, a), 19.81 (m, a). M/m = 1.1.

m/z (ES-): 542 (100 %, M^-, ^{142}Nd), 543(75 %, M^-, ^{143}Nd), 544(66 %, M^-, ^{144}Nd), 545(51 %, M^-, ^{145}Nd), 546(37 %, M^-, ^{146}Nd), 547(17 %, M^-), 548(10 %, M^-, ^{148}Nd), 549(10 %, M^-), 550(10 %, M^-, ^{150}Nd).

d_{ring}-h_{arms}-Nd(dota)

$\delta_H(D_2O$, 400 MHz, 277 K): -24.81 (m, r), -9.11 (M, r), 9.42 (M, a), 14.90 (M, a), 20.17 (m, a). M/m = 1.1. $\%d_{ring}$ = 92 %.

m/z (ES-): 548 (1 %), 549 (9 %), 550 (18 %), 551 (15 %), 552 (16 %), 553 (10 %), 554 (10 %), 555 (4 %), 557 (87 %), 558 (100 %), 559 (90 %), 560 (79 %), 561 (62 %), 562 (28 %), 563 (25 %), 564 (12 %), 565 (18 %), 566 (11 %).

h_{ring}-d_{arms}-Nd(dota)

$\delta_H(D_2O$, 400 MHz): -25.15 (m, r), -9.07 (M, r), -1.91 (r), 5-8, 9.41 (M, a), 11.83 (m, r), 14.93 (M, a), 20.19 (m, a). M/m = 1.2. $\%d_{arm}$ = 9 %.

m/z (ES-): 542 (50 %), 543 (87 %), 544 (100 %), 545 (91 %), 546 (80 %), 547 (58 %), 548 (36 %), 549 (24 %), 550 (18 %), 551 (14 %), 552 (7 %), 553 (3 %).

d_{ring}-d_{arms}-Nd(dota)

$\delta_D(H_2O$, 46 MHz): -25 (m, r), -10 (M, r), 2-10.

m/z (ES-): 550 (7 %), 551 (13 %), 552 (18 %), 553 (19 %), 554 (18 %), 555 (13 %), 556 (12 %), 557 (20 %), 558 (45 %), 559 (80 %), 560 (99 %), 561 (100 %), 562 (92 %), 563 (72 %), 564 (49 %), 565 (30 %), 566 (21 %), 567 (15 %), 568 (9 %), 569 (4 %), 570 (1 %).

h_{ring}-h_{arms}-Yb(dota)

$\delta_H(D_2O$, 200 MHz): -83.62 (M, a), -54.75 (m, a), -46.08 (M, r), -38.26 (M, a), -32.32 (m, r), -26.18 (m, a), 10.24 (m, r), 14.51 (m, r), 20.00 (M, r), 24.30 (M, r), 81.47 (m, r), 134.17 (M, r). M/m = 7.1.

m/z (ES-): 571 (91 %, M^-, ^{171}Yb), 572 (82 %, M^-, ^{172}Yb), 573 (100 %, M^-, ^{173}Yb), 574 (73 %, M^-, ^{174}Yb), 576 (31 %, M^-, ^{176}Yb).

d_{ring}-h_{arms}-Yb(dota)

δ_H(D_2O, 200 MHz): -83.31 (M, a), -54.13 (m, a), -45.71 (M, r), -38.08 (M, a), -31.75 (m, r), -25.96 (m, a), 20.18 (M, r), 24.79 (M, r), 81.42 (m, r), 135.36 (M, r). M/m = 8.2. %. d_{ring} = 90 %.

h_{ring}-d_{arms}-Yb(dota)

δ_H(D_2O, 200 MHz): -83.57 (M, a), -54.17 (m, a), -46.26 (M, r), -38.35 (M, a), -32.15 (m, r), -25.99 (m, a), 10.38 (m, r), 14.59 (m, r), 19.96 (M, r), 24.40 (M, r), 81.20 (m, r), 135.01 (M, r). M/m = 6.5. %d_{arms} = 39 %

m/z (ES-): 571 (4 %), 572 (17 %), 573 (43 %), 574 (68 %), 575 (90 %), 576 (100 %), 577 (91 %), 578 (63 %), 579 (41 %), 580 (20 %), 581 (9 %), 582 (2 %).

d_{ring}-d_{arms}-Yb(dota)

δ_D(H_2O, 46 MHz): -82.01 (M, a), -53.80 (m, a), -44.87 (M, r), -37.33 (M, a), -31.65 (m, r), -26.09 (m, a), 10.80 (m, r), 15.28 (m, r), 20.11 (M, r), 24.49 (M, r), 80.96 (m, r), 133.08 (M, r). d_{ring} = 90 %. %d_{arms} = 68 %

m/z (ES-): 572 (1 %), 573 (2 %), 574 (3 %), 575 (4 %), 576 (5 %), 577 (4 %), 578 (3 %), 579 (2 %), 580 (1 %), 581 (1 %), 582 (3 %), 583 (5 %), 584 (10 %), 585 (15 %), 586 (19 %), 587 (19 %), 588 (16 %), 589 (16 %), 590 (24 %), 591 (38 %), 592 (70 %), 593 (85 %), 594 (100 %), 595 (95 %), 596 (70 %), 597 (44 %), 598 (22 %), 599 (9 %), 600 (2 %).

6.5 Experimental for Chapter 5

6-Methylphenanthridine, 57

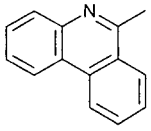

A solution of methyllithium in THF (1 mol dm^{-3}, 6 mL) was added dropwise to a stirred solution of phenanthridine (1 g, 5.59 mmol) in dry THF (100 mL) at 0 °C under an inert atmosphere of argon. After the solution had been stirred for 1 h at 0 °C a further aliquot of methyllithium solution (6 mL) was added and stirring

continued for a further 1 h at room temperature. The reaction mixture was quenched with aqueous potassium hydroxide (2 mol dm^{-3}, 50 mL). The reaction volume was then reduced to under reduced pressure and extracted with dichloromethane (2 x 50 mL). The combined organic layers were dried over anhydrous potassium carbonate. Manganese dioxide was added to the dichloromethane solution and was stirred for 4 h. The suspension was filtered and the solvents removed under reduced pressure to give an off white solid. Chromatography on silica (gradient elution CH_2Cl_2 then 25 % EtOAc-CH_2Cl_2, R_f = 0.2, CH_2Cl_2) yielded an off white solid (0.83 g, 4.30 mmol, 77 %).

Mp 52 °C.

$\delta_H(CDCl_3)$: 3.02 (s, 3H, C*H*$_3$), 7.54-7.74 (m, 3H), 7.80 (dd, 1H, J = 8.0, 8.0 Hz), 8.10 (d, 1H, J = 8.1 Hz), 8.18 (d, 1H, J = 8.1 Hz), 8.50 (d, 1H, J = 7.5 Hz), 8.58 (d, 1H, J = 7.8 Hz).

m/z (ES+): 194 ($M + H^+$)

6-(Bromomethyl)phenanthridine, 58

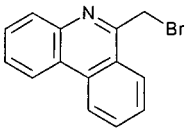

A suspension of 6-methylphenanthridine, **57**, (0.83 g, 4.3 mmol), N-bromosuccinimide (0.84 g, 4.7 mmol) and a trace amount of benzoyl peroxide in carbon tetrachloride (100 mL) was heated at reflux for 60 h under an inert atmosphere of argon. The solvents were removed under reduced pressure to give an off white solid which was used without further purification.

$\delta_H(CDCl_3)$: 5.10 (s, 1H, -C*H*$_2$Br), 7.2-8.02 (m, 4H), 8.16 (d, 1H, J = 8.0 Hz), 8.37 (d, 1H, J = 8.2 Hz), 8.59 (d, 1H, J = 7.6 Hz), 8.68 (d, 1H, J = 8.2 Hz).

m/z (ES+): 271.8 (94 %, $M + H^+$, ^{79}Br), 273.8 (100 %, $M + H^+$, ^{81}Br), 293.8 (76 %, $M + Na^+$, ^{79}Br), 295.8 (68 %, $M + Na^+$, ^{81}Br).

1-(6'-Phenanthridylmethyl)-4,7,10-tris(*tert*-butoxycarboxymethyl)-1,4,7,10-tetraazacyclododecane, 59

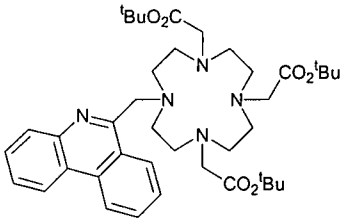

A suspension of 6-(bromomethyl)phenanthridine, **58**, (85 mg, 0.313 mmol), 1,4,7-tris(*tert*-butoxycarboxymethyl)-1,4,7,10-tetraazacyclododecane (123 mg, 0.239 mmol) and anhydrous potassium carbonate (37 mg, 0.268 mmol) in dry acetonitrile (5 mL) was heated at reflux for 18 h under an inert atmosphere of argon. The solvents were removed under reduced pressure and the residue suspended in dichloromethane (20 mL) and filtered. Removal of solvents under reduced pressure gave a crude yellow-brown solid. Column chromatography on silica (gradient elution, 0.5 %, 2 % then 4 % MeOH-CH_2Cl_2, R_f = 0.4 10 % MeoH-CH_2Cl_2) yielded a yellow solid (90 mg, 0.128 mmol, 54 %).

δ_H($CHCl_3$): 1.10 (br s, 18H, 2 –O^{t}Bu), 1.52 (s, 9H, O^{t}Bu), 1.8 – 3.4 (br, 24H), 7.42 (t, 1H, J = 7.8 Hz), 7.57 (t, 1H, J = 8.0 Hz), 7.69 (t, 1H, H-3, J = 7.9 Hz), 7.85 (t, 1H, H-2, J = 8.1 Hz), 8.03 (d, 1H, J = 7.2 Hz), 8.24 (d, 1H, H-4, J = 8.1 Hz), 8.52 (d, 1H, J = 7.8 Hz), 8.64 (d, 1H, H-1, J = 8.4 Hz).

$\delta_C\{^1H\}$($CHCl_3$): 28.0, 28.2, 51-53 (br), 53.7, 56.1, 57.6, 82.1, 82.4, 106.8, 117.8, 123.9, 124.9, 125.2, 126.9, 128.0, 128.7, 129.7, 131.2, 132.8, 143.4, 158.0, 173.1 (*C*=O), 173.4 (*C*=O).

m/z (ES+): 706 ($M + H^+$), 728 ($M + Na^+$).

1-(6'-Phenanthridylmethyl)-4,7,10-tris(carboxymethyl)-1,4,7,10-tetraazacyclododecane, 76

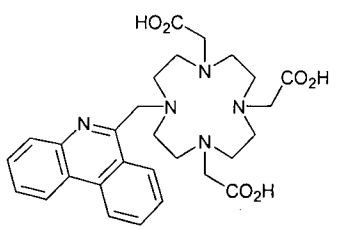

A solution of 1-(6'-phenanthridylmethyl)-4,7,10-tris(*tert*-butoxycarboxymethyl)-1,4,7,10-tetraazacyclododecane, **59**, (90 mg, 0.127 mmol) in trifluoroacetic acid (2

mL) was stirred for 18 h then the solvent was removed under reduced pressure. The resulting oil was triturated with dichloromethane (5 x 5 mL) to give a yellow solid (68 mg, 0.127 mmol, 100 %).

Mp 124 – 126 °C.

$\delta_H(CD_3OD)$: 2.9-3.9 (m, 20H), 4 .25 (s, 2H), 5.31 (s, 2H), 7.6-7.8 (m, 3H), 7.91 (dd, 1H, J = 7.8, 7.8 Hz), 8.12 (d, 1H, J = 8.4 Hz), 8.25 (d, 1H, J = 7.8 Hz), 8.63 (d, 1H, J = 7.8 Hz), 8.75 (d, 1H, J = 8.1 Hz).

$\delta_C\{^1H\}(CD_3OD)$: 49.1, 51.7, 52.3, 52.7, 55.7, 57.6, 119.9, 122.2, 122.8, 123.4, 124.5, 124.7, 128.0, 128.2. 129.5, 130.0, 132.1, 133.5, 142.0, 150.5, 168.3 (C=O), 172.6 (C=O).

ν/cm^{-1}: 3041br, 2918m, 1669s (C=O), 1427m, 1348m.

$\lambda_{max}(CH_3OH)$: 215 nm (8400 dm^3 mol^{-1} cm^{-1}), 248 nm (12100 dm^3 mol^{-1} cm^{-1}), 274 nm (1800 dm^3 mol^{-1} cm^{-1}), 304 nm (1400 dm^3 mol^{-1} cm^{-1}).

Europium complex of 76, 8

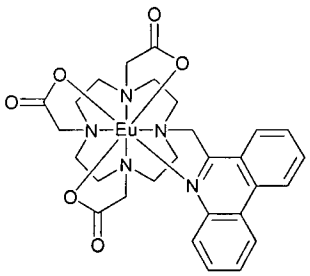

A suspension of ligand, **76**, (68 mg, 0.127 mmol) and europium(III) acetate (64 mg, 0.191 mmol) in methanol (3 mL) was stirred at 60 °C for 18 h under an atmosphere of argon after which solvents were removed under reduced pressure. Column chromatography (reverse phase silica, EtOH, R_f = 0.2, 20 % H_2O-EtOH) of the residue gave the complex (51 mg, 0.074 mmol, 59 %).

$\delta_H(CD_3OD, 200\ MHz)$: -18.5 (br m), -15.2 (br s), -13.0 (br s), -10.5, -9.9, -7.6, -4.3, -3.3, -2.4, -1.9, 7-10 (m), 20.6, 22.8, 23.9, 28.2.

m/z (ES+): 708 (M + Na^+, ^{151}Eu), 710 (M + Na^+, ^{153}Eu), 724 (M + K^+, ^{151}Eu), 726 (M + K^+, ^{153}Eu).

Φ (H_2O) = 0.063; Φ (D_2O) = 0.191; (λ_{ex} = 270 nm, measured relative to cresyl violet and rhodamine 101).

2-Bromophenanthridine, 63

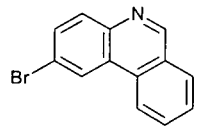

A suspension of phenanthridine (5 g, 27.9 mmol) and *N*-bromosuccinimide (5 g, 28.0 mmol) in carbon tetrachloride (60 mL) was heated at reflux in the presence of a trace amount of benzoyl peroxide for 48 h. The resultant red solution was filtered whilst hot and the remaining sticky red filtrate was washed well with further carbon tetrachloride. The solvent was removed under reduced pressure to one third of its original volume and the product allowed to crystallise. The crystals were separated and further purified by column chromatography (eluent CH_2Cl_2, R_f = 0.25, 10 % EtOH- CH_2Cl_2) to give a colourless solid (4.5 g, 17.4 mmol, 62 %).

Mp 156-159 °C (lit. 160-162.5 °C[10]).

$\delta_H(CDCl_3)$: 7.76 (dd, 1H, H-9, J = Hz), 7.83 (dd, 1H, H-3, J = Hz), 7.90 (dd, 1H, H-8, J = Hz), 8.06 (d, 1H, H-4, J = Hz), 8.07 (d, 1H, H-10, J = Hz), 8.55 (d, 1H, H-7, J = Hz), 8.72 (d, 1H, H-1, J = Hz), 9.29 (s, 1H, H-6).

m/z (ES+): 257.8 (97 %, $M^+ + 1$, ^{79}Br), 259.7 (100 %, $M^+ + 1$, ^{81}Br).

2-Cyanophenanthridine, 64

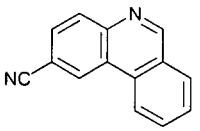

A suspension of 2-bromophenanthridine, **63**, (5.7 g, 22 mmol) and copper(I) cyanide (2.2 g, 24 mmol) in dry, degassed dimethylformamide (200 mL) was heated at 180 °C for 40 h under an inert atmosphere of argon. Solvents were removed under reduced pressure and the residue treated with hydrochloric acid (6 mol dm^{-3}, 4 L) to give an orange solution. The product (2 L batches) was extracted with dichloromethane (5 x 200 mL). More product was obtained by raising the pH of the aqueous phase to >13 with potassium hydroxide and further extraction with dichloromethane (1.5 L batches, 5 x 200 mL). The combined organic layers were dried over anhydrous potassium carbonate and then solvents removed under reduced pressure to yield a crude product. Column chromatography on silica (eluent 10 % MeOH- CH_2Cl_2, R_f = 0.25) yielded an off white solid (1.2 g, 5.88 mmol, 27 %).

Mp 199-203 °C (dec.) (lit. 200-205 °C (dec.)[11]).

$\delta_H(CDCl_3)$: 7.83 (dd, 1H, H-9, J = 7.8 ,7.8 Hz), 7.9 - 8.0 (m, 2H, H-8, H-10), 8.13 (d, 1H, H-7, J = 8.1), 8.27 (d, 1H, H-3, J = 8.4 Hz), 8.60 (d, 1H, H-4, J = 8.1 Hz), 8.93 (d, 1H, H-1, J = 1.5 Hz), 9.40 (s, 1H, H-6).

2-(Aminomethyl)phenanthridine, 51

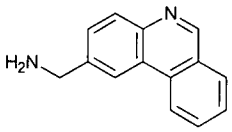

2-Cyanophenanthridine, **64**, (1.0 g, 4.90 mmol) was taken into a solution of borane-THF (100mL, 1 mol dm^{-3}) under argon and was heated at reflux for 1 week. Excess borane was quenched by the cautious addition of methanol and the solvent removed under reduced pressure. The residue was then dissolved in methanol (50 mL) and solvents were removed under reduced pressure. This was repeated three times to give a waxy solid. The residue was dissolved in aqueous hydrochloric acid (100mL, 1 mol dm^{-3}) and heated at 100 °C for 15 h. This solution was washed with diethyl ether (2 x 50 mL) then the pH was raised to >13. The basic aqueous solution was then extracted with dichloromethane (5 x 50 mL). The combined dichloromethane layers were dried over anhydrous potassium carbonate and the solvents were removed under reduced pressure to yield a pale yellow solid (0.76 g, 3.65 mmol, 74%).

$\delta_H(CDCl_3)$: 1.81 (br s, 2H, -N*H*$_2$), 4.16 (s, 2H, -C*H*$_2$-), 7.68-7.74 (m, 2H), 7.86 (dd, 1H, J = 7.1, 7.1 Hz), 8.04 (d, 1H, J = 7.8 Hz), 8.15 (d, 1H, J = 8.4 Hz), 8.52 (s, 1H, H-1), 8.64 (d, 1H, J = 8.4 Hz), 9.26 (s, 1H, H-6).

m/z (ES+): 209 ($M + H^+$), 249 ($M + K^+$).

{1-[(2'-phenanthridylmethyl)-carbamoyl]-2-methyl-propyl}-carbamic acid *tert*-butyl ester, 66

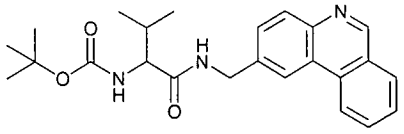

A solution of BOC-valine (1.540 g, 7.10 mmol), 2-(aminomethyl)phenanthridine, **51**, (1.476 g, 7.10 mmol), HOBT (0.958 g, 7.10 mmol), EDC (1.355 g, 7.10 mmol) and

triethylamine (1.0 mL, 7.19 mmol) in dichloromethane (50 mL) was stirred at 20 °C for 18 h. The solution then washed with water (25 mL), citric acid solution (10% in water, 25mL), and sodium hydrogen carbonate solution (5% in water, 25 mL). The combined organic layers were dried over anhydrous potassium carbonate and then solvents removed under reduced pressure to yield a crude product. Column chromatography on silica (gradient elution, CH_2Cl_2, then 4 % MeOH- CH_2Cl_2, R_f = 0.25, 5 % MeOH- CH_2Cl_2) yielded an off white crystalline solid (2.2 g, 5.40 mmol, 76 %).

Mp 118-120 °C.

$\delta_H(CDCl_3)$: 0.94 (t, 6H, $(CH_3)_2CH$-, J = 7.1 Hz), 1.35 (s, 9H, $(CH_3)_3C$-), 2.13 (sextet, 1H, $(CH_3)_2CH$-, J = 6.6 Hz), 4.08 (t, 1H, J = 8.0 Hz), 4.49 (ddd, 2H, -CH_2-, J = 5.6, 15.2, 33.9 Hz), 5.57 (d, 1H, J = 8.7 Hz), 7.40 (d, 1H, J = 8.1 Hz), 7.53 (dd, 1H, J = 7.1, 7.1 Hz), 7.64 (dd, 1H, J = 7.7, 7.7 Hz), 7.80 (d, 1H, J = 7.8 Hz), 7.88 (d, 1H, J = 8.4 Hz), 8.13 (s, 1H), 8.28 (d, 1H, J = 8.1 Hz), 9.02 (s, 1H).

$\delta_C\{^1H\}(CDCl_3)$: 18.2, 19.5, 28.4, 31.0, 43.4, 60.5, 79.8, 120.7, 121.8, 123.8, 126.2, 127.4, 128.0, 128.5, 130.1, 130.8, 132.1, 137.1, 143.5, 153.2, 156.2, 172.3.

m/z (ES+): 408 ($M + H^+$) 100%, 430 ($M + Na^+$) 80%, 815 ($2M + H^+$) 40%, 837 ($2M + Na^+$) 60%.

ν/cm^{-1}: 3294br m, 2962m, 1671m, 1646s, 1520s.

λ_{max} (MeOH): 210 nm (29000 dm^3 mol^{-1} cm^{-1}), 221 nm (23000 dm^3 mol^{-1} cm^{-1}), 249 nm (42000 dm^3 mol^{-1} cm^{-1}), 273 nm (sh) (9300 dm^3 mol^{-1} cm^{-1}), 294 nm (6700 dm^3 mol^{-1} cm^{-1}), 331 nm (2400 dm^3 mol^{-1} cm^{-1}), 347 nm (2300 dm^3 mol^{-1} cm^{-1}).

$[\alpha]_D^{20}$ = 14.0° (c = 1.08, MeOH).

2-Amino-*N*-(2'-phenanthridylmethyl)-3-methyl-butyramide trifluoroethanoic acid salt, 67

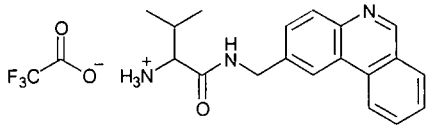

A solution of BOC-protected valine, **66**, (870 mg, 2.14 mmol) in trifluoroacetic acid (2 mL) was stirred at room temperature for 18 h. Removal of solvents under reduced

pressure gave an oil which was triturated with dichloromethane (5 x 5 mL) to give a yellow solid (0.9 g, 2.14 mmol, 100 %).

Mp 99-101 °C.

$\delta_H(CD_3OD)$: 1.11 (dd, 6H, $(CH_3)_2CH$-, J = 1.8, 6.6 Hz), 2.33 (sextet, 1H, $(CH_3)_2CH$-, J = 6.6 Hz), 3.95 (d, 1H, ^+H_3N-CH-, J = 5.7 Hz), 4.66 (dd, 2H, -CH_2-Ar, J = 15.9, 49.2 Hz), 7.70 (d, 1H, J = 8.7 Hz), 7.74 – 7.86 (m, 2H), 7.99 (dd, 1H, J = 7.5, 7.5 Hz), 8.24 (d, 1H, J = 8.1 Hz), 8.29 (s, 1H), 8.34 (d, 1H, J = 8.4 Hz), 9.36 (s, 1H).

$\delta_C\{^1H\}(CD_3OD)$:

m/z (ES+): 308 (M^+) 100%, 615 ($2M^+$) 5%.

λ_{max} (MeOH): 223 nm (8900 dm^3 mol^{-1} cm^{-1}), 248 nm (19200 dm^3 mol^{-1} cm^{-1}), 276 nm (sh) (3500 dm^3 mol^{-1} cm^{-1}), 297 nm (2700 dm^3 mol^{-1} cm^{-1}), 333 nm (690 dm^3 mol^{-1} cm^{-1}), 350 nm (390 dm^3 mol^{-1} cm^{-1}).

$[\alpha]_D^{20}$ = +15.9° (c = 2.5, MeOH).

N-(2'phenanthridylmethyl)-2-(chloromethylamino)-3-methyl-butyramide, 68

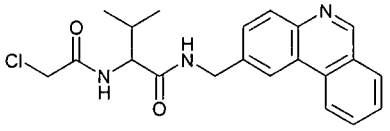

A solution of chloroethanoic acid (39 mg, 0.413 mmol), 2-amino-*N*-(2'-phenanthridylmethyl)-3-methyl-butyramide trifluoroethanoic acid salt, **67**, (173.7 mg, 0.412 mmol), HOBT (55.5 mg, 0.411 mmol), EDC (79.1 mg, 0.413 mmol) and triethylamine (0.15 mL, 1.08 mmol) in dry tetrahydrofuran (50 mL) was stirred at 20 °C for 18 h. Solvents were removed under reduced pressure. The resulting residue was partitioned between dichloromethane (50 mL) and water (50 mL). The organic layer was washed with aqueous citric acid (10%, 50 mL), and aqueous sodium hydrogen carbonate (5%, 50 mL). The organic layer was dried over anhydrous potassium carbonate and then solvents removed under reduced pressure to yield a crude product. Column chromatography on silica (gradient elution, CH_2Cl_2, 2% then 10 % MeOH- CH_2Cl_2, R_f = 0.54, 10 % MeOH- CH_2Cl_2) yielded an off white crystalline solid (50 mg, 0.13 mmol, 32 %).

Mp >220 °C.

δ_H($CDCl_3$:CD_3OD, 10:1): 0.91 (dd, 6H, $(CH_3)_2CH$-, J = 3.5, 6.5 Hz), 2.07 (sextet, 1H, $(CH_3)_2CH$-, J = 6.8 Hz), 4.00 (s, 2H, CH_2Cl), 4.18 (d, 1H, N-CH-CO, J = 7.5 Hz), 4.61 (dd, 2H, -CH_2-Ar, J = 15.0, 31.2 Hz), 7.57 (d, 1H, J = 8.1 Hz), 7.66 (dd, 1H, J = 7.5, 7.5 Hz), 7.82 (dd, 1H, J = 7.7, 7.7 Hz), 7.98 (d, 1H, J = 8.1 Hz), 8.02 (d, 1H, 8.4 Hz), 8.41 (s, 1H), 8.55 (d, 1H, J = 8.1 Hz), 9.13 (s, 1H).

m/z (ES+): 384 ($M + H^+$), 406 ($M + Na^+$).

1-{N-[1-((2'-phenanthridylmethyl)-carbamoyl)-2-methyl-propyl]-carbamoylmethyl}-4,7,10-tris(*tert*-butoxycarboxymethyl)-1,4,7,10-tetraazadodecane, 69

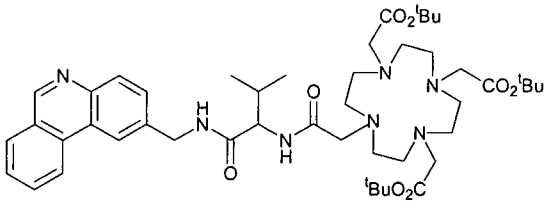

A suspension of N-(2'phenanthridylmethyl)-2-(chloromethylamino)-3-methyl-butyramide, **68**, (50 mg, 0.130 mmol), 1,4,7-tris(*tert*-butoxycarboxymethyl)-1,4,7,10-tetraazacyclododecane (67 mg, 0.130 mmol), caesium carbonate (42.3 mg, 0.130 mmol) and potassium iodide (21.6 mg, 0.130 mmol) in dry acetonitrile (5 mL) was heated at reflux for 18 h under an inert atmosphere of argon. Removal of solvent under reduced pressure yielded a residue which was suspended in dichloromethane (20 mL) and filtered; the filter cake was washed well with dichloromethane (3 x 20 mL). Removal of solvent under reduced pressure gave a crude yellow-brown solid. Column chromatography on silica (gradient elution, 0.5 %, 2 % then 4 % MeOH-CH_2Cl_2, R_f = 0.65, 10 % MeOH- CH_2Cl_2) yielded a yellow solid (101 mg, 0.117 mmol, 90 %).

δ_H($CDCl_3$): 0.9 (m, 6H, -CH_3), 1.4 (m, 27H, ^{t}Bu), 1.8 – 4.0 (br m, 24H), 4.3 (m, 1H), 4.6 (m, 2H), 4.8 (m, 2H), 7.66 (t, 1H, J = 7.5 Hz), 7.8 – 7.9 (m, 2H), 7.97 (d, 1H, J = 8.0 Hz), 8.05 (d, 1H, 8.2 Hz), 8.45 (m, 1H), 8.86 (m, 1H), 9.19 (s, 1H).

$\delta_C\{^1H\}$($CDCl_3$): 16.7, 18.8, 21.8, 26.7, 26.9, 27.2, 28.7, 29 (br), 41 (br), 47 (br), 52 (br m), 54.5, 80.9, 123.1 (Ar), 125.3 (Ar), 126.4 (Ar), 127.3 (Ar), 128.9 (Ar), 130.2 (Ar), 131.7 (Ar), 142.4 (Ar), 152.2 (Ar), 170.5 (*C*=O), 170.7 (*C*=O), 171.0 (*C*=O), 171.3 (*C*=O).

m/z (ES+): 884 ($M + Na^+$).

ν/cm^{-1} (gg): 3000w, 1710s, 1650m.

1-{N-[1-((2'-Phenanthridylmethyl)-carbamoyl)-2-methyl-propyl]-carbamoylmethyl}-4,7,10-tris(carboxymethyl)-1,4,7,10-tetraazadodecane, 70

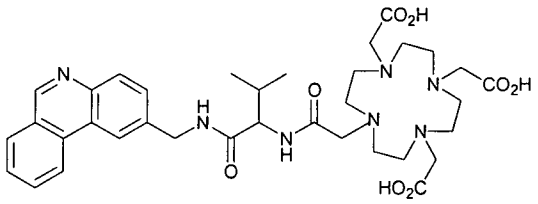

A solution of the tris(*t*-butyl ester), **69**, (101 mg, 0.117 mmol) in trifluoroacetic acid (2 mL) was stirred for 18 h. Removal of the solvent under reduced pressure gave an oil which was triturated with dichloromethane (5 x 5 mL) to give an off white solid (80 mg, 0.115 mmol, 98 %). This compound was used without further purification.

δ_H(d-TFA): 1.08 (s, 6H, -CH_3),3.2 – 4.4 (br m, 16H, ring), 6.67 (br s, 8H, NCH_2CO), 5.01 (dd, 2H, J = 15.0, 70.1 Hz), 8.4-8.8 (m, 3H, Ar), 8.1-8.2 (m, 2H, Ar), 9.0-9.1 (m, 2H, Ar), 9.70 (s, 1H, Ar).

$\delta_C\{^1H\}$(d-TFA): 16.8, 17.8, 24.8, 29.5, 31.4, 44.2, 60.3, 66.8, 122.2, 122.9, 123.2, 124.0, 126.0, 129.9, 131.2, 131.8, 132.0, 133.0, 133.9, 136.0, 139.4, 140.7, 169.4 (*C*=O).

Europium complex of 70, 71

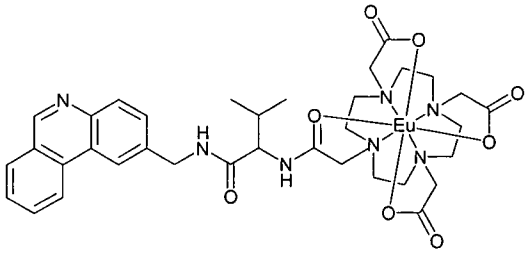

A suspension of ligand, **70**, (80 mg, 0.115 mmol) and europium(III) acetate (56 mg 0.173 mmol) in methanol (3 mL) was stirred at 60 °C for 18 h under an atmosphere of argon after which solvents were removed under reduced pressure. Preparative thin layer chromatography of a portion of the reaction mixture (Alumina, gradient elution, CH_2Cl_2, 2 %, 4 %, 10 % MeOH in CH_2Cl_2) gave the complex by collection of the baseline fraction.

m/z (ES+): 444 ($M + 2Na^+$, ^{151}Eu, 90 %), 445 ($M + 2Na^+$, ^{153}Eu, 100 %), 864 ($M + Na^+$, ^{151}Eu, 10 %), 866 ($M + Na^+$, ^{153}Eu, 10 %).

Φ (H_2O) = 0.0038; Φ (D_2O) = 0.012; (λ_{ex} = 270 nm, measured relative to cresyl violet and rhodamine 101).

6.6 References for chapter 6

[1] Demas J. N., Crosby G. A., *J. Phys. Chem.*, **1971**, 75, 8, 991.

[2] Handbook of Organic Photochemistry, Sciano J. C., CRC Press, 1989, Boca Raton, Florida.

[3] Lehn J. M., Simon J., Wagner J., *Nouv. J. Chem.*, **1977**, 1, 77.

[4] Miyazawa T., Yamada T., Kuwata S., *Bull. Chem. Soc. Jpn.*, **1984**, 57, 3605.

[5] M. Woods, PhD thesis, University of Durham, 1998.

[6] Graf E., Lehn J.-M., *Helv. Chim. Acta*, **1981**, 64, 1040.

[7] Pettit G. R., Smith R. L., *Can. J. Chem.*, **1964**, 42, 572.

[8] Swinkels D. W., van Duynhoven J. P. M., Hilbers C. W., Tesser G. I., *Recl. Trav. Chim. Pays-Bas*, **1991**, 110, 124.

[9] Parker D., Pulukkody K., Smith F. C., Batsonov A. S., Howard J. A. K., J. Chem. Soc., Dalton Trans., 1994, 689.

[10] Gilman H., Eisch J., *J. Am. Chem. Soc.*, **1955**, 77, 6379.

[11] Parker D., Senanayake K., Williams J. A. G., *J. Chem. Soc., Perkin Trans. 2*, **1998**, 2129.

Appendices

Appendix A

Conferences, Lectures and Research Colloquia

The author attended the following colloquia between October 1996 and September 1999.

1996

October 16 Professor Ojima, Guggenheim Fellow, State University of New York at Stony Brook
Silylformylation and Silylcarbocyclisations in Organic Synthesis

October 22 Professor Lutz Gade, Univ. Wurzburg, Germany
Organic transformations with Early-Late Heterobimetallics: Synergism and Selectivity

October 22 Professor B. J. Tighe, Department of Molecular Sciences and Chemistry, University of Aston
Making Polymers for Biomedical Application - can we meet Nature's Challenge?
Joint lecture with the Institute of Materials

October 23 Professor H. Ringsdorf (Perkin Centenary Lecture), Johannes Gutenberg-Universitat, Mainz,
Germany
Function Based on Organisation

November 13 Dr G. Resnati, Milan
Perfluorinated Oxaziridines: Mild Yet Powerful Oxidising Agents

November 18 Professor G. A. Olah, University of Southern California, USA
Crossing Conventional Lines in my Chemistry of the Elements

November 19 Professor R. E. Grigg, University of Leeds
Assembly of Complex Molecules by Palladium-Catalysed Queueing Processes

November 27 Dr Richard Templer, Imperial College, London
Molecular Tubes and Sponges

December 3 Professor D. Phillips, Imperial College, London
"A Little Light Relief" -

December 4 Professor K. Muller-Dethlefs, York University
Chemical Applications of Very High Resolution ZEKE Photoelectron Spectroscopy

December 11 Dr Chris Richards, Cardiff University
Sterochemical Games with Metallocenes

1997

January 15 Dr V. K. Aggarwal, University of Sheffield
Sulfur Mediated Asymmetric Synthesis

January 16 Dr Sally Brooker, University of Otago, NZ
Macrocycles: Exciting yet Controlled Thiolate Coordination Chemistry

February 18 Professor Sir James Black, Foundation/King's College London
My Dialogues with Medicinal Chemists

March 4 Professor C. W. Rees, Imperial College
Some Very Heterocyclic Chemistry

March 5 Dr J. Staunton FRS, Cambridge University
Tinkering with biosynthesis: towards a new generation of antibiotics

March 19 Dr Katharine Reid, University of Nottingham
Probing Dynamical Processes with Photoelectrons

October 8 Professor E Atkins, Department of Physics, University of Bristol
Advances in the control of architecture for polyamides: from nylons to genetically engineered silks to monodisperse oligoamides

October 22 Professor R J Puddephatt (RSC Endowed Lecture), University of Western Ontario
Organoplatinum chemistry and catalysis

October 23 Professor M R Bryce, University of Durham, Inaugural Lecture
New Tetrathiafulvalene Derivatives in Molecular, Supramolecular and Macromolecular
Chemistry: controlling the electronic properties of organic solids

October 29 Professor R Peacock, University of Glasgow
Probing chirality with circular dichroism

October 28 Professor A P de Silva, The Queen's University, Belfast
Luminescent signalling systems"

November 5 Dr M Hii, Oxford University
Studies of the Heck reaction

November 11 Professor V Gibson, Imperial College, London
Metallocene polymerisation

November 12 Dr J Frey, Department of Chemistry, Southampton University
Spectroscopy of liquid interfaces: from bio-organic chemistry to atmospheric chemistry

November 19 Dr G Morris, Department of Chemistry, Manchester Univ.
Pulsed field gradient NMR techniques: Good news for the Lazy and DOSY

November 25 Dr R Withnall, University of Greenwich
Illuminated molecules and manuscripts

November 26 Professor R W Richards, University of Durham, Inaugural Lecture
A random walk in polymer science

December 2 Dr C J Ludman, University of Durham
Explosions

December 3 Professor A P Davis, Department. of Chemistry, Trinity College Dublin.
Steroid-based frameworks for supramolecular chemistry

1998

January 14 Professor D Andrews, University of East Anglia
Energy transfer and optical harmonics in molecular systems

January 20 Professor J Brooke, University of Lancaster
What's in a formula? Some chemical controversies of the 19th century

January 21 Professor D Cardin, University of Reading
Aspects of metal and carbon cluster chemistry

February 3 Dr J Beacham, ICI Technology
The chemical industry in the 21st century

February 4 Professor P Fowler, Department of Chemistry, Exeter University
Classical and non-classical fullerenes

February 17 Dr S Topham, ICI Chemicals and Polymers
Perception of environmental risk; The River Tees, two different rivers

February 18 Professor G Hancock, Oxford University
Surprises in the photochemistry of tropospheric ozone

February 24 Professor R Ramage, University of Edinburgh
The synthesis and folding of proteins

March 11 Professor M J Cook, Dept of Chemistry, UEA
How to make phthalocyanine films and what to do with them.

March 18 Dr J Evans, Oxford University
Materials which contract on heating (from shrinking ceramics to bullet proof vests

October 23 Professor J C Scaiano, Department of Chemistry, University of Ottawa, Canada
In Search of Hypervalent Free Radicals, RSC Endowed Lecture

October 27 Professor A Unsworth, University of Durham
What's a joint like this doing in a nice girl like you?
In association with The North East Polymer Association

October 28 Professor J P S Badyal, Department of Chemistry, University of Durham
Tailoring Solid Surfaces, Inaugural Lecture

November 4 Dr N Kaltscoyannis, Department of Chemistry, UCL, London
Computational Adventures in d & f Element Chemistry

November 3 Dr C J Ludman, Chemistry Department, University of Durham
Bonfire night Lecture

November 10 Dr J S O Evans, Chemistry Department, University of Durham
Shrinking Materials

November 11 Dr M Wills, Department of Chemistry, University of Warwick
New Methodology for the Asymmetric Transfer Hydrogen of Ketones

November 12 Professor S Loeb, University of Windsor, Ontario, Canada
From Macrocycles to Metallo-Supramolecular Chemistry

November 17 Dr J McFarlane, Glasgow University
Nothing but Sex and Sudden Death!

November 24 Dr B G Davis, Department of Chemistry, University of Durham
Sugars and Enzymes

December 1 Professor N Billingham, University of Sussex
Plastics in the Environment - Boon or Bane
In association with The North East Polymer Association.

January 19 Dr J Mann, University of Reading
The Elusive Magic Bullet and Attempts to find it?

January 20 Dr A Jones, Department of Chemistry, University of Edinburgh
Luminescence of Large Molecules: from Conducting Polymers to Coral Reefs

January 27 Professor K Wade, Department of Chemistry, University of Durham
Foresight or Hindsight? Some Borane Lessons and Loose Ends

May 11 Dr John Sodeau, University of East Anglia
Ozone Holes and Ozone Hills

Appendix B

Publications

'Non-radiative deactivation of the excited states of europium, terbium and ytterbium complexes by proximate energy-matched OH, NH and CH oscillators: an improved luminescence method for establishing solution hydration states.'

Beeby A., Clarkson I. M., Dickins, R. S., Faulkner S., Parker D., Royle L., de Sousa A., S., Williams J. A. G., Woods M., *J. Chem. Soc., Perkin Trans. 2*, **1999**, 493.

'Lanthanide-containing reversed micelles: A structural and luminescence study.'

Beeby A., Clarkson I. M., Eastoe J., Faulkner S., Warne B., *Langmuir*, **1997**, 13, 5816.

Appendix C

Computer Programs

The following programs were written using National Instruments LabVIEW 5.0 ™.

map calc.vi
E:\labview\Squirrel Map\map calc.vi
Last modified on 17/06/99 at 14:59
Printed on 19/11/99 at 13:42

Connector Pane

map calc.vi

Front Panel

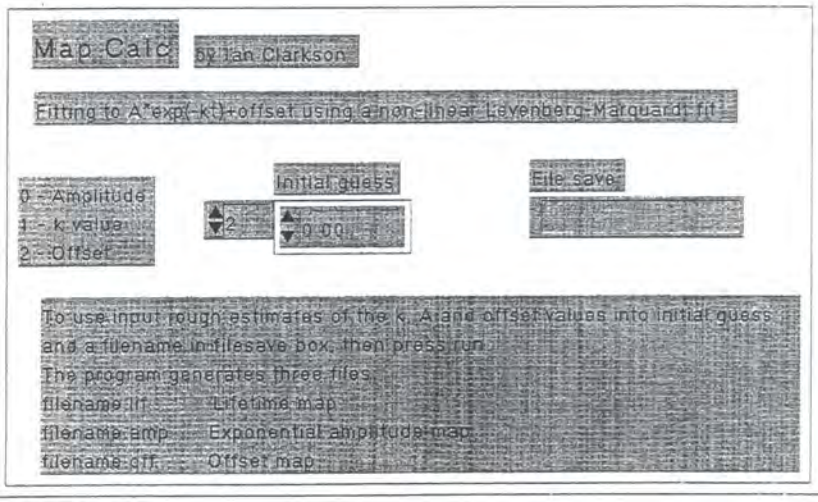

Block Diagram

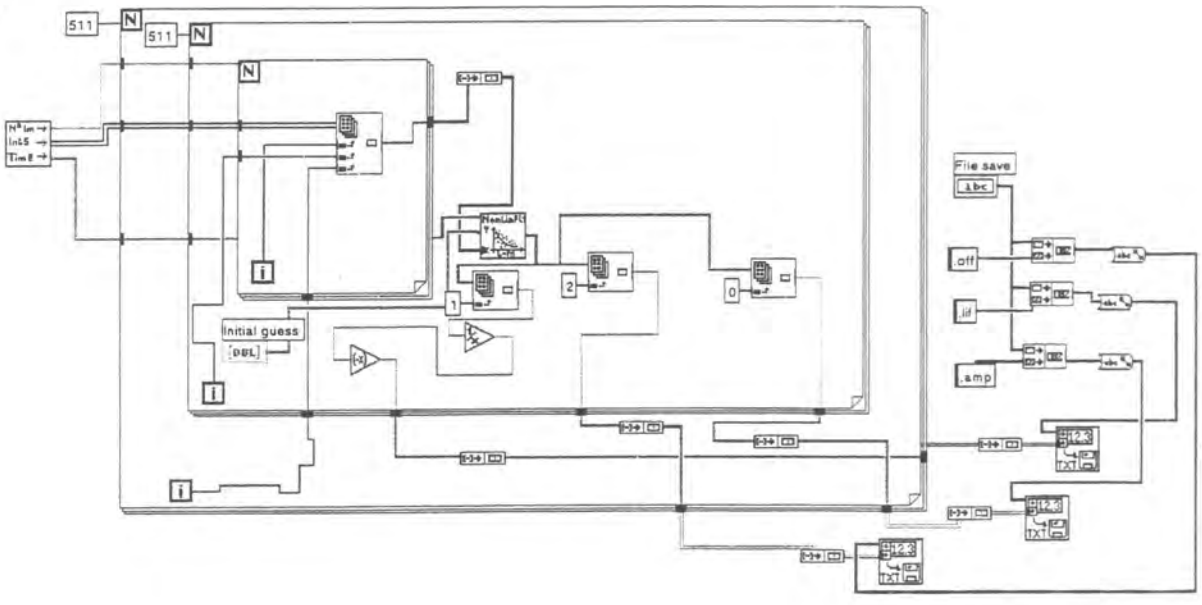

Read to 3d arrary.vi
E:\labview\Squirrel Map\Stuff\Read to 3d arrary.vi
Last modified on 23/03/99 at 15:57
Printed on 19/11/99 at 13:45

Connector Pane

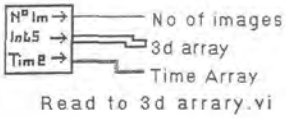

Front Panel

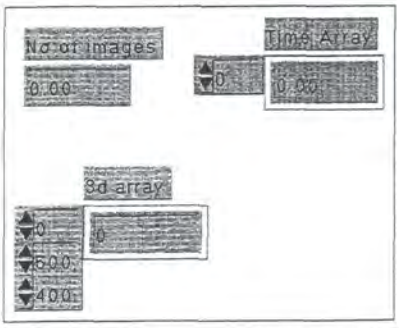

Block Diagram

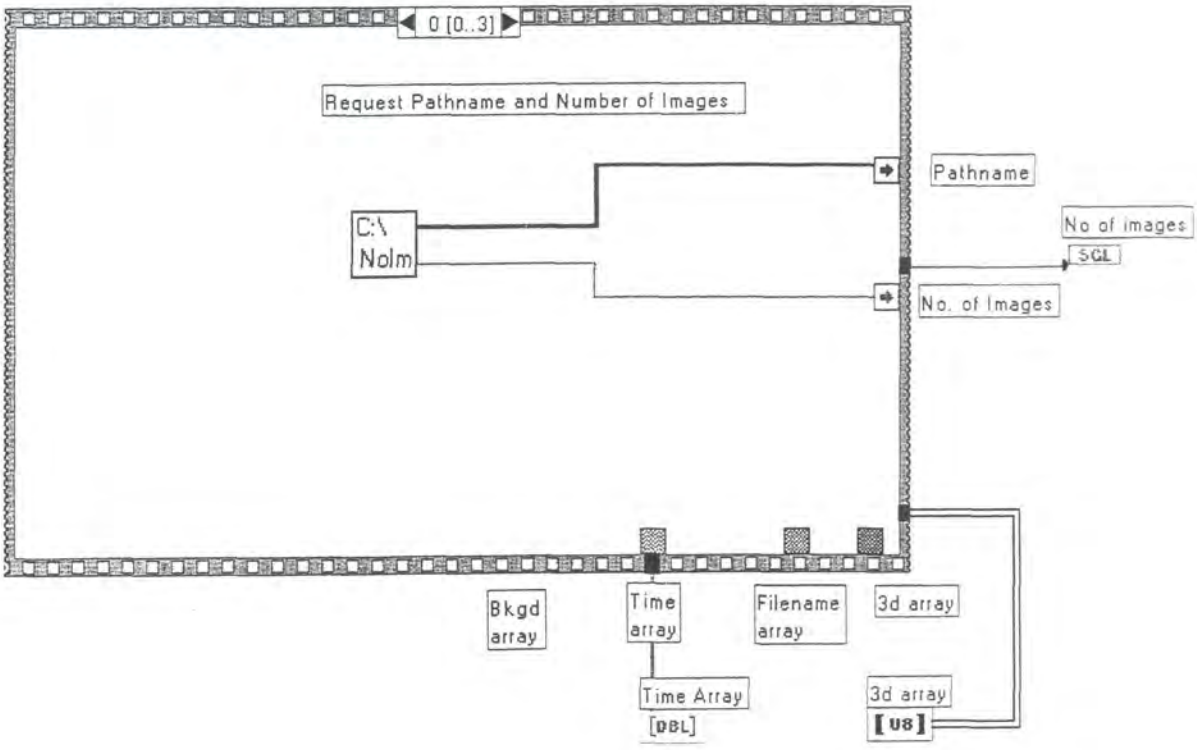

Read to 3d arrary.vi
E:\labview\Squirrel Map\Stuff\Read to 3d arrary.vi
Last modified on 23/03/99 at 15:57
Printed on 19/11/99 at 13:45

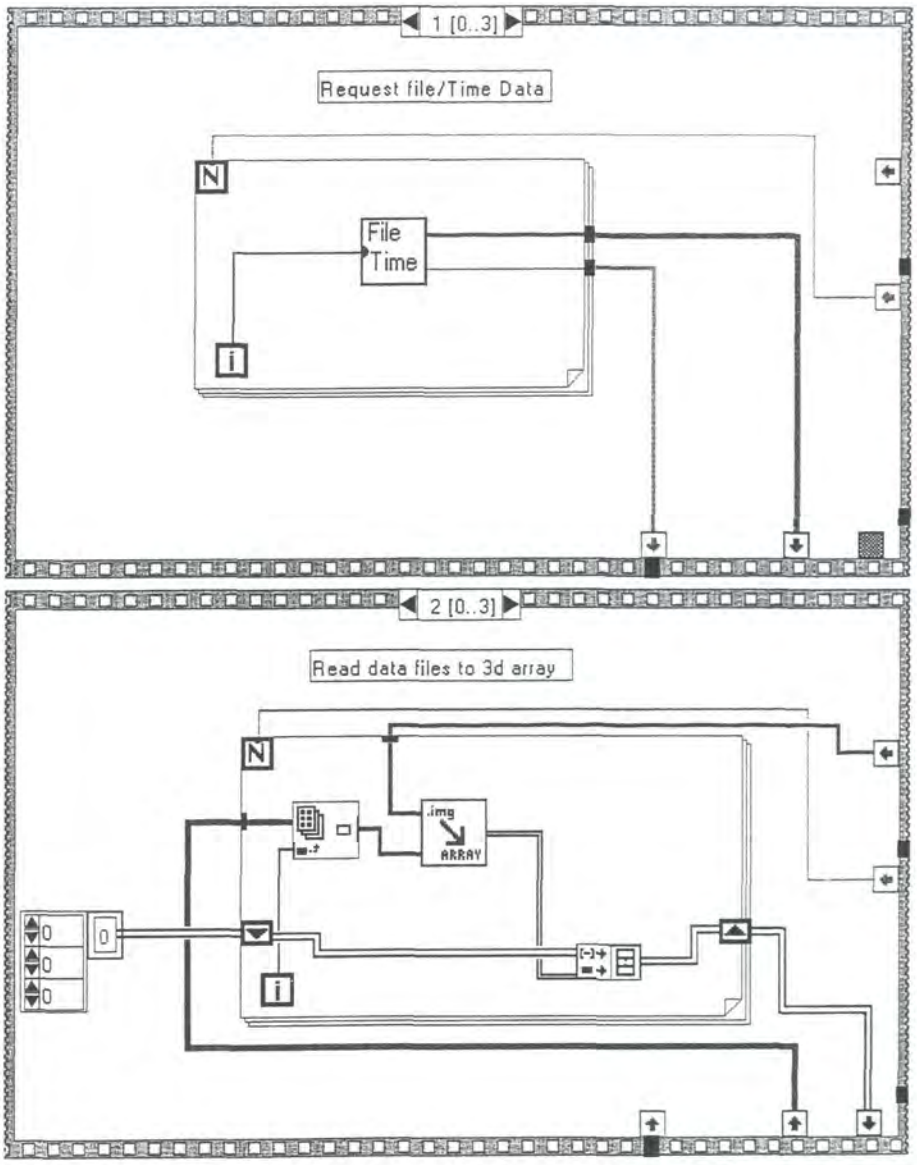

Read to 3d arrary.vi
E:\labview\Squirrel Map\Stuff\Read to 3d arrary.vi
Last modified on 23/03/99 at 15:57
Printed on 19/11/99 at 13:45

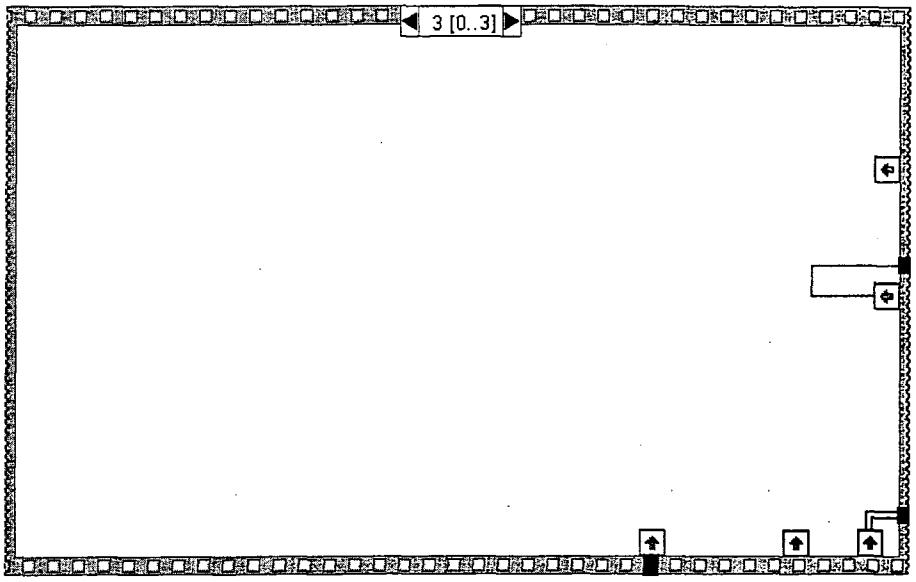

No of images.vi
E:\labview\Squirrel Map\Stuff\No of images.vi
Last modified on 05/05/99 at 18:57
Printed on 19/11/99 at 13:46

Connector Pane

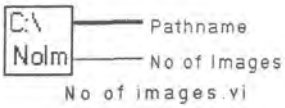

Front Panel

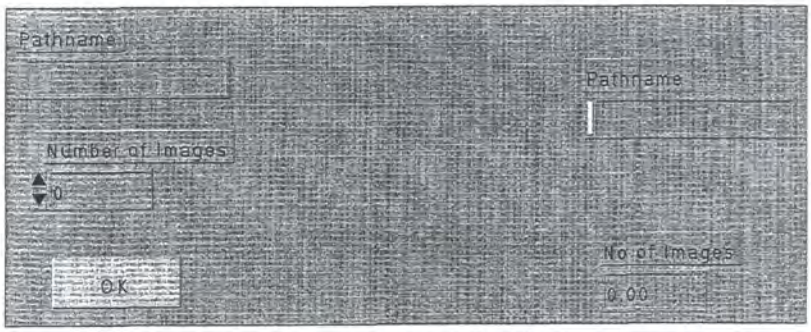

Block Diagram

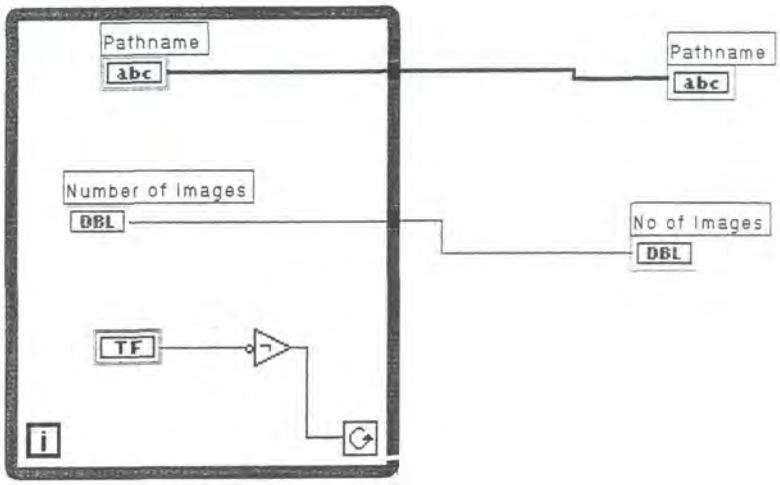

File Time Request.vi
E:\labview\Squirrel Map\Stuff\File Time Request.vi
Last modified on 05/05/99 at 18:57
Printed on 19/11/99 at 13:47

Connector Pane

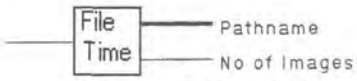

File Time Request.vi

Front Panel

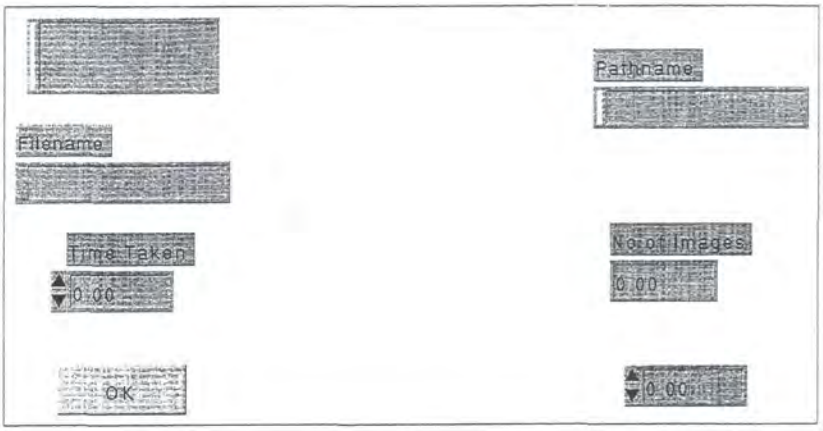

Block Diagram

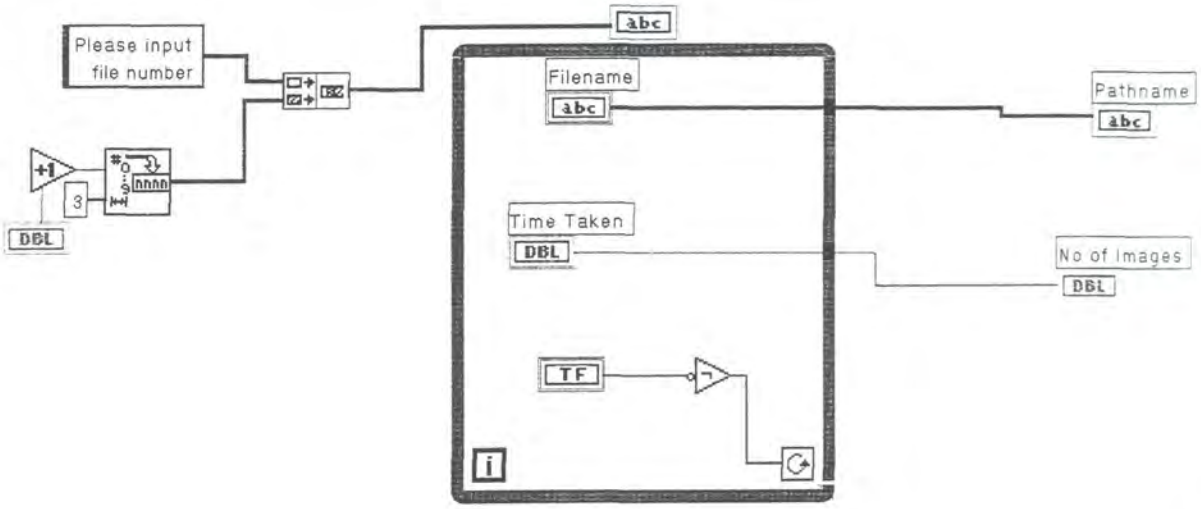

img to array.vi
E:\labview\Programs\img to array.vi
Last modified on 09/09/99 at 17:11
Printed on 19/11/99 at 13:47

Connector Pane

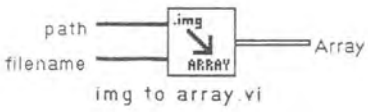

Front Panel

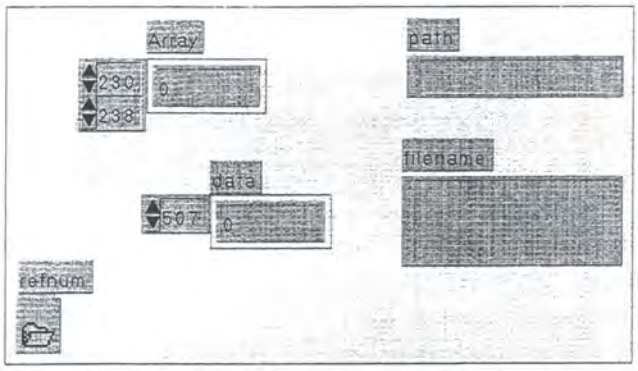

Block Diagram

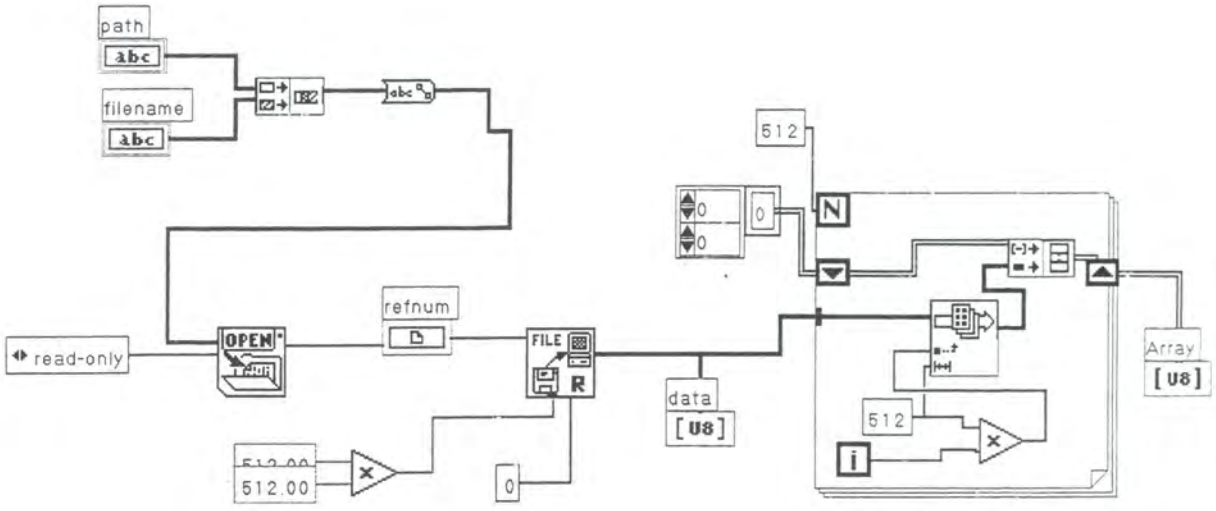

viewer3.vi
E:\labview\Squirrel Map\viewer3.vi
Last modified on 16/07/99 at 17:30
Printed on 19/11/99 at 13:50

Connector Pane

viewer3.vi

Front Panel

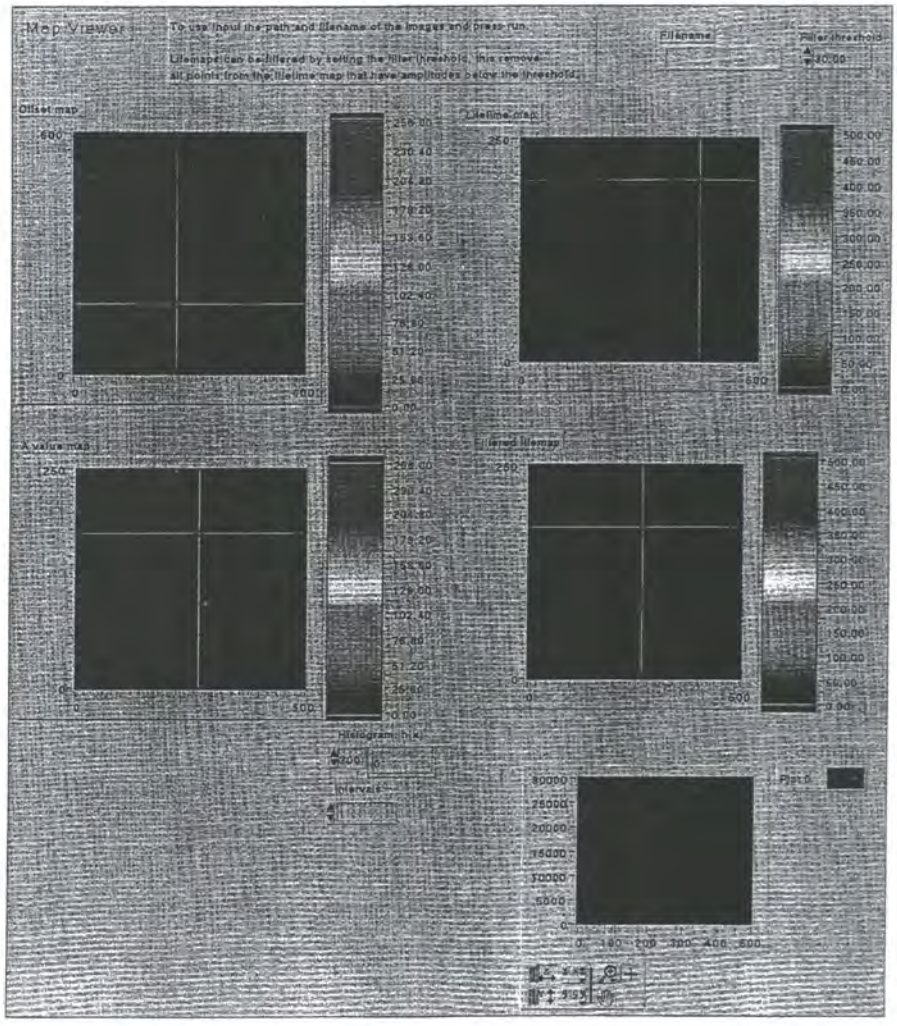

Block Diagram